

C.2

82

Evaluation of Air Injection in a Sudden Expansion Diffuser for Real-Time Afterburning Application

S. E. Stephens
Sverdrup Technology, Inc.

January 1991

Final Report for Period January 22 through April 5, 1989

**TECHNICAL REPORTS
FILE COPY**

PROPERTY OF U.S. AIR FORCE
AEDC TECHNICAL LIBRARY

Approved for public release; distribution is unlimited.

**ARNOLD ENGINEERING DEVELOPMENT CENTER
ARNOLD AIR FORCE BASE, TENNESSEE
AIR FORCE SYSTEMS COMMAND
UNITED STATES AIR FORCE**



NOTICES

When U. S. Government drawings, specifications, or other data are used for any purpose other than a definitely related Government procurement operation, the Government thereby incurs no responsibility nor any obligation whatsoever, and the fact that the Government may have formulated, furnished, or in any way supplied the said drawings, specifications, or other data, is not to be regarded by implication or otherwise, or in any manner licensing the holder or any other person or corporation, or conveying any rights or permission to manufacture, use, or sell any patented invention that may in any way be related thereto.

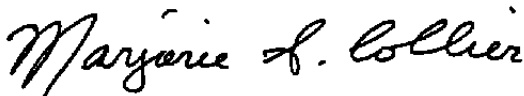
Qualified users may obtain copies of this report from the Defense Technical Information Center.

References to named commercial products in this report are not to be considered in any sense as an endorsement of the product by the United States Air Force or the Government.

This report has been reviewed by the Office of Public Affairs (PA) and is releasable to the National Technical Information Service (NTIS). At NTIS, it will be available to the general public, including foreign nations.

APPROVAL STATEMENT


This report has been reviewed and approved.



MARJORIE S. COLLIER
Directorate of Technology
Deputy for Operations

Approved for publication:

FOR THE COMMANDER



KEITH L. KUSHMAN
Technical Director
Directorate of Technology
Deputy for Operations

REPORT DOCUMENTATION PAGE			Form Approved OMB No. 0704-0188	
Public reporting burden for this collection of information is estimated to average 1 hour per response, including the time for reviewing instructions, searching existing data sources, gathering and maintaining the data needed, and completing and reviewing the collection of information. Send comments regarding this burden estimate or any other aspect of this collection of information, including suggestions for reducing this burden, to Washington Headquarters Services, Directorate for Information Operations and Reports, 1215 Jefferson Davis Highway, Suite 1204, Arlington, VA 22202-4302, and to the Office of Management and Budget, Paperwork Reduction Project (0704-0188), Washington, DC 20503				
1. AGENCY USE ONLY (Leave blank)	2. REPORT DATE January 1991	3. REPORT TYPE AND DATES COVERED Final, January 22, 1989 -- April 5, 1989		
4. TITLE AND SUBTITLE Evaluation of Air Injection in a Sudden Expansion Diffuser for Real-Time Afterburning Application		5. FUNDING NUMBERS PE-65807F		
6. AUTHOR(S) Stephens, S. E., Sverdrup Technology, Inc., AEDC Group				
7. PERFORMING ORGANIZATION NAME(S) AND ADDRESS(ES) Arnold Engineering Development Center/DOT Air Force Systems Command Arnold AFB, TN 37389-5000		8. PERFORMING ORGANIZATION REPORT NUMBER AEDC-TR-90-29		
9. SPONSORING/MONITORING AGENCY NAME(S) AND ADDRESS(ES) Arnold Engineering Development Center/DO Air Force Systems Command Arnold AFB, TN 37389-5000		10. SPONSORING/MONITORING AGENCY REPORT NUMBER		
11. SUPPLEMENTARY NOTES Available in Defense Technical Information Center (DTIC).				
12a. DISTRIBUTION/AVAILABILITY STATEMENT Approved for public release; distribution is unlimited.		12b. DISTRIBUTION CODE		
13. ABSTRACT (Maximum 200 words) Altitude testing of advanced hydrogen-fueled propulsion systems will require techniques to deal with unburned hydrogen in the engine exhaust stream. One approach is real-time afterburning. This approach would inject oxidizer in the test facility exhaust diffuser and burn off the excess hydrogen before it reached any facility machinery. A combined experimental and computational study was conducted to evaluate the feasibility of this approach. The experimental study tested a sudden expansion diffuser with injection both upstream and downstream of the step. Engine air was delivered through either a Mach 3.0 or 0.8 nozzle. The acquired data evaluated mixing of the nonreacting streams using measured temperatures and a Crocco relationship. Wall and pitot pressures were used to evaluate diffuser performance. The PARC computer program was used to predict the flow field at two test conditions. The results showed that good mixing can be obtained with the configuration at penalty of loss in maximum diffuser pressure rise. The PARC program did an excellent job of predicting the flow-field pressures and shock structure; however, it was less satisfactory for predicting mixing based on temperature distribution.				
14. SUBJECT TERMS hydrogen-fueled propulsion systems gas handling techniques		PARC code diffuser performance		15. NUMBER OF PAGES 87
				16. PRICE CODE
17. SECURITY CLASSIFICATION OF REPORT UNCLASSIFIED	18. SECURITY CLASSIFICATION OF THIS PAGE UNCLASSIFIED	19. SECURITY CLASSIFICATION OF ABSTRACT UNCLASSIFIED		20. LIMITATION OF ABSTRACT SAME AS REPORT

PREFACE

The work reported herein was conducted at the Arnold Engineering Development Center (AEDC), Air Force Systems Command (AFSC), at the request of the Directorate of Technology (DOT). The results were obtained by Sverdrup Technology, Inc., AEDC Group (a Sverdrup Corporation Company), operating contractor of the propulsion test facilities, AEDC, AFSC, Arnold Air Force Base, Tennessee. The test program was conducted in the Engine Test Facility (ETF) Research Test Cell R1A1 from January 27, 1989 to April 5, 1989 under Air Force Project No. DA31EW, "Advanced Propulsion Test Techniques." The AEDC Air Force Project Manager was Ms. Marjorie S. Collier. The Sverdrup Project Manager was Mr. John L. Jordan. Technical consultant on the project was Dr. R. J. Schulz of the University of Tennessee Space Institute. The manuscript was submitted for publication on November 28, 1990.

CONTENTS

	<u>Page</u>
1.0 INTRODUCTION	5
2.0 TEST APPARATUS	6
2.1 Test Facility	6
2.2 Test Instrumentation	7
3.0 TEST DESCRIPTION	8
3.1 Test Conditions	8
3.2 Test Procedures	8
3.3 Data Reduction	9
3.4 Measurement System Uncertainty	9
4.0 FLOW-FIELD COMPUTATIONAL MODEL	9
5.0 RESULTS	10
5.1 Mach 3.0 Configuration	10
5.2 Mach 0.8 Configuration	17
6.0 CONCLUSIONS AND RECOMMENDATIONS	19
REFERENCES	21

ILLUSTRATIONS

<u>Figure</u>	<u>Page</u>
1. Test Apparatus	23
2. R1A1 Instrumentation Location Schematic	26
3. Total Temperature and Pitot Pressure Rakes	27
4. Crocco Number — Mach 3.0 Configuration, No Injection	28
5. Crocco Number — Upstream Injection = 0.25 lbm/sec	29
6. Crocco Number — Upstream Injection = 0.50 lbm/sec	30
7. Crocco Number — Upstream Injection = 1.0 lbm/sec	31
8. Crocco Number — Downstream Injection = 0.50 lbm/sec	32
9. Crocco Number — Downstream Injection = 1.0 lbm/sec	33
10. Crocco Number — Downstream Injection = 2.0 lbm/sec	34
11. Crocco Number — Combined Injection = 0.75 lbm/sec	35
12. Crocco Number — Combined Injection = 1.50 lbm/sec	36
13. Crocco Number — Combined Injection = 3.0 lbm/sec	37
14. Mixedness Parameter versus Axial Distance for Mach 3.0 Configuration	38

<u>Figure</u>	<u>Page</u>
15. Typical Diffuser Breakdown Curve	41
16. Diffuser Breakdown Curve for Combined Upstream/ Downstream Injection in the Mach 3.0 Configuration	42
17. Wall Pressure versus Axial Distance	43
18. PARC Prediction of Total Temperature versus Experimental Data, Case 2	46
19. PARC Prediction of Total Temperature versus Experimental Data, Case 3	50
20. PARC Prediction of Pitot Pressure versus Experimental Data, Case 2	54
21. PARC Prediction of Pitot Pressure versus Experimental Data, Case 3	58
22. PARC Prediction of Wall Pressure, Case 2	62
23. PARC Prediction of Wall Pressure, Case 3	63
24. Crocco Number — Mach 0.8 Configuration, No Injection	64
25. Crocco Number — Upstream Injection = 0.25 lbm/sec	65
26. Crocco Number — Upstream Injection = 0.50 lbm/sec	66
27. Crocco Number — Upstream Injection = 1.0 lbm/sec	67
28. Crocco Number — Downstream Injection = 0.50 lbm/sec	68
29. Crocco Number — Downstream Injection = 1.0 lbm/sec	69
30. Crocco Number — Downstream Injection = 2.0 lbm/sec	70
31. Crocco Number — Combined Injection = 0.75 lbm/sec	71
32. Crocco Number — Combined Injection = 1.5 lbm/sec	72
33. Crocco Number — Combined Injection = 3.0 lbm/sec	73
34. Mixedness Parameter versus Axial Distance for Mach 0.8 Configuration	74
35. Diffuser Breakdown Curve for Mach 0.8 Configuration with Downstream Injection	77
36. Wall Pressure versus Axial Distance, Mach 0.8 Configuration	78

TABLES

1. Measurement Uncertainties	81
NOMENCLATURE	82

1.0 INTRODUCTION

Proposed testing of hydrogen-fueled air-breathing propulsion systems for hypersonic vehicles in the Engine Test Facility (ETF) of the Arnold Engineering Development Center (AEDC) presents an exhaust gas handling challenge. The exhaust gas will contain unburned hydrogen under several engine conditions, including normal operation, flameouts, in-flight start attempts, no-lights, relights, and fuel system leakage. The potentially explosive nature of the exhaust products poses a hazard. Exhaust gas handling techniques must be identified to allow test and evaluation of the desired engine conditions.

The handling of unburned hydrogen in exhaust gases is not new in the ETF. Rocket propulsion systems typically produce large amounts of unburned hydrogen. The exhaust becomes combustible when combined with air from leakages in the facility exhaust ducting. For rocket engine testing in the ETF, nitrogen dilution is used to reduce the amount of available oxidizer in the facility exhaust ducting to a level below the oxidizer lean combustion limit (OLCL).

Dilution techniques are not feasible for many conditions expected during testing of air-breathing hypersonic propulsion systems (Ref. 1). Diluent flow rates required to reach the OLCL during some conditions exceed exhaust plant volume flow rate capacities. Therefore, an exhaust gas handling technique other than nitrogen dilution is needed.

The possible fuel-to-air ratio (F/A) of the exhaust gas composition that may occur in the diffuser can be divided into two categories. The first category is referred to as overstoichiometric (overstoich, for short). This exists when there is more hydrogen than required for complete combustion with the available oxygen. This may occur in a direct-connect test of a hydrogen-fueled engine. There may be a large amount of unburned hydrogen being exhausted by the engine into the facility ducting, but only a small amount of oxygen caused by relatively small air in-leakages.

The second category is referred to as understoichiometric (or understoich) and occurs when there is more than enough oxygen available to burn all the hydrogen present. The understoich condition is likely to occur during free-jet testing, where a large amount of air by-passes the engine and is collected by the exhaust diffuser.

One exhaust gas handling approach is real-time hydrogen afterburning. Conceptually, this technique relies on controlled combustion in the facility exhaust ducting to reduce the free hydrogen to below the fuel lean combustion limit (FLCL). It is applicable to both understoich and overstoich conditions. For overstoich conditions, additional oxidizer must be injected into the ducting to permit effective afterburning.

An experimental database is required to both assess the feasibility of and validate an analytical model of exhaust gas afterburning. To obtain this database, an experimental study was conducted to evaluate mixing an injected oxidizer in an exhaust diffuser flow. The effect of injection on diffuser performance was also evaluated. Predictions of the mixing and diffuser performance were made using a computational model. The predictions were then compared to the experimental data.

2.0 TEST APPARATUS

2.1 TEST FACILITY

The test program was conducted in the AEDC ETF Research Test Cell R1A1. The test apparatus is shown in Fig. 1. An overall test cell schematic is shown in Fig. 1a. The tests were designed to simulate injection and mixing of an oxidizer in a diffuser flow. Engine exhaust was simulated using heated air. The simulated exhaust flow is denoted in Fig. 1 as primary air. Simulated oxidizer flow was injected downstream in the cell exhaust diffuser and/or just downstream of a sudden expansion located at the diffuser exit. Unheated air was used for this flow, which is denoted in Fig. 1 as secondary air.

The primary air is supplied from the von Kármán Facility (VKF) high-pressure air (HPA) system. The primary air is heated as it passes through a natural-gas-fired, clean-air heat exchanger. It then enters the cell through either a convergent Mach 0.8, or convergent-divergent Mach 3.0 nozzle. The two different Mach number nozzles allow simulation of tests at either started or unstarted diffuser conditions.

The Mach 0.8 primary air nozzle, Fig. 1b, has an exit diameter of 4.5 in. The Mach 3.0 nozzle, Fig. 1c, has a throat diameter of 2.64 in. and expands to an exit diameter of 5.43 in. through a 10-deg half-angle cone. The 15.62-in.-diam test cabin is designed to permit variation of the spacing between nozzle exit plane and diffuser entrance plane in discrete steps of 0, 4, and 8 in. The complete test program was conducted with the spacing between nozzle exit and diffuser inlet maintained at 4 in.

The nozzle exhaust is captured by a cylindrical diffuser. The diffuser is 7.98 in. in diameter and 40 in. long. The diffuser empties into a 15.62-in. "burner" duct through a rearward-facing step. This configuration is frequently referred to as a sudden expansion burner.

Secondary air, the simulated injected oxidizer, enters the system through either or both of two sets of injectors. Each set consists of eight injectors directed radially inward toward the duct centerline with one manifold supplying all eight injectors. Air is supplied to the manifolds by an auxiliary air supply system. The system is capable of delivering approximately 5 lbm/sec total airflow at 110 psia and ambient temperature to the secondary air manifolds.

The first set of injectors is located 20 in. upstream of the sudden expansion. The injectors are uniformly spaced at 45-deg increments around the diffuser circumference. The second set of injectors is located 8 in. downstream of the sudden expansion and are axially aligned with the eight upstream injectors. Figure 1d is a photograph of the manifolds and the injectors.

2.2 TEST INSTRUMENTATION

The locations and nomenclature of the test instrumentation are shown in Fig. 2. The measurements were made to provide data to determine mixing and diffuser performance as a function of primary and secondary flow conditions. Mixing performance was determined by measuring total temperatures in the burner duct. Diffuser performance was determined by measuring wall static pressure and burner duct pitot pressures.

The burner duct conditions were surveyed with two total temperature and two pitot pressure rakes. The rakes had a total of 13 temperature probes and 12 pressure probes set on equal areas as shown in Fig. 3. The rakes could be mounted in the burner duct in any of four axial locations. These locations were 1.19, 1.71, 2.73, and 4.78 burner duct diameters downstream of the sudden expansion. Relocation of the rake station was accomplished by the reordering of five interchangeable burner duct sections.

The total temperature rakes were usually positioned at 0- and 22.5-deg angular locations, and the total pressure rakes were positioned at 180- and 202.5-deg angular locations measured clockwise from the top of the duct looking downstream, as shown in Fig. 3. Installation of the rakes in this manner allowed data to be gathered both directly downstream and between adjacent secondary flow injectors. For symmetry checks, the temperature and pressure probes were exchanged so that the pressure rakes were located at 0 and 22.5 deg, and the temperature rakes were located at 180- and 202.5-deg rotation. For tests where the survey rakes were positioned at an $L/D = 1.19$ or 1.71 , the rakes could not be installed at the 180-deg position because of facility hardware interference. An alternate rake orientation at 225-deg was used instead of the 180-deg orientation.

The primary, upstream secondary, and downstream secondary airflow rates were measured using critical flow venturis. The primary flow venturi has a 0.95-in.-diam throat, whereas the upstream and downstream flow venturis have 0.91- and 1.034-in.-diam throats, respectively.

Air flows were calculated based on total temperature and total pressure measurements of the air flowing into the critical flow venturi. Wall static pressure taps were located along the diffuser and burner duct to measure pressure recovery and to locate gas dynamic shocks in the system.

All temperature measurements were made with either copper-constantan (CC) or Chromel® -Alumel® (CA) thermocouple junctions. All pressures were measured with bonded, strain-gage-type pressure transducers. Instrument system calibrations performed during the testing are traceable to the National Institute of Standards and Technology (NIST). Each link in the traceability chain to the NIST is maintained and documented by the AEDC Precision Measurement Equipment Laboratory (Ref. 2).

3.0 TEST DESCRIPTION

3.1 TEST CONDITIONS

Heated primary air was supplied to the test cell from the VKF HPA system. The VKF HPA flow was regulated using a pressure control valve. Operation in this mode allowed a constant flow rate to be maintained when the test cell pressure was maintained below the value required for critical flow through the primary airstream venturi. Primary air flow was typically set at 5 lbm/sec. A natural-gas-fired, indirect heater was used to obtain nonvitiated primary air at the desired temperature level. The heater could be operated with automatically operated set point controls or operated in manual mode.

Secondary flow was delivered to the upstream and downstream secondary flow manifolds from the auxiliary air supply system. Flow to either manifold could be turned on or off via a manually operated shutoff valve.

3.2 TEST PROCEDURES

Before each test, the test cell instrumentation was calibrated *in situ* at ambient conditions. After adequate ambient calibrations were completed, the test cell was subjected first to a pressure of 20 psia and then to a vacuum of 6 psia. *In situ* pressure calibrations were made at both the pressure and vacuum conditions. Operations of the data acquisition and data recording systems were verified before each test.

During testing, the flow rate and total temperature of the primary airstream and the flow rate of the secondary airstream were set at predetermined values. After the system had stabilized, as indicated by a variation in rake total temperature, TTR-n, of less than $\pm 5^{\circ}\text{F}$ and a variation in rake total pressure, PTR-n, of less than ± 0.2 psia, steady-state data were recorded. Nominally, the primary airflow rate was maintained at 5.0 lbm/sec, and the secondary air flow was set at discrete points ranging between 0 and 3.0 lbm/sec in various upstream and downstream injection combinations as shown in the following table, where X indicates combinations evaluated during the test program.

Upstream Injection, lbm/sec	Downstream Injection, lbm/sec			
	0	0.50	1.0	2.0
0	X	X	X	X
0.25	X	X		
0.50	X		X	
1.0	X			X

After all planned flow rate combinations were tested, several points were repeated. When time permitted during the tests, the total temperature and total pressure probe positions were reversed and the test matrix repeated for flow symmetry checks.

3.3 DATA REDUCTION

The AEDC/ETF digital data acquisition system was used to record all steady-state data collected during the testing. Engineering units data were processed and printed in near real-time after processing by the AEDC VAX 8600 central computer. A control room CRT display of selected parameters was used to set conditions and display near real-time values of critical, calculated parameters during testing.

3.4 MEASUREMENT SYSTEM UNCERTAINTY

Measuring devices, ranges, and steady-state uncertainty, based on analysis methods used in Ref. 3, are presented in Table 1.

4.0 FLOW-FIELD COMPUTATIONAL MODEL

The PARC computer code was used to model the characteristics of the flow field, including the mixing of the primary and secondary flows in the diffuser and burner duct. The PARC code is a general purpose, multidimensional Navier-Stokes equation solver that has been successfully applied to a wide range of fundamental and practical propulsion-related problems, (Refs. 4 and 5). Among its past applications are problems concerning supersonic nozzle flows, free and wall-bounded shear layers, and rearward-facing steps. Recent successful calibrations (Ref. 6) for flows with elements similar to those of the current investigation support its application here.

The PARC code was used to predict the flow-field characteristics for three test conditions. The hardware configuration for each of these used the Mach 3.0 primary nozzle. The injection configuration varied among the cases as shown in the following table:

Case	Primary Flow Rate, lbm/sec	Secondary Flow Rate, lbm/sec	
		Upstream	Downstream
1	5.0	0	0
2	5.0	0.5	1.0
3	5.0	1.0	2.0

As indicated by this table, Case 1 employed no injection. Axial flow-field symmetry was assumed and the flow field for Case 1 was computed with the two-dimensional (2-D) (axisymmetric) version of the PARC code. For Cases 2 and 3, which include injection, the assumption of flow-field axisymmetry is no longer valid. However, circumferential periodicity of the flow field does exist since both the upstream and downstream secondary injection jets are placed every 45 deg. Thus, the required computational grid was only 22.5 deg in the circumferential direction.

5.0 RESULTS

The objective of the experimental study was to collect a database to evaluate the effect of injection on mixing and diffuser performance. No attempt was made to simulate, or evaluate, combustion characteristics.

Tests were conducted to simulate two different engine configurations: Mach = 3.0 engine exhaust (diffuser normally started) and Mach = 0.8 engine exhaust (diffuser unstarted). Tests were conducted at each engine configuration for several different secondary flow injection conditions. Primary and secondary air mixing and diffuser performance were evaluated first for the Mach 3.0 engine exhaust configuration, then for the Mach 0.8 engine exhaust configuration.

5.1 MACH 3.0 CONFIGURATION

5.1.1 Mixing Performance

Afterburning requires fuel and oxidizer species that are well mixed. In overstoich applications, the fuel source is the unburned fuel contained in the engine exhaust, here simulated by primary flow, and the oxidizer source is the injected gas, here simulated by secondary flow. For afterburning with injection to be successful, the primary and secondary flows must be well mixed.

A Crocco analogy was used to relate measured temperatures to a theoretical species distribution. The Crocco analogy assumes that the turbulent diffusion of the total temperature is the same as the turbulent diffusion of species, i.e., that the turbulent Lewis number is unity. The analogy is stated in the equation

$$Cr_i = \frac{T_{tr_i} - T_{t_s}}{T_{t_p} - T_{t_s}} = \frac{Y_i - Y_s}{Y_p - Y_s}$$

where:

- Cr = Crocco number
- T_{tr} = rake probe total temperature, °R
- T_t = total temperature, °R
- Y = mass fraction of chemical species of interest
- i = point of interest in mixed flow field
- s = secondary flow
- p = primary flow

Using this equation, if the total temperature at a point in the mixed flow field is the same as the secondary flow total temperature, then the Crocco number at this point is zero, and the species are identical to that contained in the unmixed secondary flow. Conversely, if the total temperature at a point is the same as the primary flow, then the Crocco number is unity, and the species are identical to the primary flow. For the case of a perfectly mixed flow, the Crocco number will be constant throughout, with a value between 0 and 1.

Plots of Crocco number for the Mach 3.0 configuration are shown in Figs. 4 through 13. These plots illustrate the functional relationship between Crocco number and radial position for various axial distances and injection flow rates. The flow conditions and corresponding figure numbers are shown in the following table:

Figure	Upstream Injection Flow Rate	Downstream Injection Flow Rate	Combined Injection Flow Rate
4	$W_u = 0 \text{ lbm/sec}$	$W_d = 0 \text{ lbm/sec}$	$W_s = 0 \text{ lbm/sec}$
5	$= 0.25 \text{ lbm/sec}$	$= 0 \text{ lbm/sec}$	$= 0.25 \text{ lbm/sec}$
6	$= 0.50 \text{ lbm/sec}$	$= 0 \text{ lbm/sec}$	$= 0.50 \text{ lbm/sec}$
7	$= 1.0 \text{ lbm/sec}$	$= 0 \text{ lbm/sec}$	$= 1.0 \text{ lbm/sec}$
8	$= 0 \text{ lbm/sec}$	$= 0.50 \text{ lbm/sec}$	$= 0.50 \text{ lbm/sec}$
9	$= 0 \text{ lbm/sec}$	$= 1.0 \text{ lbm/sec}$	$= 1.0 \text{ lbm/sec}$
10	$= 0 \text{ lbm/sec}$	$= 2.0 \text{ lbm/sec}$	$= 2.0 \text{ lbm/sec}$
11	$= 0.25 \text{ lbm/sec}$	$= 0.50 \text{ lbm/sec}$	$= 0.75 \text{ lbm/sec}$
12	$= 0.50 \text{ lbm/sec}$	$= 1.0 \text{ lbm/sec}$	$= 1.50 \text{ lbm/sec}$
13	$= 1.0 \text{ lbm/sec}$	$= 2.0 \text{ lbm/sec}$	$= 3.0 \text{ lbm/sec}$

Each plot in Figs. 4 through 13 shows two lines of Crocco number corresponding to different circumferential measurement locations. One line is measured in the same circumferential plane as the injectors, and is denoted as 0-deg, while the other is in a plane located halfway between injectors, and is denoted as 22.5 deg. Each of the figures indicate that there is less than a 3-percent variation of Crocco number in the circumferential direction at the measurement locations. This implies that all circumferential variations have abated within 1.17 diam of the sudden expansion.

The plots do show that at an axial location of 1.71 diam, the fifth probe (counting from the centerline) on the 0-deg rake is measuring a significantly different temperature than its 22.5-deg counterpart. This is true for all of the downstream and combined injection case data. However, the data was acquired over successive data points in one test only. Because of the severity of the variation and its uniqueness, it is believed that the data were taken with a malfunction in the instrumentation and recording system and are not a valid representation of the actual flow, i.e. a bad measurement.

Figure 4 shows the case of zero secondary flow injection. By definition, the Crocco numbers should be 1.0 for all positions; however, the calculated values, based on the test data, are less than 1.0. It is believed that the reason for this is attributable to the presence of a recirculation. A recirculation would cause a part of the flow to have an axial velocity vector that is not in the downstream direction. When the flow is not close to axial, the temperature probes are no longer measuring an accurate recovery temperature. An inaccurate temperature measurement leads to an inaccurate Crocco number calculation. Figure 4d shows that Crocco number is constant and near unity, indicating that recirculation does not extend to that

measurement station, 4.78 diam downstream of the expansion. The remaining difference is probably caused by heat loss from the system between the primary and secondary upstream temperature measurements and the rake temperature probes.

It is logical to ask what effect recirculation has on the data points with injection. The obtained data do not lend themselves to calculating the presence, or size, of a recirculation zone. A crude indication can be obtained by comparing plots of Crocco number at different axial locations. For the no-injection case, Figs. 4a through d, the average value of the Crocco number increases significantly with downstream distance. In fact, the average value at the 4.78 downstream diam is approximately the same as the maximum value of Crocco number at the 1.19-diam location. Since heat addition to the flow is improbable, the only plausible explanation is that the upstream locations were not measuring the total temperature, which indicates a recirculation present at the upstream location.

Examination of Figs. 5 through 13 shows that the average value of Crocco number does not increase with distance to the same degree as the no-injection case. Figures 5 and 6 show moderate increase in average Crocco number, whereas the rest of the figures show very little change. It appears that recirculation does not play a significant role in the cases of flow with injection, with the possible exception of the cases of low and moderate upstream-only injection.

Reduction in the radial gradient in Crocco number indicates mixing improves as the flow travels away from the step. For example, the Crocco plots for the case of combined upstream/downstream injection of 0.75 lbm/sec are shown in Fig. 11. At the axial location farthest upstream, 1.19 diam downstream of the sudden expansion (Fig. 11a), there is a large gradient in Crocco number. Crocco values range from 0.94 at the centerline to 0.68 at the diffuser wall. As the flow moves downstream, the gradient diminishes to 0.04 (0.77 to 0.73) indicating better mixing at a distance of 4.78 diam downstream from the step, Fig. 11d.

The absolute value of the Crocco number is not as important in this study as is its variation. Therefore, a mixedness parameter was defined to quantify the mixing of the flow. This mixedness parameter is defined by,

$$M = \left[\frac{1}{n} \sum_{i=1}^n \left(\frac{Cr_i - Cr_{avg}}{Cr_{avg}} \right)^2 \right]^{1/2}$$

where

- M = mixedness parameter
- n = number of measurement probes, and
- avg = mass averaged value

The mixedness parameter is essentially a root-mean-square of Crocco number deviations relative to a mass-averaged value. Large values of M , close to unity, correspond to large average deviations, whereas small values of M , close to zero, correspond to near-uniform, or well-mixed, conditions.

Plots of the mixedness parameter versus axial distance are shown for the Mach 3.0 configuration in Fig. 14. Figure 14a shows M for the upstream injection case, and Figs. 14b and c show the downstream injection and combined upstream/downstream injection cases, respectively. For all three cases, the most evident feature is that the mixedness parameter is decreasing with distance. This is consistent with an expected increase in mixing with distance.

As secondary flow rate increases, the amount of mixing increases. For the upstream injection case (Fig. 14a), the deviation in Crocco number drops from 6 to 3 percent for the low flow rate, whereas for the high flow rate, the deviation drops from 7 to 0.5 percent. A similar result is true for the downstream and combined injection cases.

The plots of the mixedness parameter indicate that the downstream injection mixes better than upstream injection. Comparing Figs. 14a and b shows that near the step, the mixedness parameter is high (poor mixing) for the downstream injection case. This is expected since the downstream injection jets are close to the measurement stations. However, at the farthest measurement station, 4.78 diam, the downstream injection case has mixed better (smaller mixedness parameters) than the upstream injection case. The results of the combined injection case are nearly identical to the downstream injection case, in spite of the additional mass flow. The exception is that the highest mass flow rate for combined injection shows a higher degree of mixing at the measurement station closest to the step. The combined injection may therefore be a good compromise between a desired initial mixedness and a large degree of overall mixing.

5.1.2 Diffuser Pumping Performance

One approach to evaluating diffuser (pumping) performance is to relate cell pressure to diffuser exit pressure with both terms normalized by the driving, or primary, nozzle total pressure. Figure 15 shows an example of a plot relating these parameters. The plot is known as a diffuser breakdown curve. The curve shows that for a sufficiently low ratio of exit pressure to driving pressure, the diffuser is started (cell pressure becomes independent of the exit pressure). Conversely, for higher pressure ratios, the diffuser is unstarted (cell pressure is a function of the exit pressure).

Diffuser systems usually contain some hysteresis in the breakdown curve. That is, the transition point between started and unstarted is dependent on the direction from which it

is approached. Going from unstarted to started, the transition point is referred to as the starting point, or starting pressure ratio, whereas in the reverse direction, the point is referred to as the operating point, or operating pressure ratio.

Figure 16 shows the data acquired for the Mach 3.0 configuration case with combined secondary injection. The diffuser was started for nearly all data points with a cell pressure ratio of 0.01. The secondary flow had no effect on cell pressure provided the system remained started. The data show that the exit pressure increased slightly with the secondary flow; however, this is because of the manner in which the back pressure was maintained in the experimental apparatus.

Several data points were attained for elevated exit pressure ratios. Figure 16 shows that the unstarted condition was attained at raised exit pressure ratios for two different injection flow rates. The curve illustrates that as the secondary flow is increased, the operating point moves to the left, that is, the diffuser unstarts at lower values of P_e/P_t . The operating pressure ratio for the case of 1.5 lbm/sec secondary injection is approximately 0.125 with a maximum rise ratio $[(P_e/P_t)/(P_c/P_t)]$ of 12.5. For the case of 3.0 lbm/sec injection, the operating pressure ratio is 0.10 with a maximum rise ratio of 10. This implies that to operate with secondary flow, the facility exhaust system will be required to maintain lower pressures at the burner duct exit than would be required without secondary flow. Since no data were taken at an unstarted, no-injection condition, a direct evaluation of the data relative to no secondary flow is not possible.

The data for the cases of upstream and downstream secondary injection are not presented herein but indicate similar performance trends. The cell pressure ratios were the same with no effect of secondary flow rate on started diffuser performance. Again, no data were taken at unstarted conditions.

Wall static pressure was recorded at several axial locations at each flow condition. The wall pressure profile data are presented in Fig. 17. Figure 17a shows the wall pressure for the upstream injection cases; and Figs. 17b and c show the wall pressure for the downstream and combined injection cases, respectively. The pressure recovery profile in the diffuser and burner ducts is a function of the overall pressure ratio and the injection characteristics. For the case of upstream injection, Fig. 17a, there is a pressure rise just downstream of the injection, and a second pressure rise at the sudden expansion corresponding to a velocity decrease. As secondary flow increases, the first pressure rise increases in magnitude. The downstream injection case, Fig. 17b, places the pressure rise at the diffuser exit for low flow rates and moves upstream with increasing flow rate. As expected, the combined injection case, Fig. 17c, is a combination of these effects.

5.1.3 Results of PARC Code Predictions

The PARC code was used to predict the flow field for the three cases of 0, 1.5, and 3.0 lbm/sec combined upstream/downstream secondary flow. These are noted as Cases 1, 2, and 3, respectively. The primary nozzle and injection conditions were set as boundary conditions along with the burner duct exit pressure. The code failed to converge for Case 1. More specifically, the shock location oscillated in the duct, yielding a constantly changing flow field. The system is inherently unstable and not conducive to time-accurate flow-field computations. Cases 2 and 3 did converge however, and the results are presented herein.

The PARC code predictions of mixing for Case 2 can be compared to the experimental data directly using plots of temperature versus radius, as given in Fig. 18. Comparisons are made at axial locations of $x = 1.19, 1.71, 2.73$, and 4.78 diam from the sudden expansion. The PARC code predicts less mixing than the test data indicate, although the overall trends are similar with the exception of the $x = 4.78$ diam case, Fig. 18d. At this distance, the data show a very flat profile, whereas the PARC code predicts a strong gradient in temperature. The discrepancy is probably caused by inaccuracies in the PARC code turbulent mixing model.

There are two comparisons, corresponding to 0 and 22.5 deg circumferential location, for each axial station. The PARC code predicts slightly less circumferential mixing than indicated by the test data. At the $x = 1.19$ diam location, Figs. 18a and b, the predictions show that there is a circumferential variation in the flow field not indicated by the test data. By the next measurement station, $x = 1.71$ diam shown in Figs. 18c and d, the predicted circumferential variation is nearly gone.

The results for Case 3 are not as good as Case 2. The comparisons of temperature versus radius for Case 3 results are shown in Fig. 19. The test data show nearly uniform temperature profiles throughout the eight measurement stations. The PARC code, however, predicts strong gradients in temperature. At $x = 1.19$ and 1.71 diam, Figs. 19a through d, PARC predicts a hot core flow. As radius increases, the gas temperature drops rapidly, then increases slowly over the outer half-radius. Neither the hot core flow nor the outer temperature gradient are indicated by the test data. At the last two measurement stations, Figs. 19e through h, the code predicts the hot core flow and a temperature drop only. The test data indicate a cooler, uniform profile.

The inaccuracies of the total temperature predictions for Cases 2 and 3 are believed to be caused by inaccuracies in the PARC turbulent mixing model. The mixing model has been upgraded since the calculations were performed; however, the flow field has not been recalculated with this revision.

Direct comparisons of the rake pitot pressures can also be made. Figures 20 and 21 show the comparisons of PARC-predicted rake pitot pressure to experimental data for Cases 2 and 3, respectively. Both cases show excellent agreement. Very little circumferential variation is indicated by either the test data or the PARC predictions. The $x = 1.19$ diam plots, Figs. 20a and b, show very good agreement on the location and slope of the radial gradient in pitot pressure. The bump on the 22.5-deg plot near the wall is attributable to a predicted, localized velocity spike that is not indicated by the test data. The test apparatus did not have a pitot pressure probe on the centerline (radius = 0), so no comparison is available at this point. Comparisons at the last measurement station show that the code predicts the region of the pitot pressure gradient to be closer to the centerline than the test data show; in fact, because of the lack of a centerline probe, the gradient is not detected at all. The results for Case 3 are comparable to Case 2.

The PARC-computed cell pressure is shown in the breakdown curve presented in Fig. 16. The code used specified exit pressure and primary nozzle total pressure for boundary conditions in the cell pressure calculation. The code did a poor job of predicting the cell pressure. As with the mixing, the inaccuracy of the turbulent mixing model is believed to be the reason.

The PARC code predictions of wall pressure versus axial distance are shown in Figs. 22 and 23. Figure 22 shows the profile for Case 2. Agreement with the measured pressures is very good from the sudden expansion downstream, including the region in the vicinity of the downstream injector. However, upstream of the expansion in the vicinity of the upstream injector, significant differences in trend and level exist. In contrast, the computed wall pressure distribution for Case 3 shown in Fig. 23, indicates good agreement with the measured wall pressures in the vicinity of the upstream injector while differing by as much as 20 percent at the sudden expansion and in the vicinity of the downstream injector. However, the predicted trend of wall pressure versus distance does agree well with the measurements.

5.2 MACH 0.8 CONFIGURATION

5.2.1 Mixing Performance

Plots of the functional relationship of Crocco number, calculated from experimental data, to duct radial position at $x = 1.19, 1.71, 2.73,$ and 4.78 diam from the sudden expansion step for the Mach 0.8 configuration are shown in Figs. 24 through 33. The flow conditions and corresponding figure numbers are shown in the following table:

Figure	Upstream Injection Flow Rate	Downstream Injection Flow Rate	Combined Injection Flow Rate
24	$W_u = 0$ lbm/sec	$W_d = 0$ lbm/sec	$W_s = 0$ lbm/sec
25	$= 0.25$ lbm/sec	$= 0$ lbm/sec	$= 0.25$ lbm/sec
26	$= 0.50$ lbm/sec	$= 0$ lbm/sec	$= 0.50$ lbm/sec
27	$= 1.0$ lbm/sec	$= 0$ lbm/sec	$= 1.0$ lbm/sec
28	$= 0$ lbm/sec	$= 0.50$ lbm/sec	$= 0.50$ lbm/sec
29	$= 0$ lbm/sec	$= 1.0$ lbm/sec	$= 1.0$ lbm/sec
30	$= 0$ lbm/sec	$= 2.0$ lbm/sec	$= 2.0$ lbm/sec
31	$= 0.25$ lbm/sec	$= 0.50$ lbm/sec	$= 0.75$ lbm/sec
32	$= 0.50$ lbm/sec	$= 1.0$ lbm/sec	$= 1.50$ lbm/sec
33	$= 1.0$ lbm/sec	$= 2.0$ lbm/sec	$= 3.0$ lbm/sec

As with the Mach 3.0 configuration, there are two lines of Crocco numbers on each plot corresponding to the 0- and 22.5-deg circumferential locations. The plots indicate that there is no circumferential variation at any of the measurement stations at any injection condition.

The case of no secondary flow injection is shown in Fig. 24. As with the Mach 3.0 configuration, the Crocco values are slightly less than unity. The difference is constant throughout the length of the burner duct. Combined with the flat profiles, this indicates that heat loss may be the major cause of the deviations from unity Crocco number. The effect, however, is small, so the results for the injection cases are still qualitatively valid.

For the points with secondary flow injection, the Mach 0.8 data show that the flow is very well mixed in the radial direction before it reaches the first measurement location, $x = 1.19$ diam. Figures 25 through 27 show that for the case of upstream injection, the flow is well mixed. For the downstream and combined injection cases, Figs. 28 through 33, the data indicate a reverse gradient in Crocco number near the sudden expansion. The core flow is cooler than flow near the wall because the injected flow has penetrated to the centerline and displaced the primary flow from the core to the wake region behind the injection jet. As the flow moves downstream, however, the flow quickly mixes out to a uniform value.

The small radial gradient of Crocco number shown in Figs. 24 through 33 indicates that the flow is well mixed for the Mach 0.8 configuration. The plot of mixedness parameter versus distance is given in Fig. 34. The plot shows that the flow is well mixed prior to reaching the first rake position, with the upstream injection case, Fig. 34a, being slightly more mixed than either of the two other cases. For all of the injection cases, nearly all of the mixing occurs within 2 diam of the sudden expansion.

5.2.2 Diffuser Pumping Performance

A diffuser breakdown curve for the Mach 0.8 configuration with downstream injection is shown in Fig. 35. This curve shows cell pressure versus diffuser exit pressure with both terms normalized by the primary nozzle total pressure. Supersonic flow in the diffuser is a necessary condition for a started diffuser. Because the primary nozzle is operating subsonically and the exit pressure is not low enough to accelerate the flow, the diffuser is unstarted.

Because the diffuser is unstarted, exit pressure and cell pressure are not independent in the Mach 0.8 configuration. For the Mach 0.8 configuration tests, the primary nozzle conditions were maintained via an upstream choked venturi, whereas the cell pressure was controlled via the exhaust plant. For the higher mass flow rates, slightly lower exit pressures must be used to maintain cell pressure. This is reflected in Fig. 35. For increasing injection mass flow rates, slightly lower values of P_e/P_t are set to obtain the same cell pressure ratios, P_c/P_t . For two injection conditions, no injection and 1.0 lbm/sec, the exit pressure was intentionally lowered to map the unstarted leg of the diffuser breakdown curve. The points for the 1.0-lbm/sec case lie only slightly to the left of the corresponding points for the no-injection case.

The axial distribution of wall static pressure as a function of distance for various secondary air injection configurations is presented in Fig. 36. Figure 36a shows the wall pressure for the upstream injection cases, and Figs. 36b and c show the wall pressure for the downstream and combined injection cases, respectively. For the upstream injection case, Fig. 36a shows the pressure rise decreases slightly as the secondary flow increases. Because the configuration is an unstarted diffuser, the profile is very flat. The strong adverse pressure gradient, (large pressure rise) cannot be maintained with the subsonic flow condition. For the downstream and combined injection cases, the pattern is the same. As secondary flow is increased, the overall pressure ratio decreases.

6.0 CONCLUSIONS AND RECOMMENDATIONS

A combined experimental and computational research program was conducted to investigate transverse injection and mixing in a sudden expansion diffuser system and to evaluate the effects on diffuser performance. The following conclusions are based on results presented in the preceding sections:

1. The tested sudden expansion duct configuration with transverse injectors provided good mixing for both the Mach 3.0 and 0.8 conditions. Deviations in Crocco

number average less than 1 percent from the mean at a distance of 4 duct diam for the Mach 3.0 configuration and 2 duct diam for the Mach 0.8 configuration.

2. With injection ports spaced circumferentially at 45-deg intervals, all angular variations greater than 1.0 percent of Crocco number in the flow field dissipate within 1.2 diam of the sudden expansion.
3. As secondary flow is increased, mixing improves.
4. The cell pressure obtained by a started diffuser is not affected by secondary flow that is introduced in the diffuser/burner ducts.
5. The maximum rise ratio that can be obtained in the diffuser/burner ducts decreases as secondary flow is introduced in the diffuser/burner ducts since back pressure is decreasing.
6. Oxidizer injection through normal jets appears suitable to provide oxidizer and exhaust gas mixing, provided the rise ratio penalty is acceptable.
7. The PARC code prediction of the diffuser/burner duct pressure field is in excellent agreement with the test data. However, PARC predictions of mixing, based on total temperature comparisons, agree with the test data in overall trends only. Further, the code did a poor job of predicting cell pressure with the started diffuser. These shortcomings are believed to be caused by use of an inaccurate turbulent mixing model.

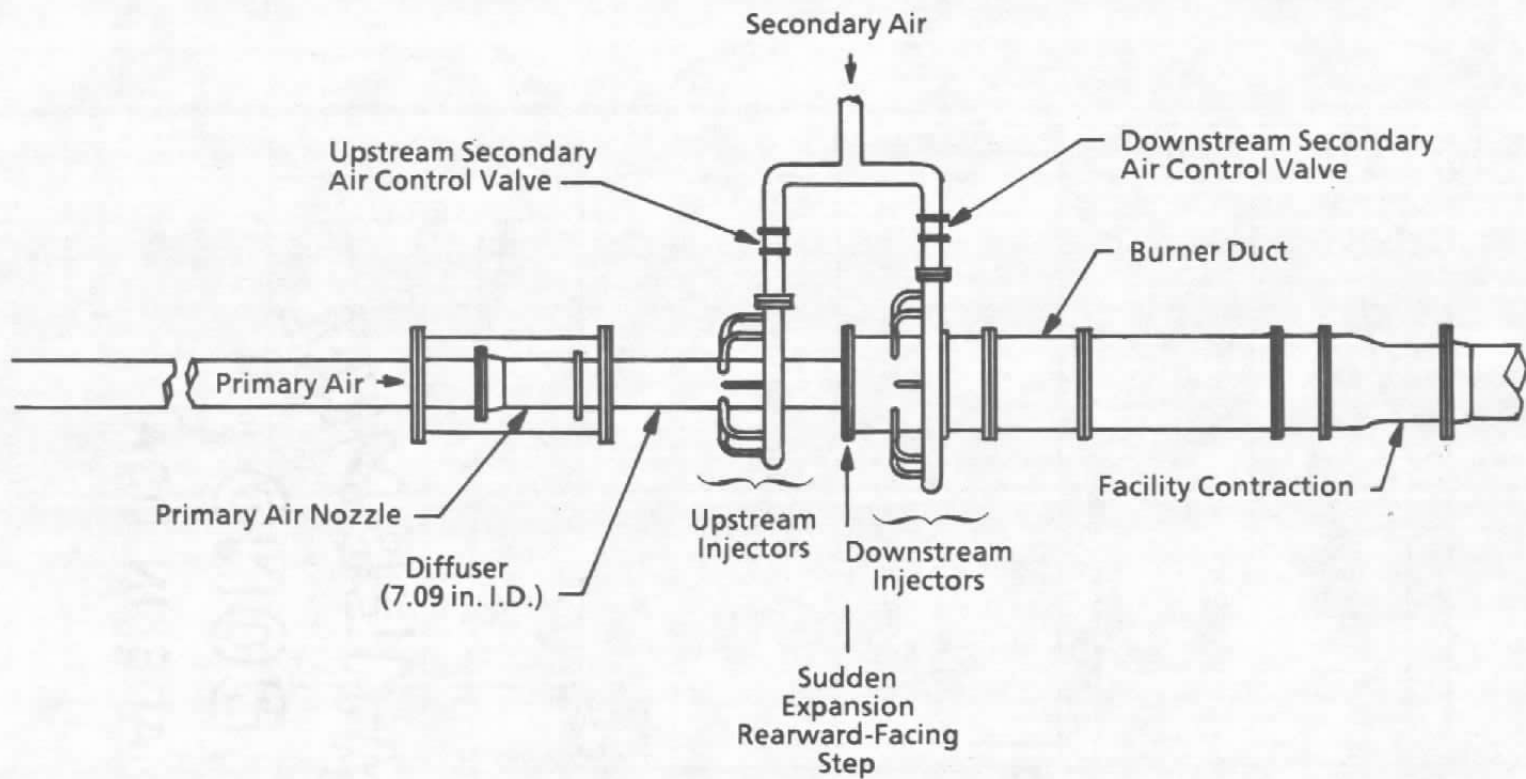
The following recommendations are made for future study:

1. Studies of the amount of mixing oxidizer and exhaust gas required to achieve flammable mixtures for afterburning should be studied.
2. A second generation of experiments using reacting flows should be conducted to evaluate ignition, flameholding, stability, and other important combustion parameters.
3. Future applications of the PARC code should use an improved turbulent mixing model. Such a model has become available since the work reported here was conducted.

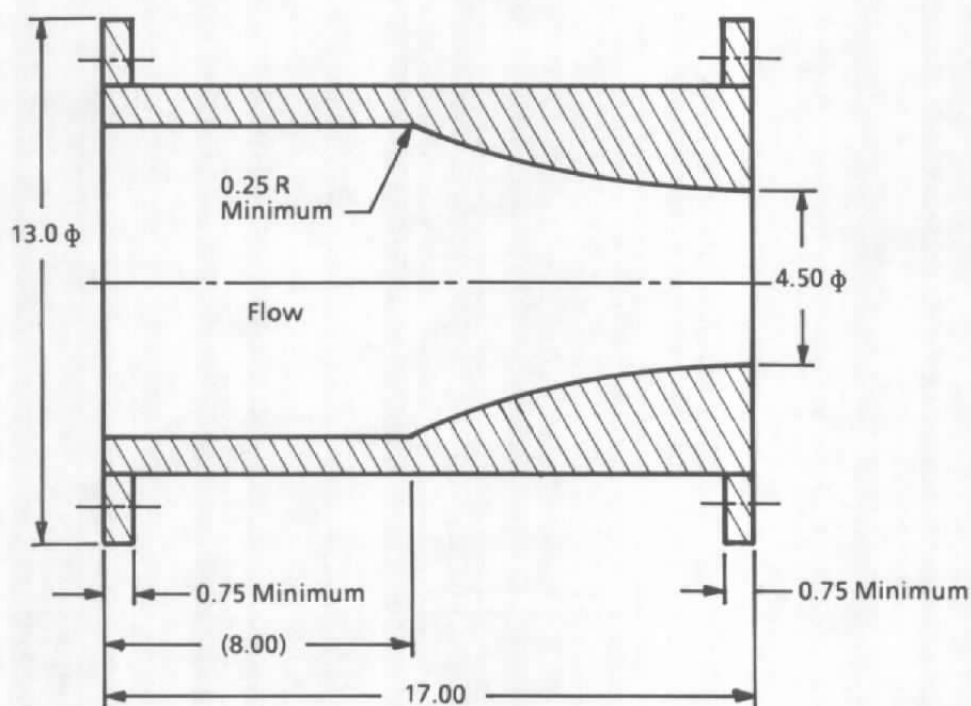
4. Either the PARC code should be modified to include finite rate chemistry, or a different Navier-Stokes code with chemistry should be obtained. Such a code will be needed to apply second-generation subscale experiments to full-scale development.

REFERENCES

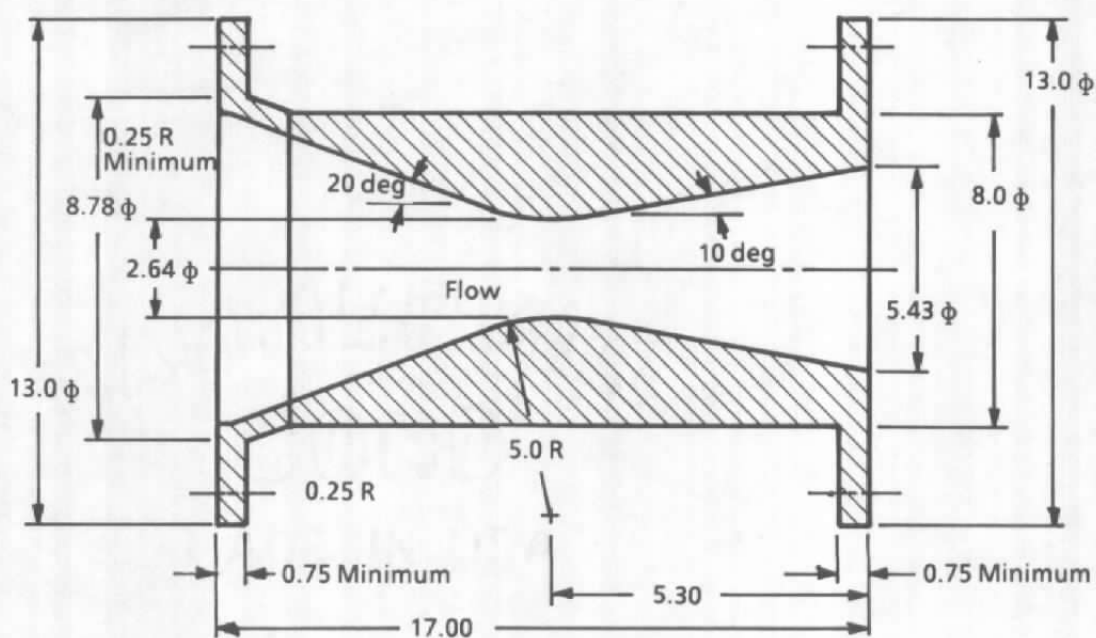
1. Stephens, S. E, Jordan, J. L., and Schulz, R. J. "Hydrogen Rich Exhaust Gas Handling Studies at AEDC." AIAA Paper No. 88-3019, July 1988.
2. Owens, C. L. "Calibration Capabilities of ETF Instrument Branch." AEDC-TR-67-18 (AD-648707), March 1967.
3. Abernethy, R. B. and Thompson, J. W. "Handbook, Uncertainty in Gas Turbine Measurements." AEDC-TR-73-5 (AD-755356), February 1973.
4. Cooper, G. K., Garrard, G. D., and Phares, W. J. "PARC Code Validation for Propulsion Flows." AEDC-TR-88-32, January 1989.
5. Phares, W. J. et al. "Application of Computational Fluid Dynamics to Test Facility and Experiment Design." AIAA-86-1733, AIAA/ASME/SAE/ASEE 22nd Joint Propulsion Conference, June 16-18, 1986.
6. Garrard, G. D. and Phares, W. J. "PARC Code Calibration for Propulsion-Type Flows." AEDC-TR-90-7, July 1990.



a. Test cell schematic
 Figure 1. Test apparatus.

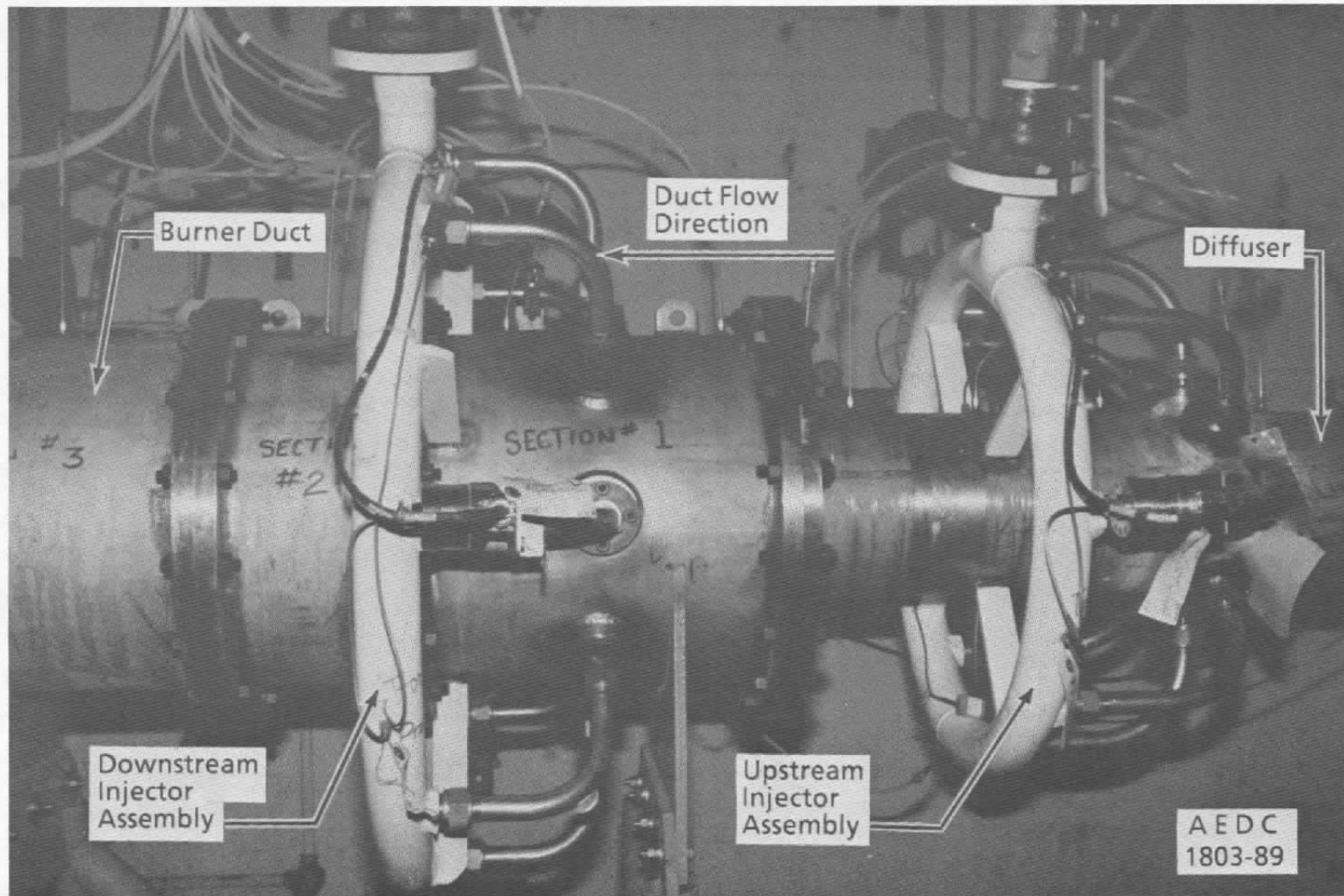


b. Mach 0.8 nozzle



c. Mach 3.0 nozzle

Figure 1. Continued.



d. Upstream and downstream injectors
Figure 1. Concluded.

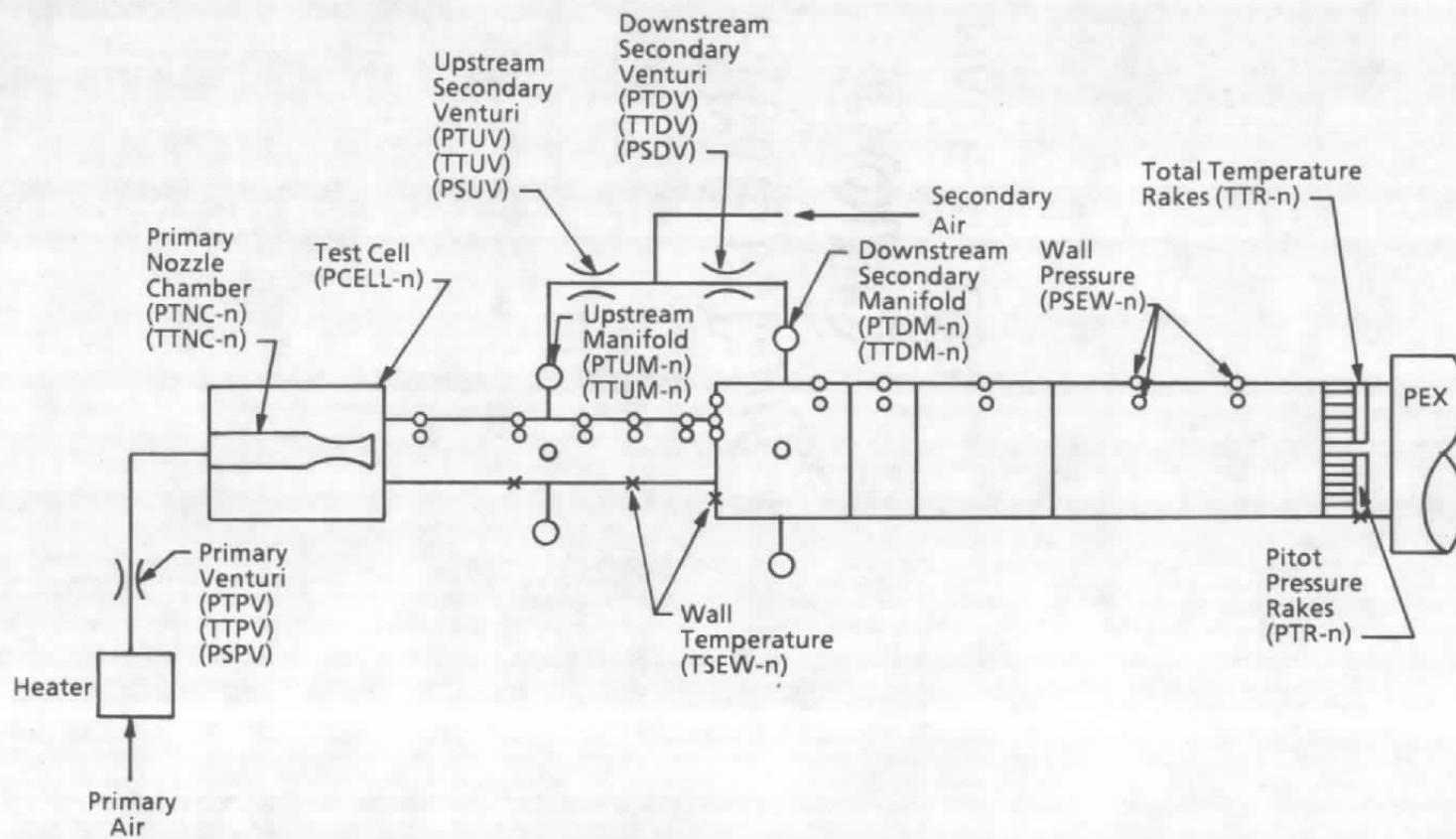


Figure 2. R1A1 instrumentation location schematic.

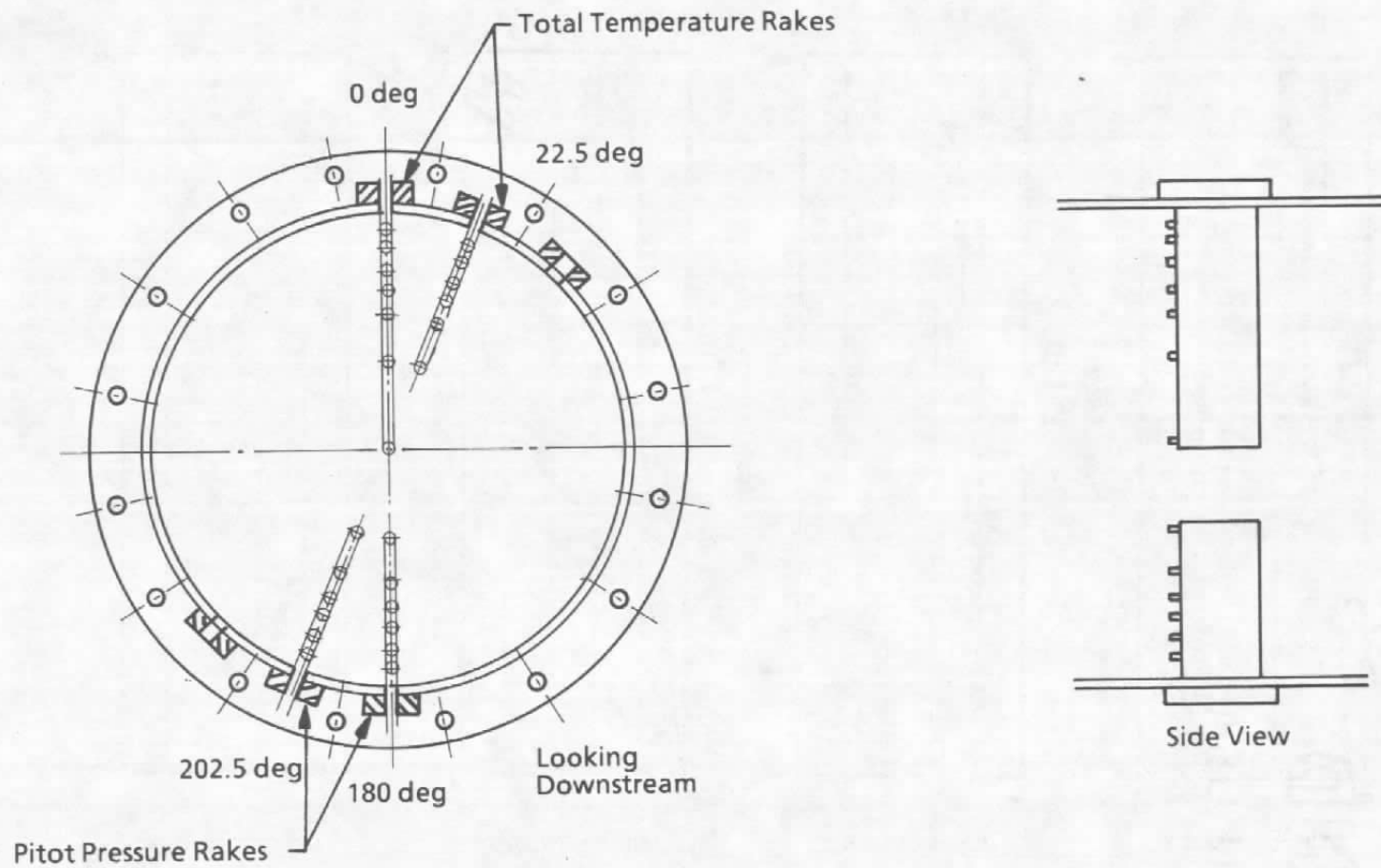


Figure 3. Total temperature and pitot pressure rakes.

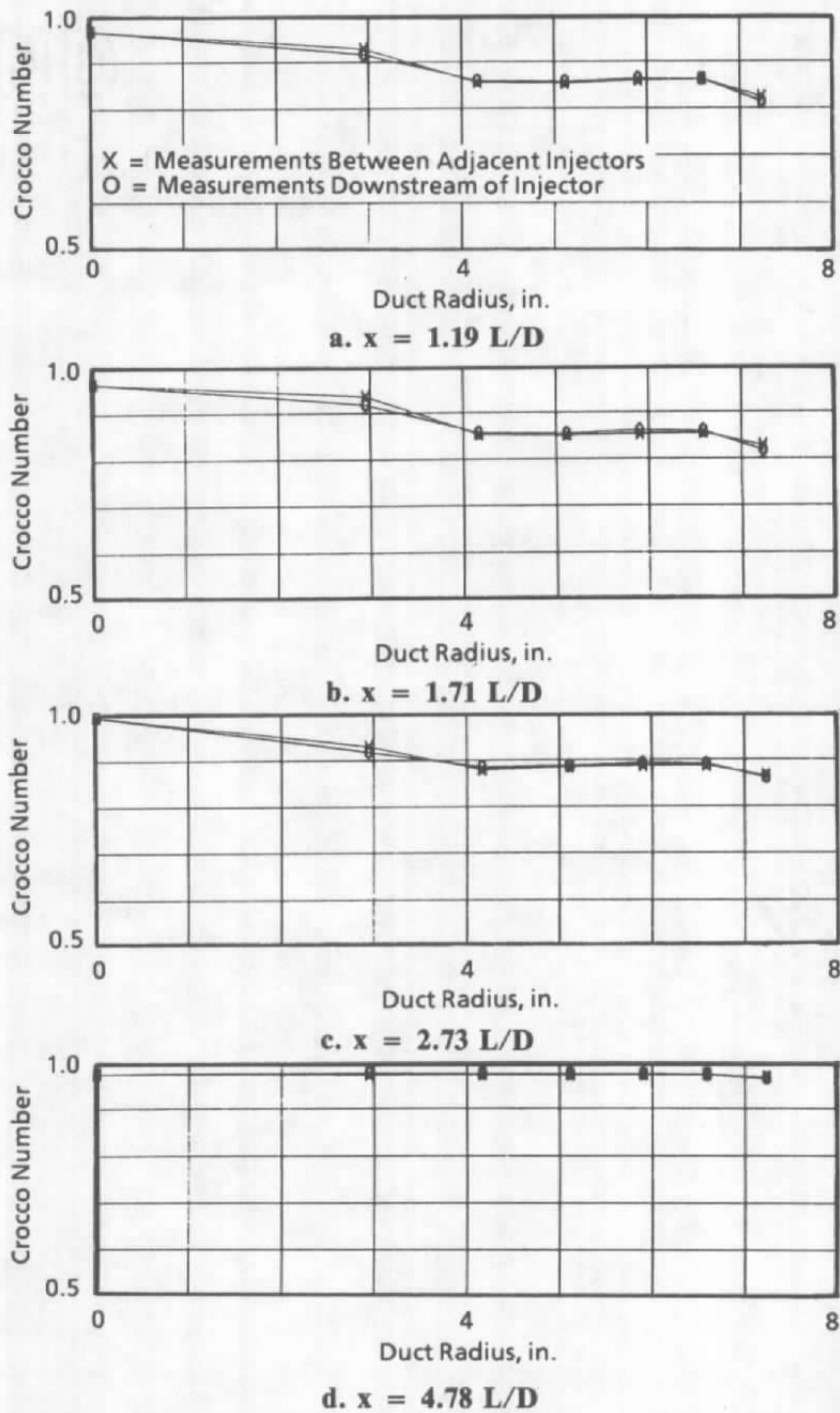


Figure 4. Crocco number — Mach 3.0 configuration, no injection.

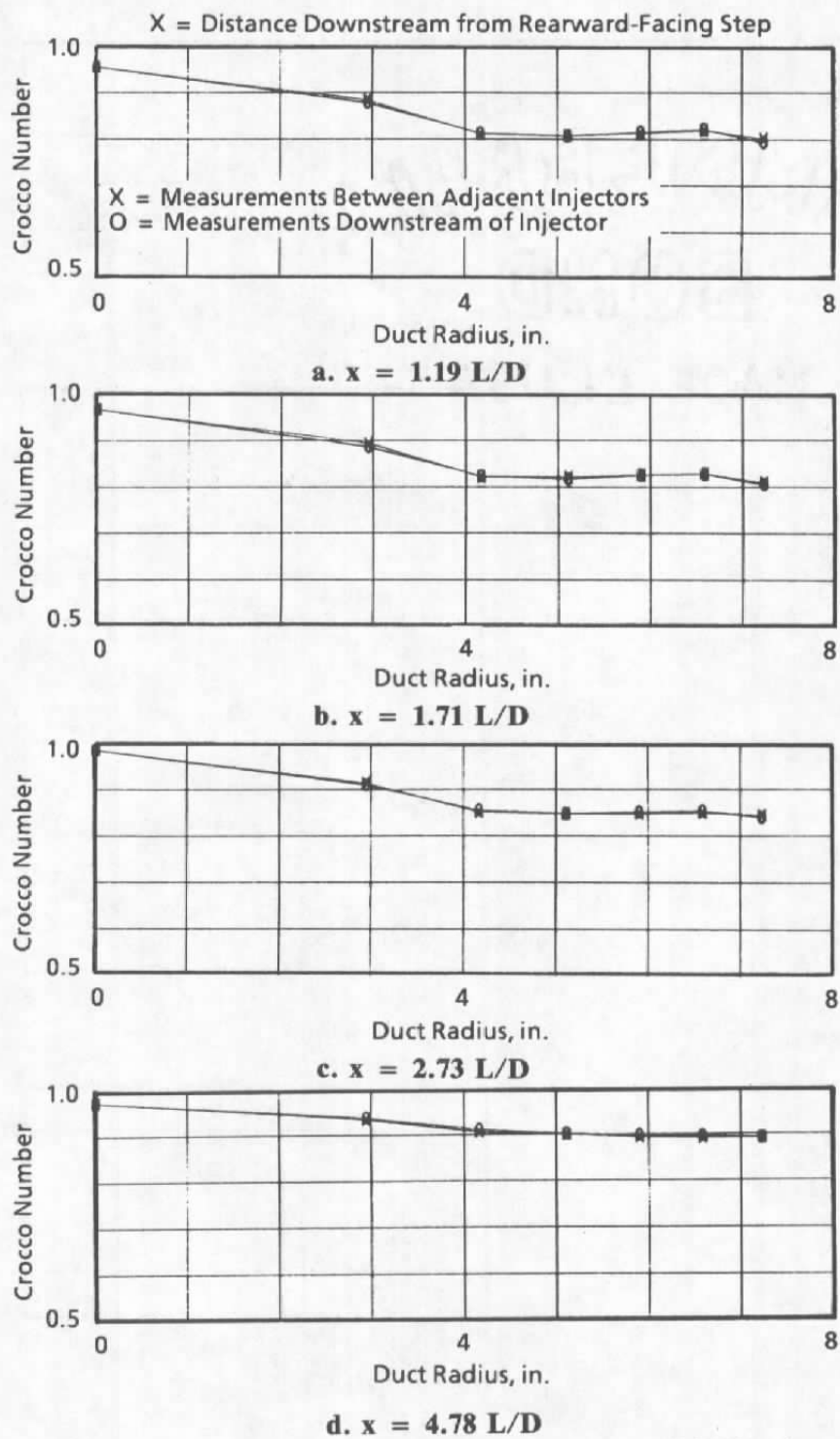
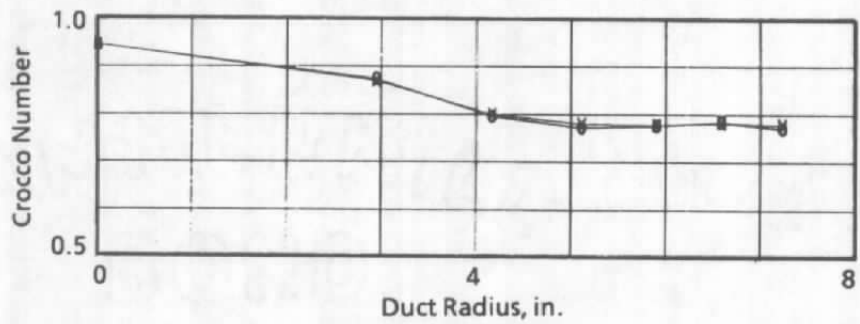
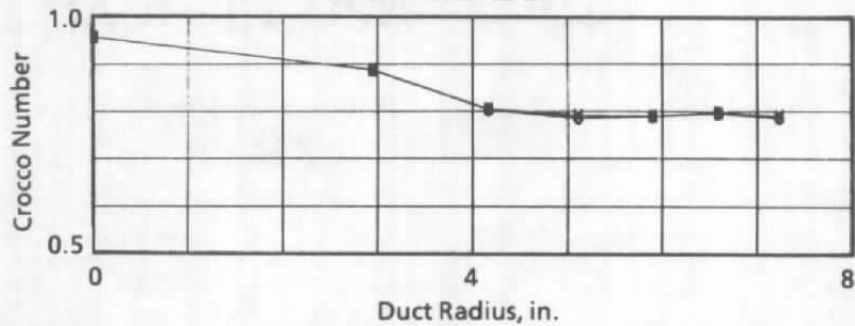


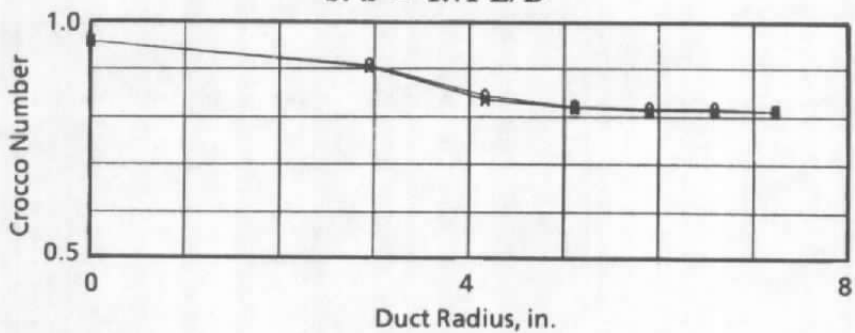
Figure 5. Crocco number — upstream injection = 0.25 lbm/sec.



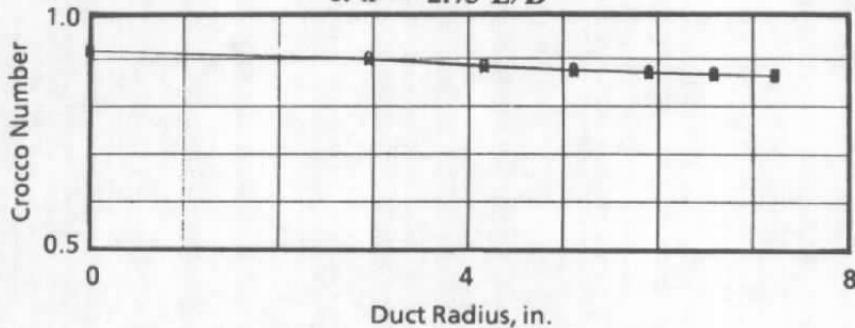
a. $x = 1.19 L/D$



b. $x = 1.71 L/D$



c. $x = 2.73 L/D$



d. $x = 4.78 L/D$

Figure 6. Crocco number — upstream injection = 0.50 lbm/sec.

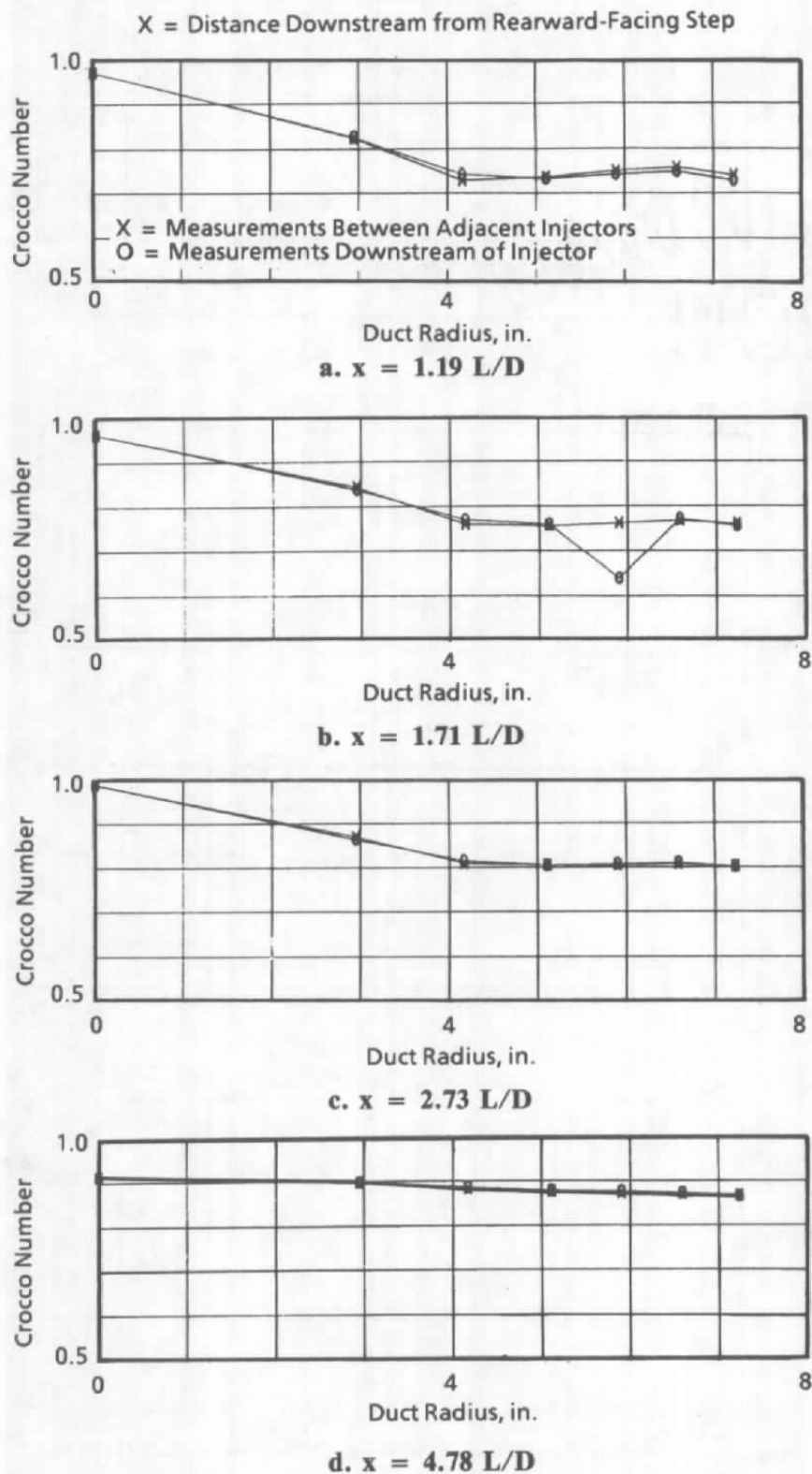
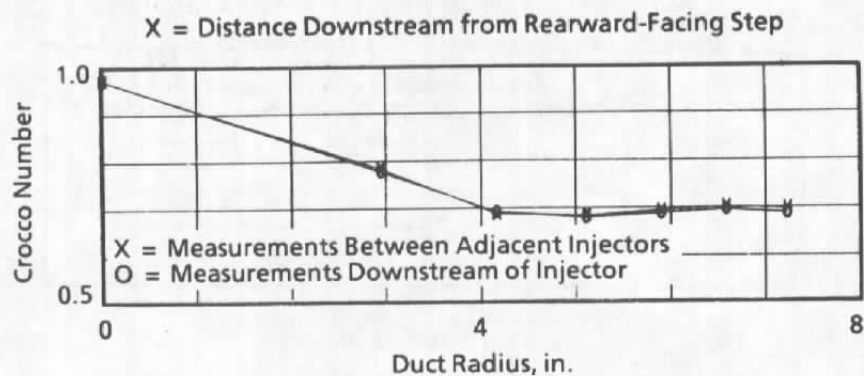
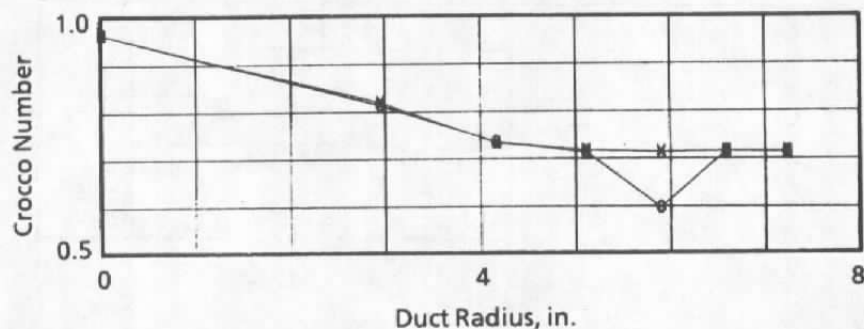


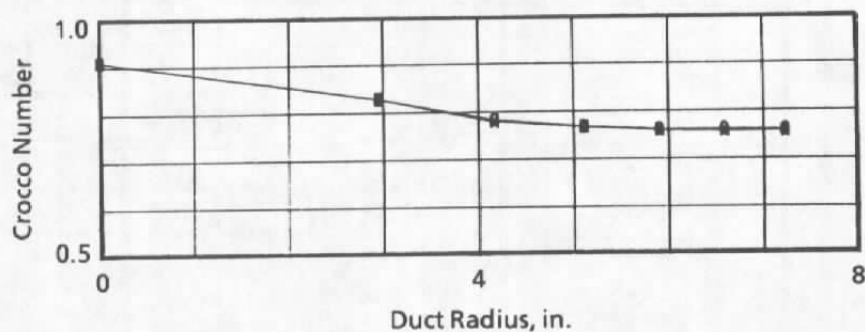
Figure 8. Crocco number — downstream injection = 0.50 lbm/sec.



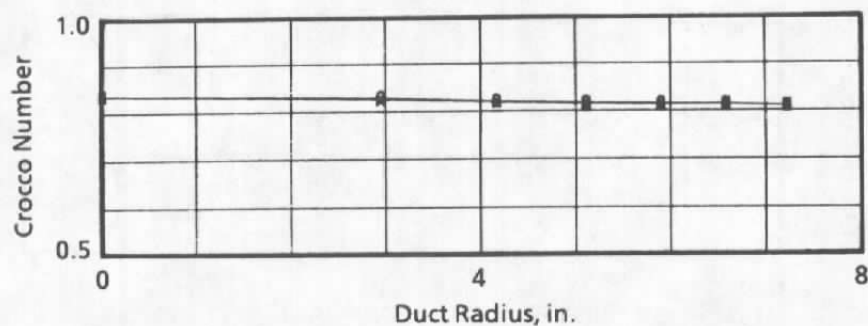
a. $x = 1.19 L/D$



b. $x = 1.71 L/D$



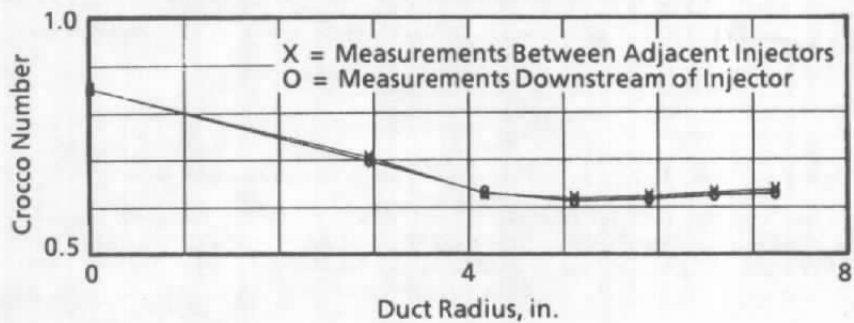
c. $x = 2.73 L/D$



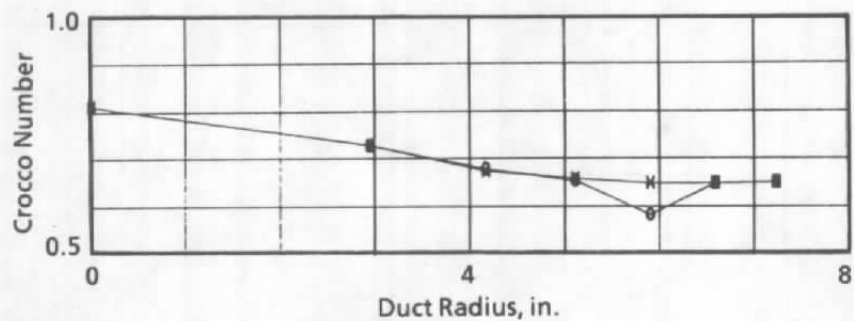
d. $x = 4.78 L/D$

Figure 9. Crocco number — downstream injection = 1.0 lbm/sec.

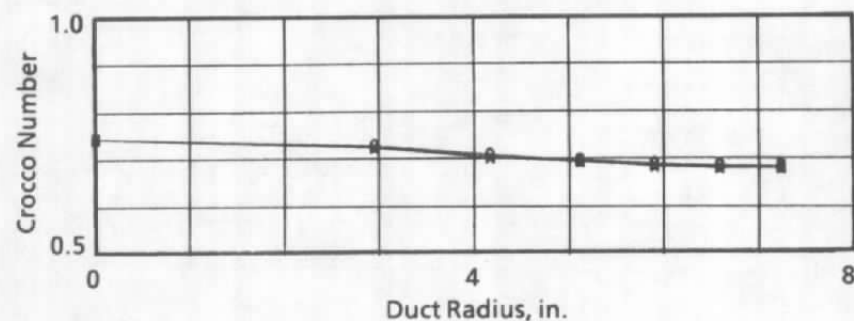
X = Distance Downstream from Rearward-Facing Step



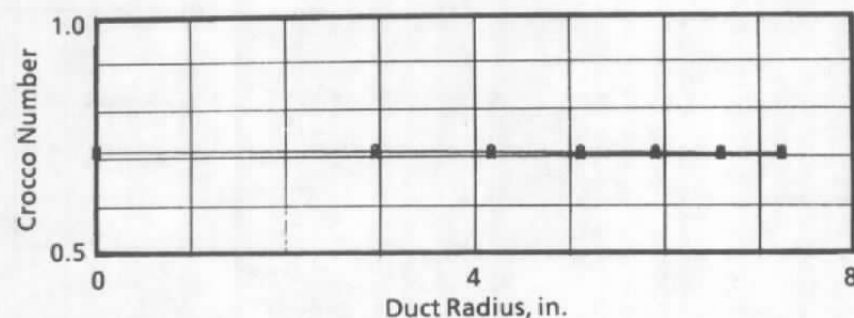
a. $x = 1.19 L/D$



b. $x = 1.71 L/D$

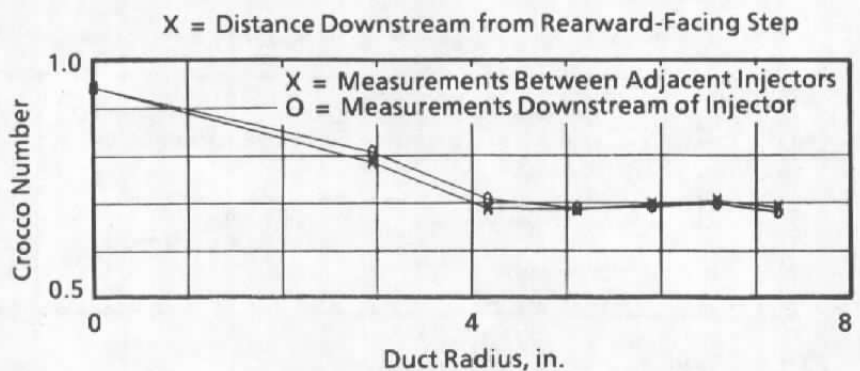


c. $x = 2.73 L/D$

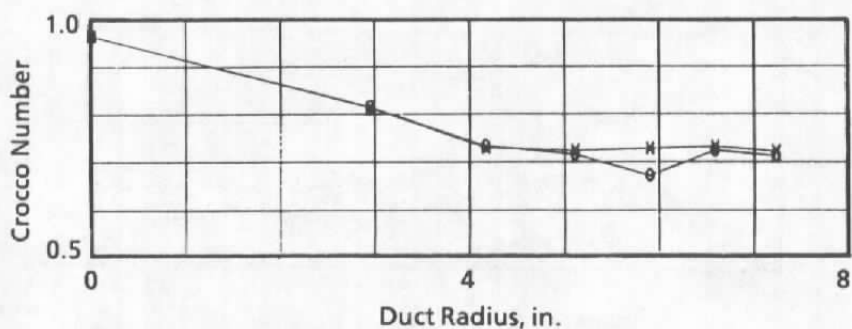


d. $x = 4.78 L/D$

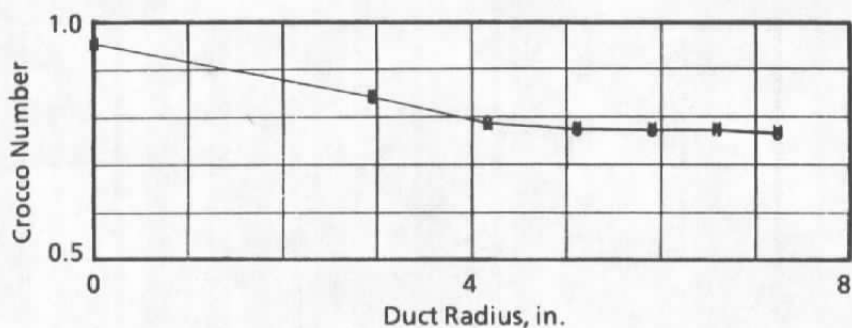
Figure 10. Crocco number — downstream injection = 2.0 lbm/sec.



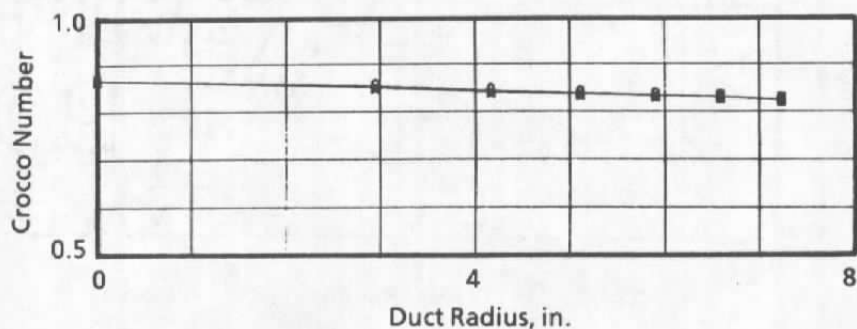
a. $x = 1.19 L/D$



b. $x = 1.71 L/D$



c. $x = 2.73 L/D$



d. $x = 4.78 L/D$

Figure 11. Crocco number — combined injection = 0.75 lbm/sec.

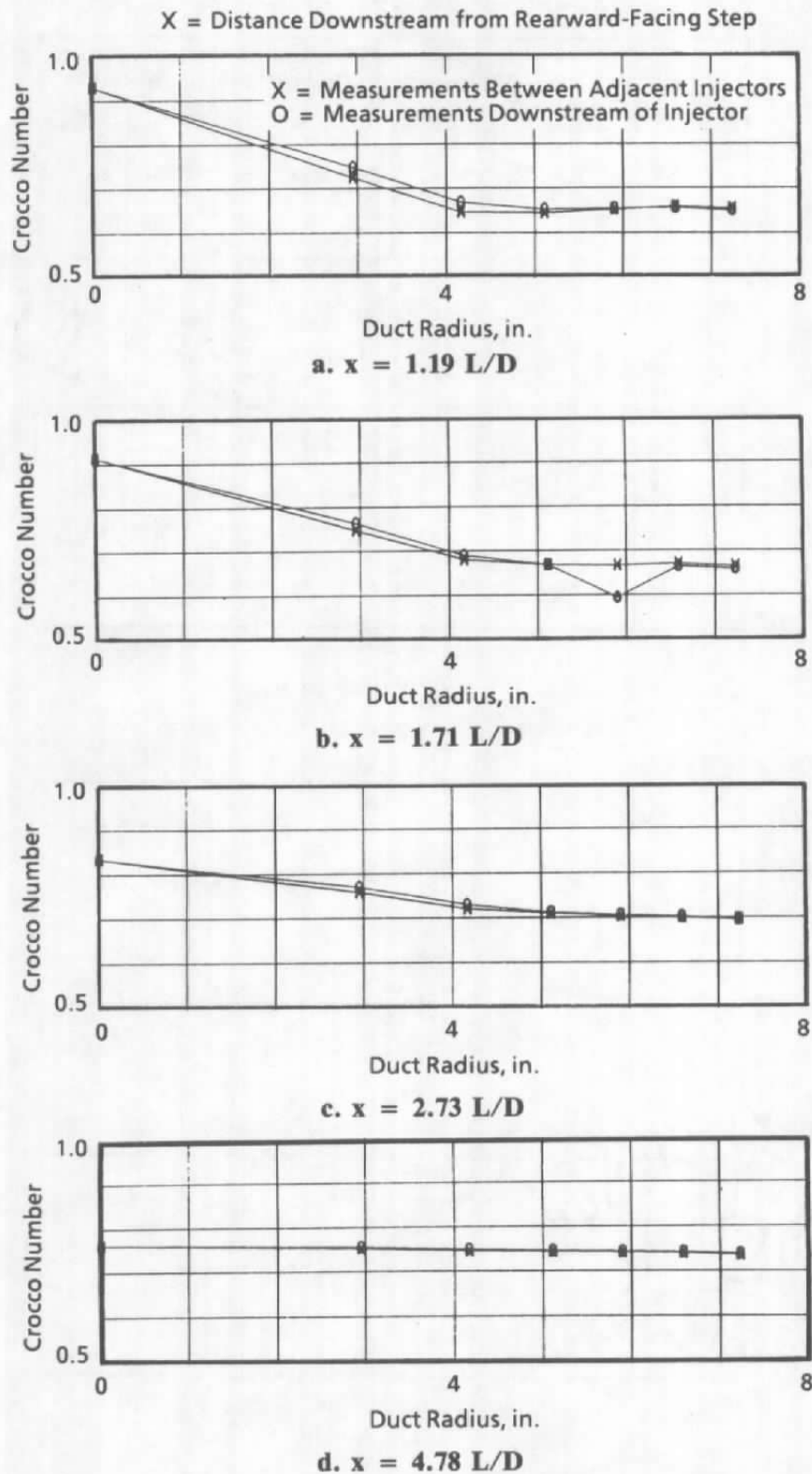


Figure 12. Crocco number — combined injection = 1.5 lbm/sec.

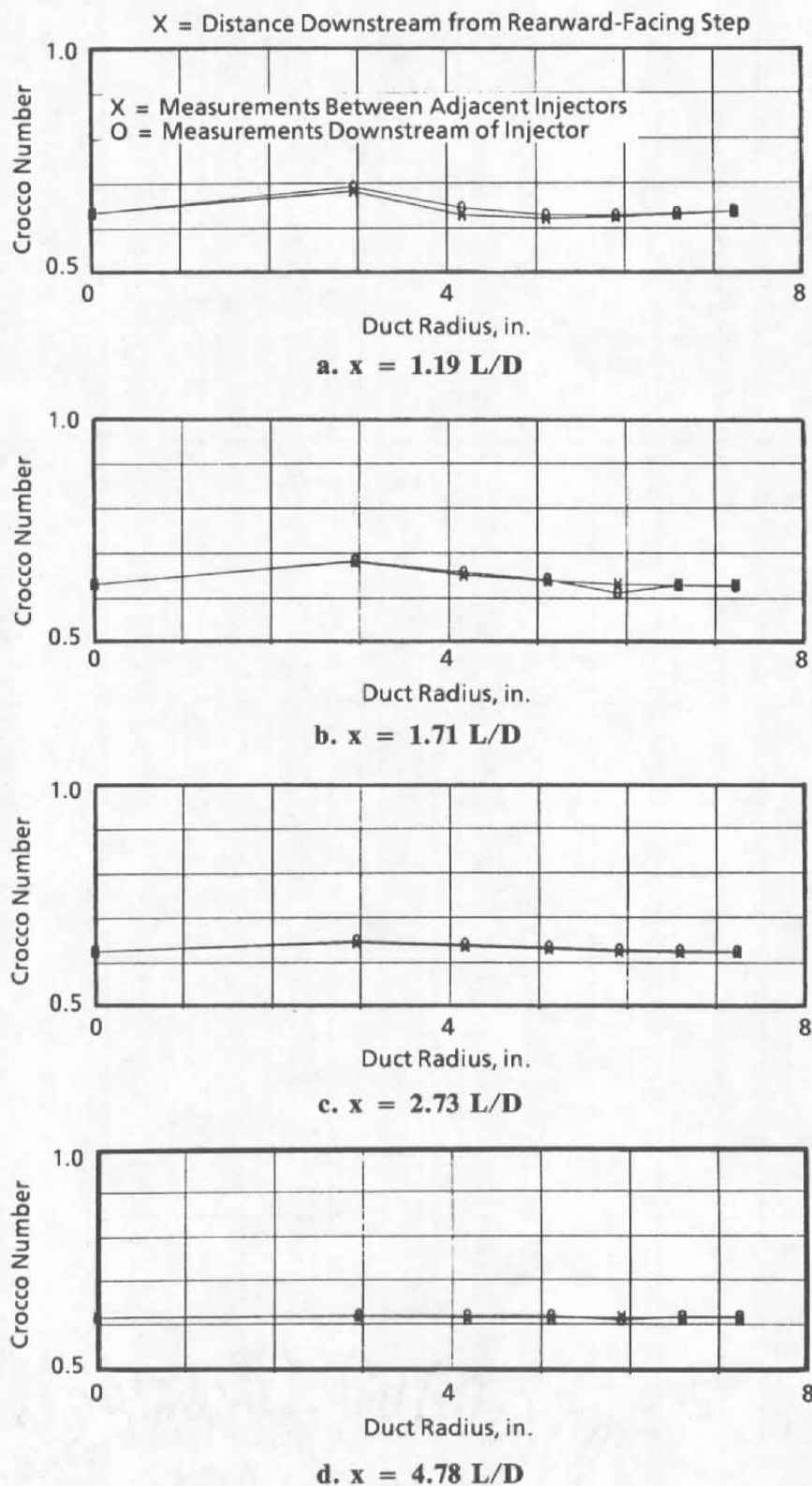
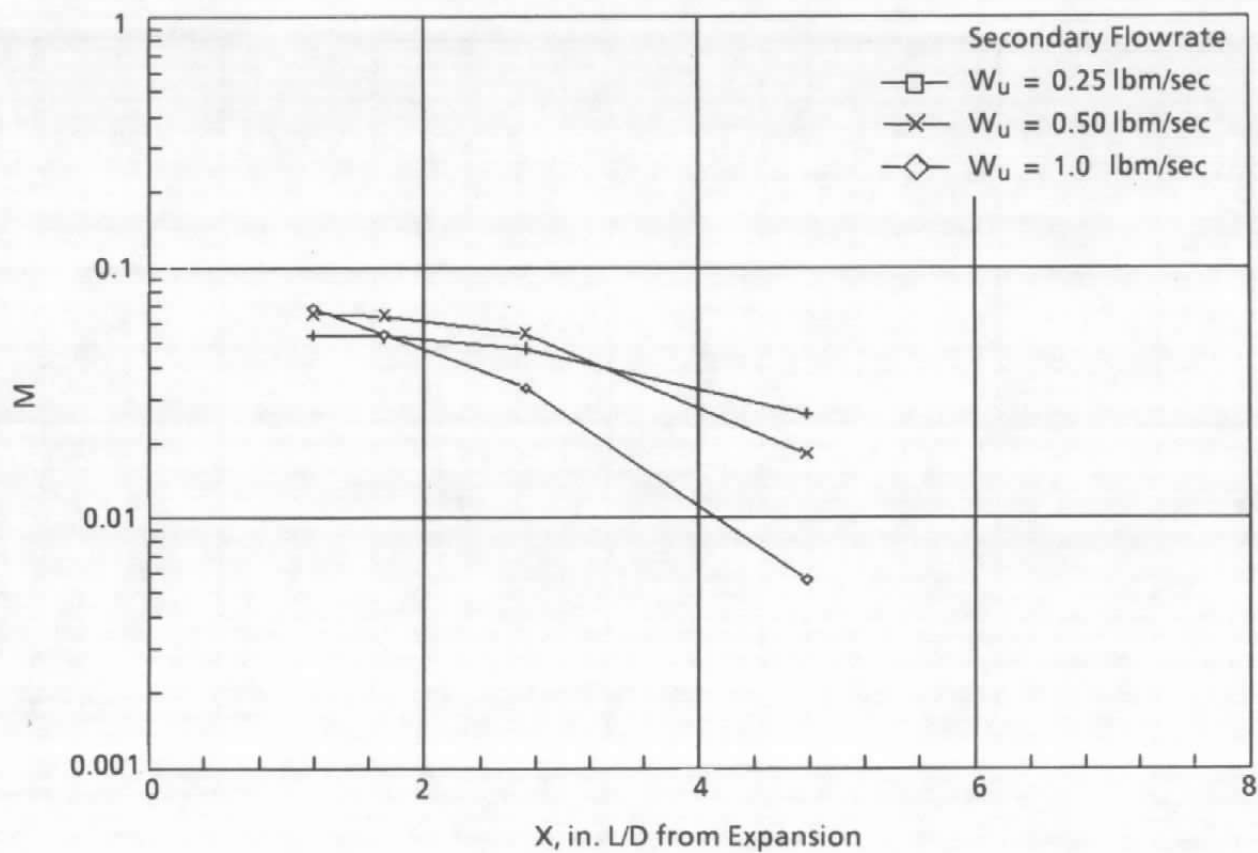
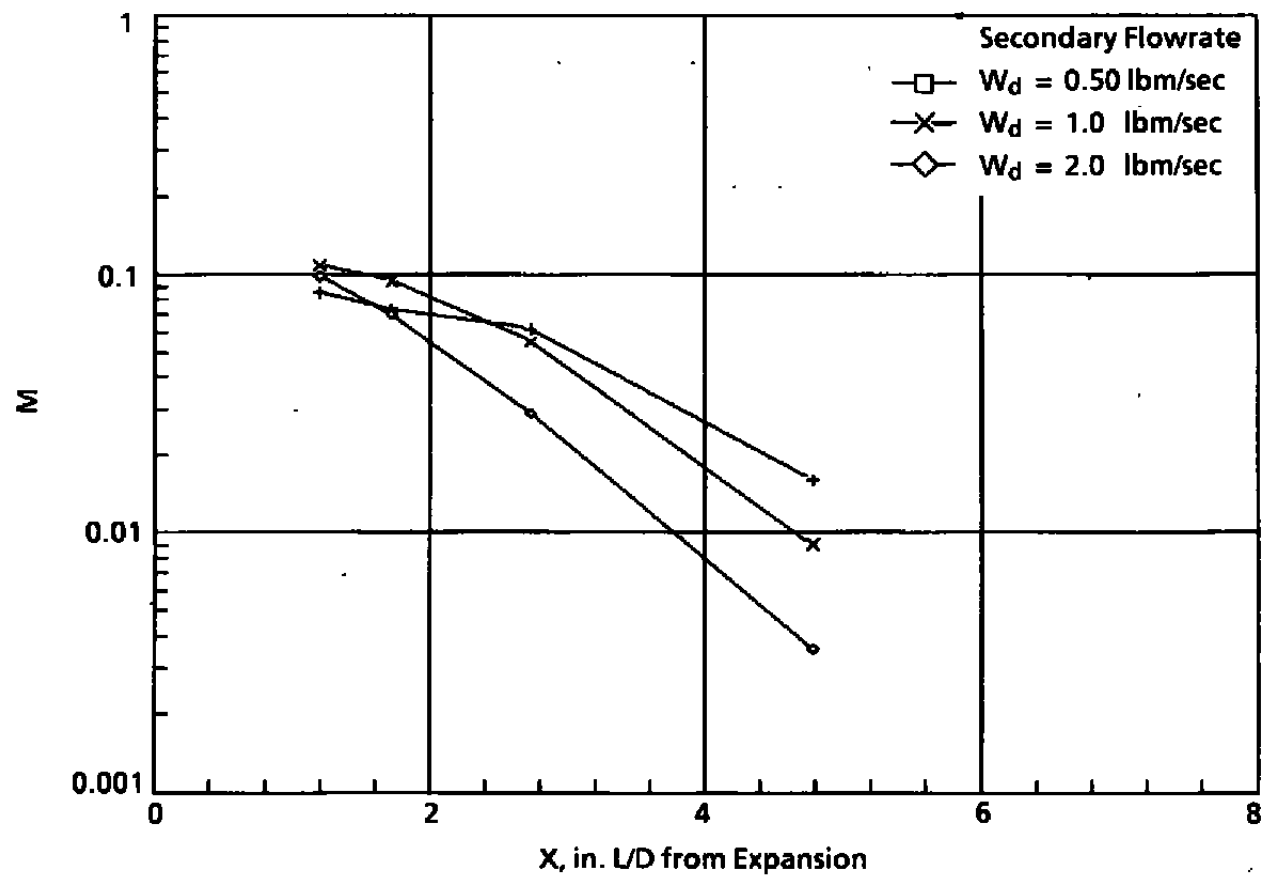


Figure 13. Crocco number — combined injection = 3.0 lbm/sec.

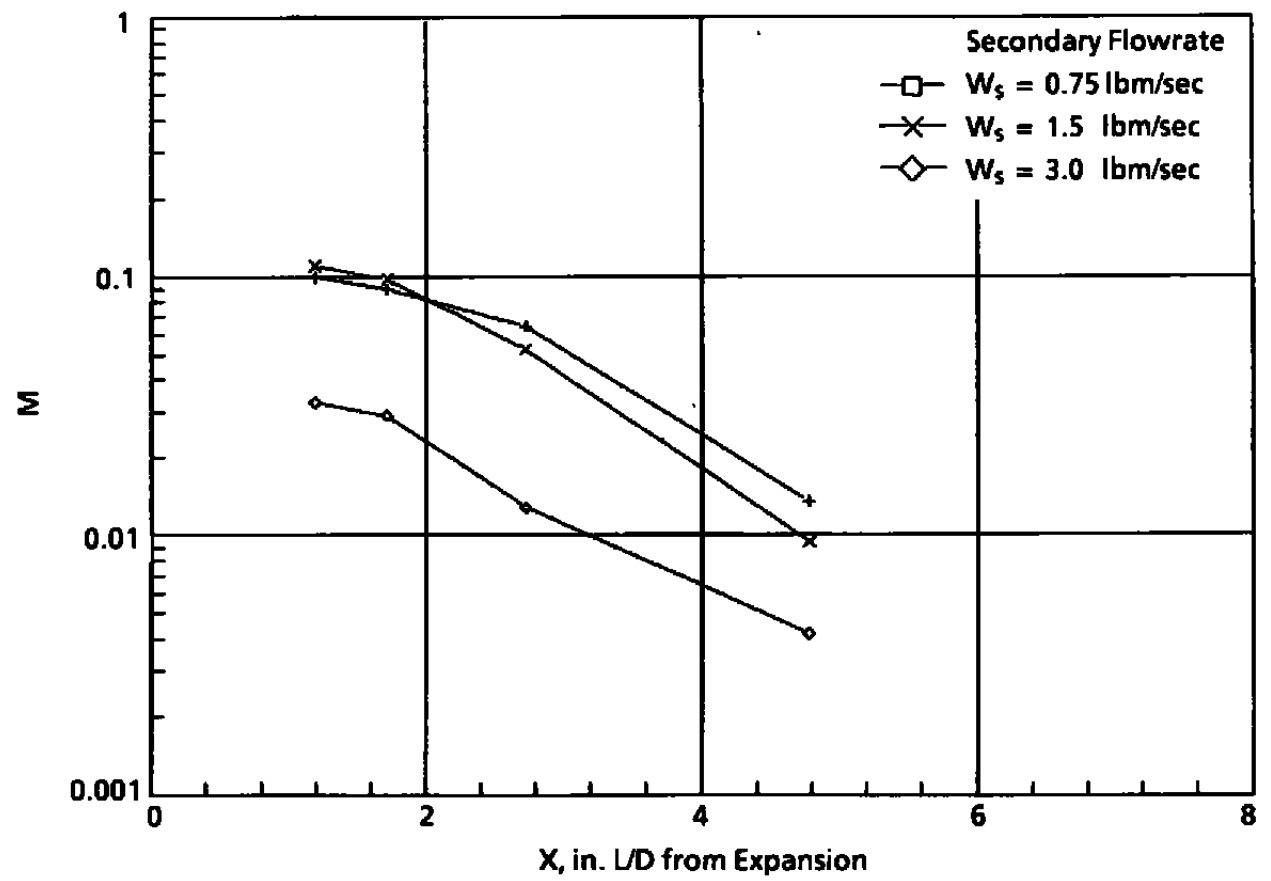


a. Upstream injection

Figure 14. Mixedness parameter versus axial distance for mach 3.0 configuration.



b. Downstream injection
Figure 14. Continued.



c. Combined upstream/downstream injection
Figure 14. Concluded.

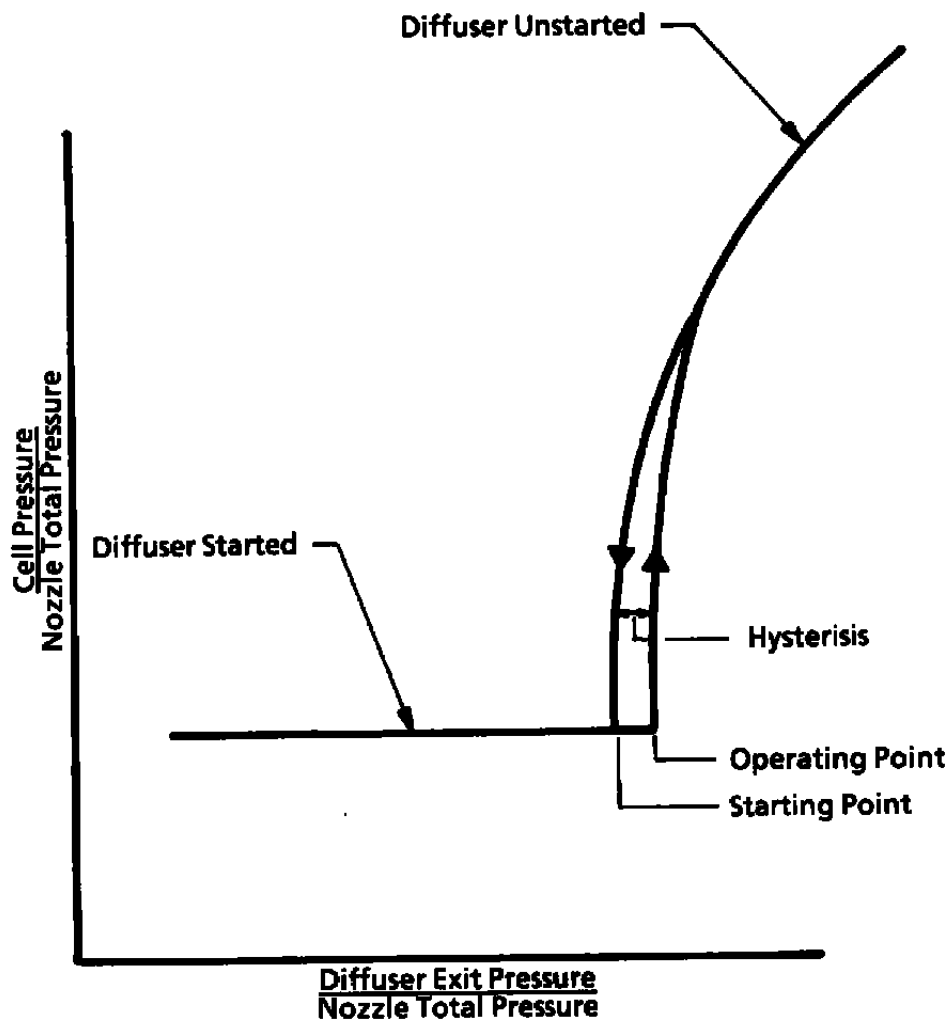


Figure 15. Typical diffuser breakdown curve.

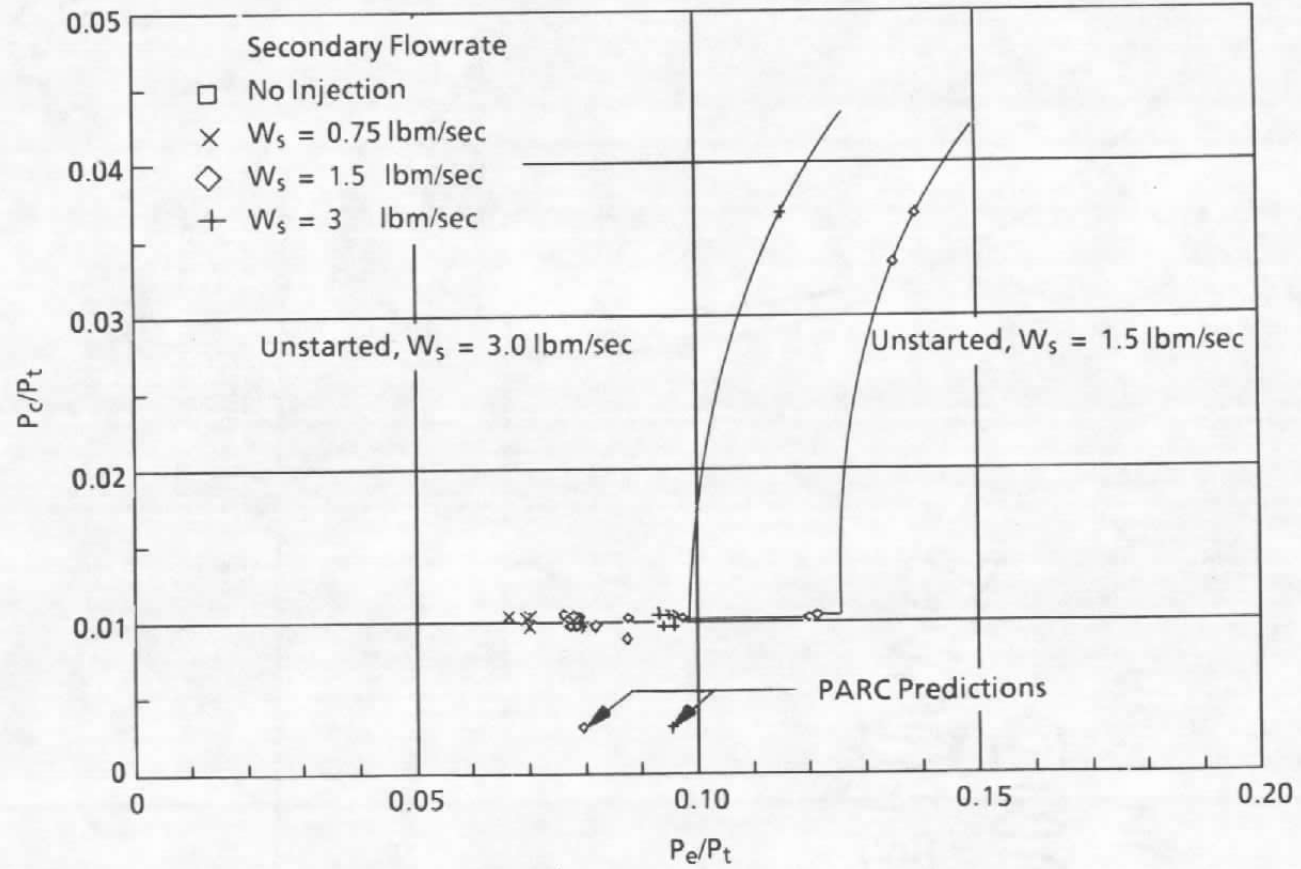
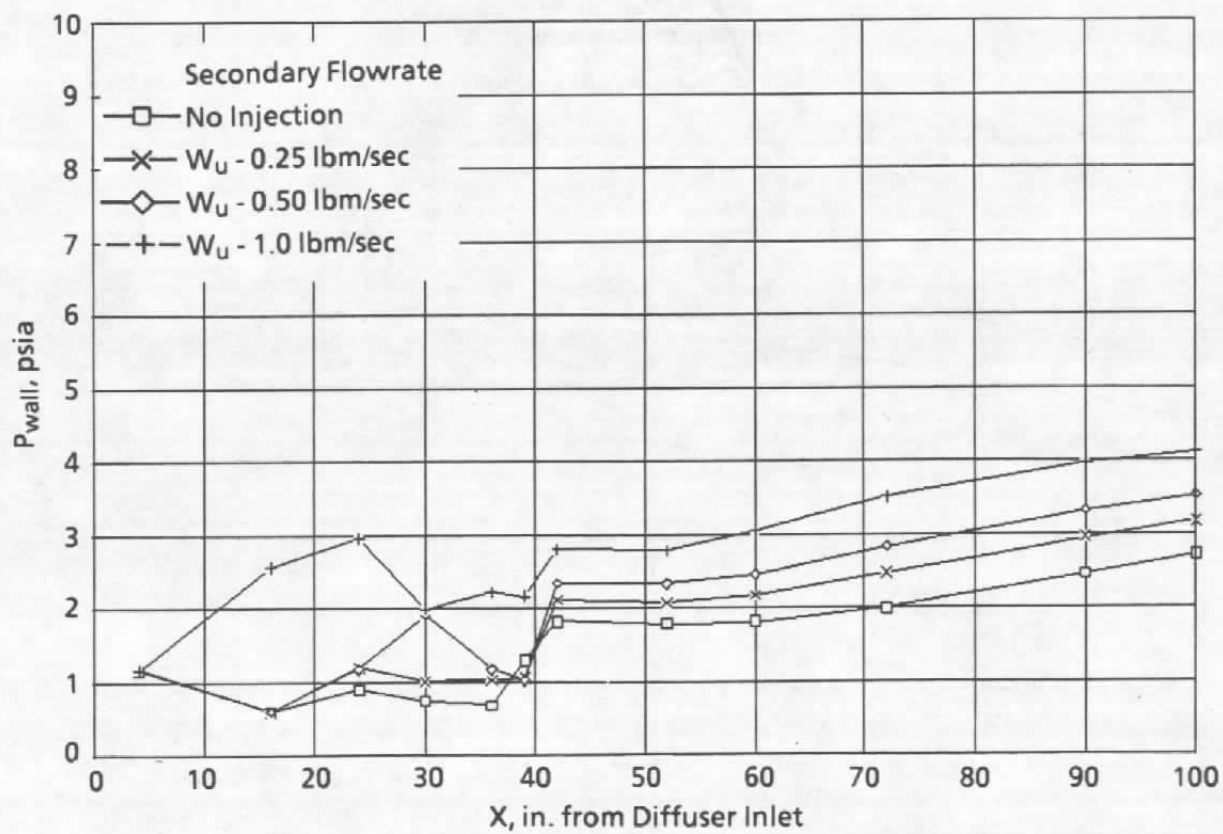
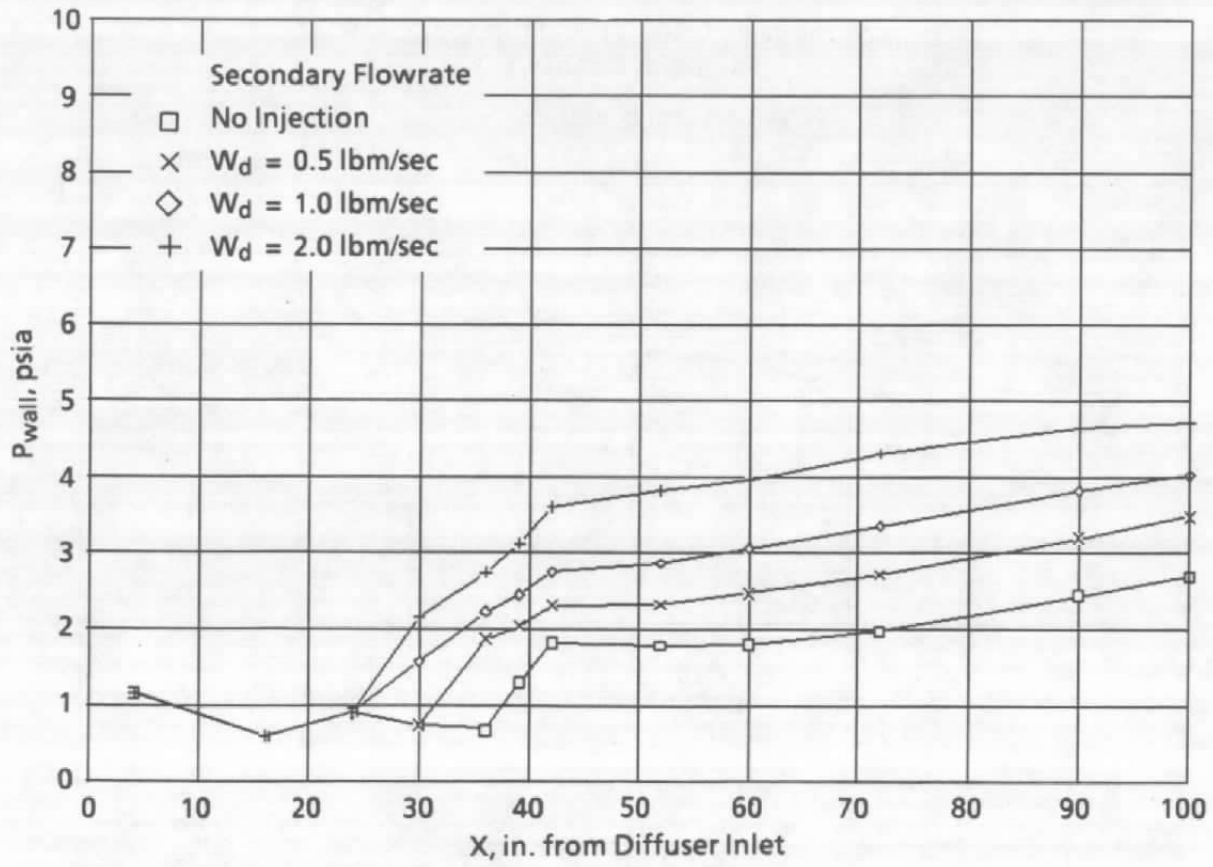


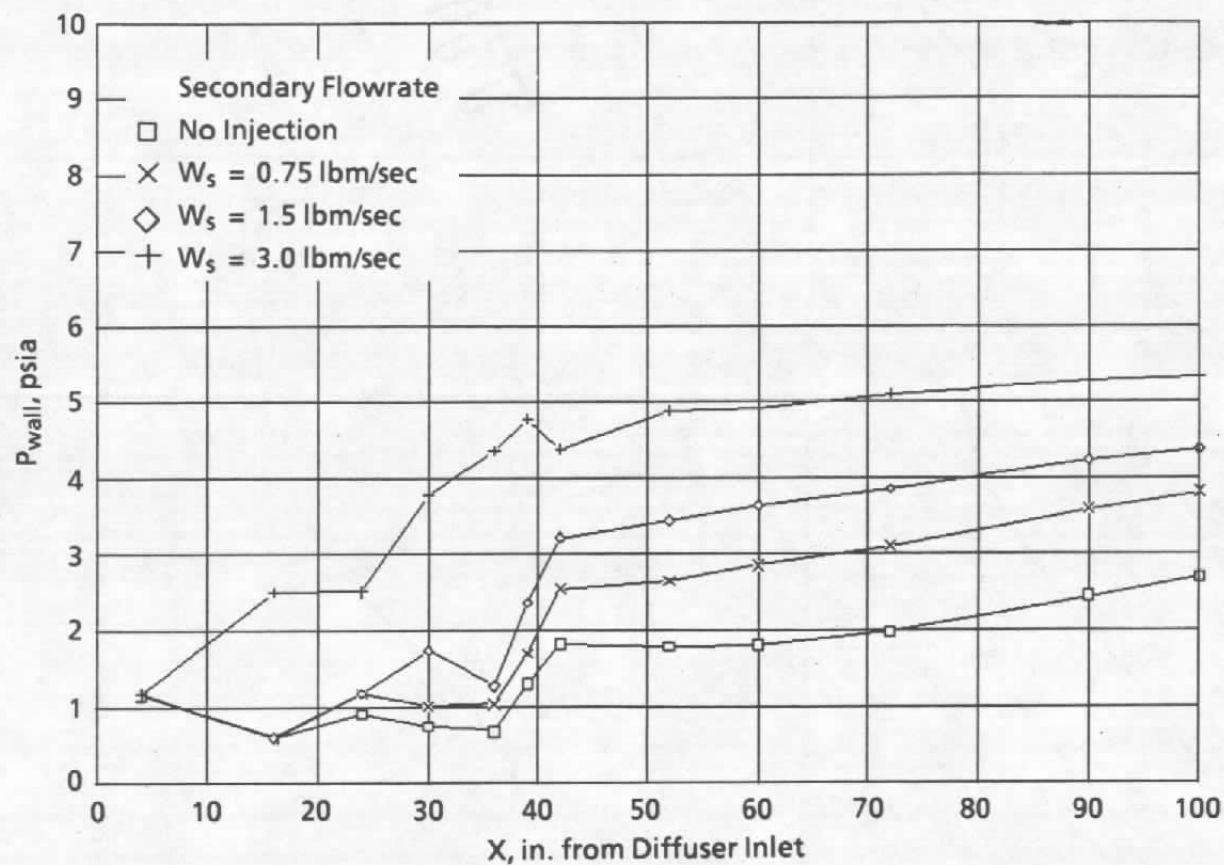
Figure 16. Diffuser breakdown curve for combined upstream downstream injection in the Mach 3.0 configuration.



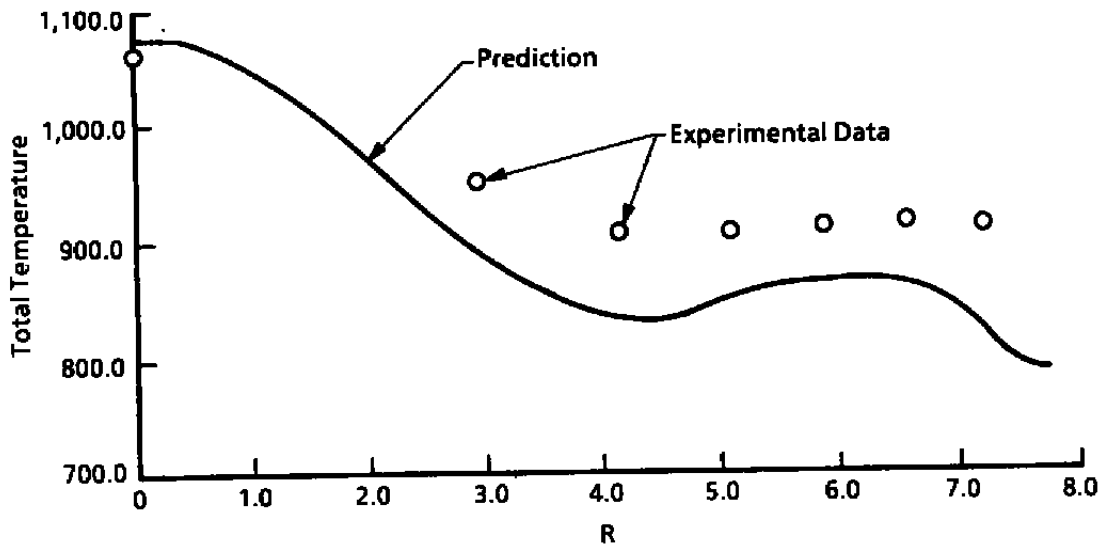
a. Upstream injection
Figure 17. Wall pressure versus axial distance.



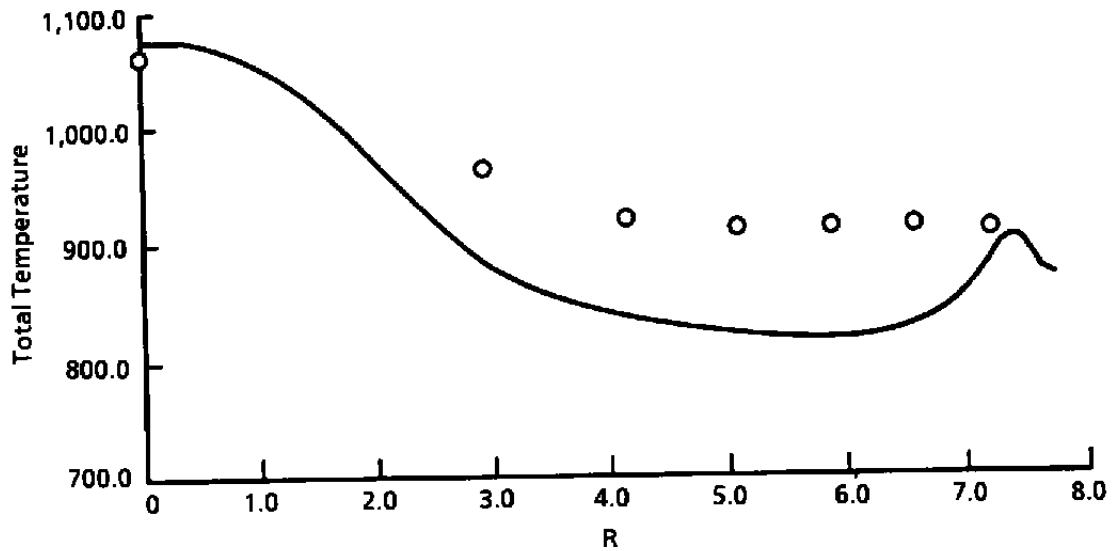
b. Downstream injection
Figure 17. Continued.



c. Combined upstream/downstream injection
Figure 17. Concluded.

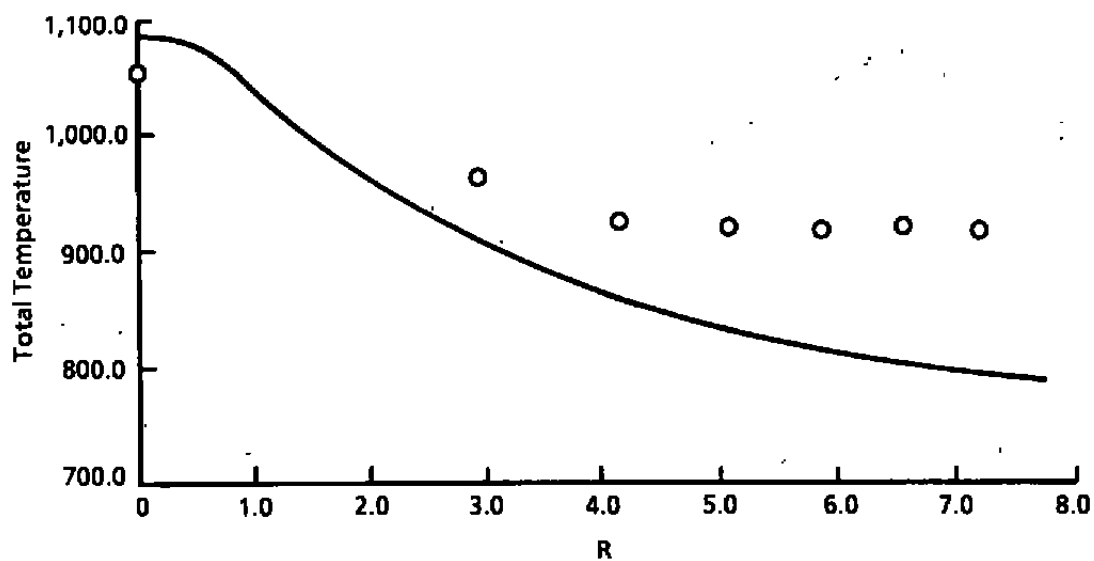


a. $x = 1.19 \text{ diam}$, $\theta = 0 \text{ deg}$

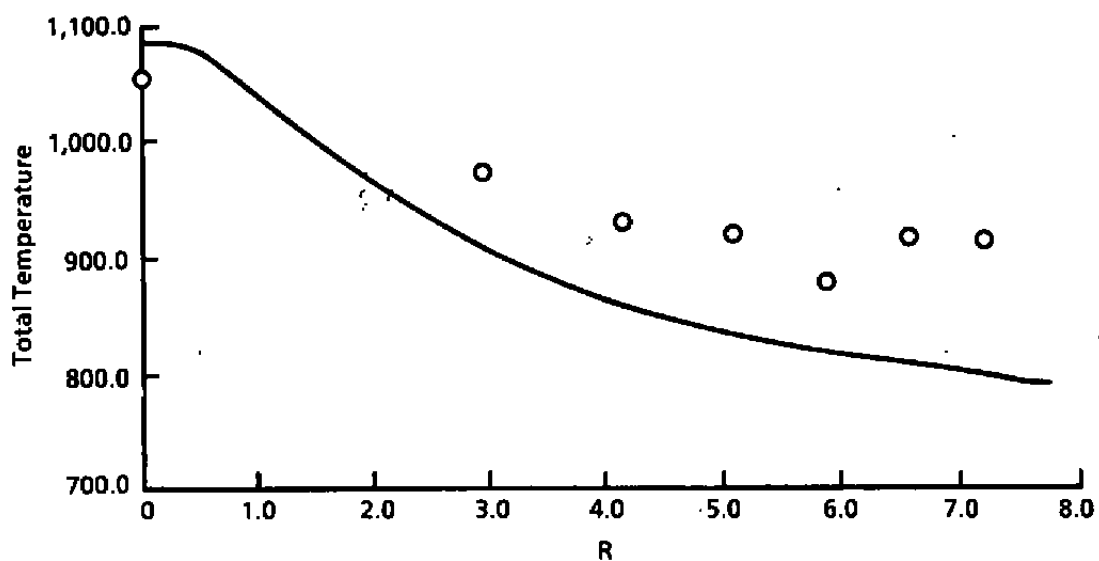


b. $x = 1.19 \text{ diam}$, $\theta = 22.5 \text{ deg}$

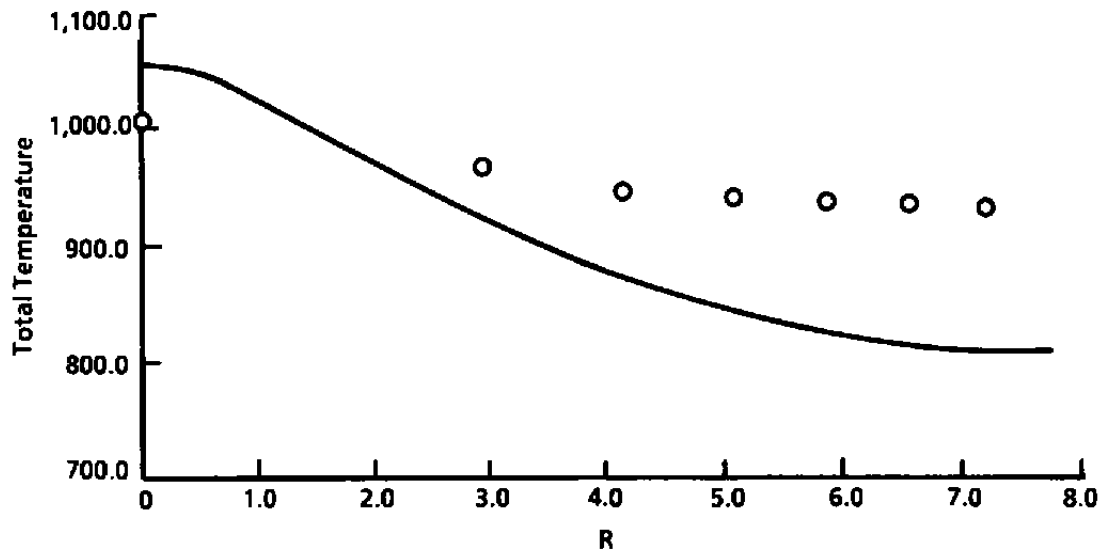
Figure 18. PARC prediction of total temperature versus experimental data, Case 2.



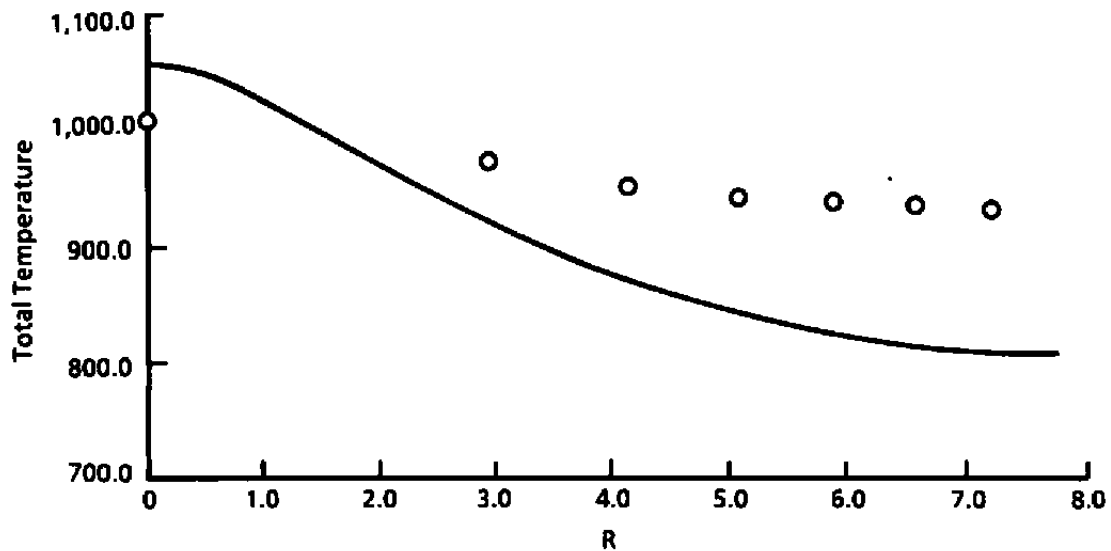
c. $x = 1.71$ diam, $\theta = 0$ deg



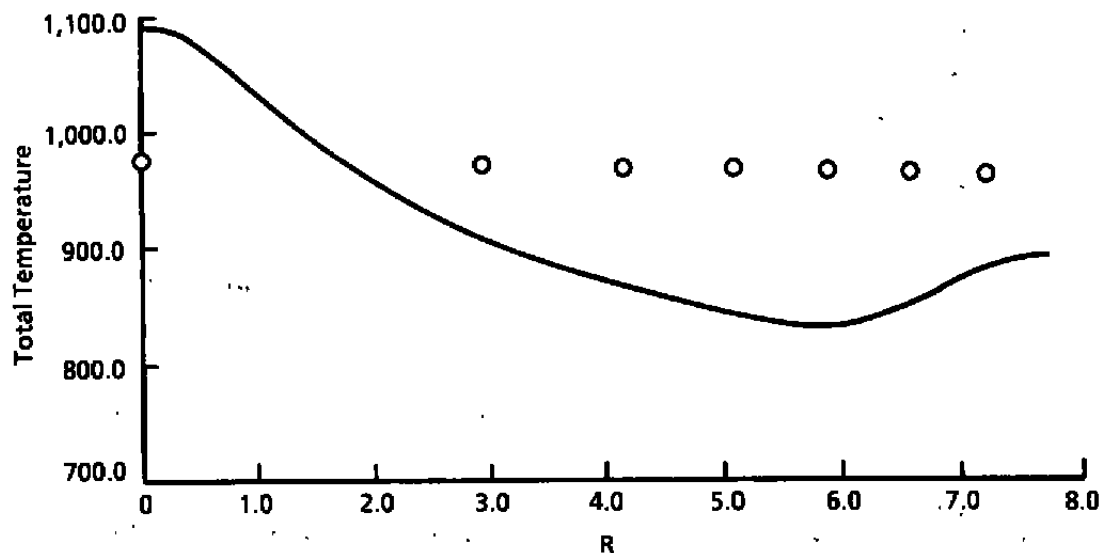
d. $x = 1.71$ diam, $\theta = 22.5$ deg
Figure 18. Continued.



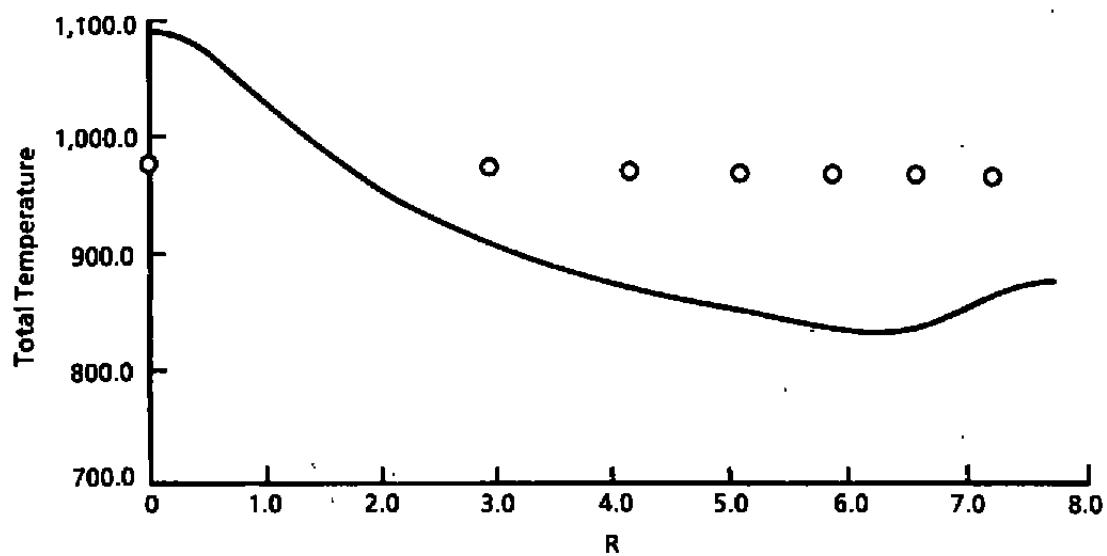
e. $x = 2.73$ diam, $\theta = 0$ deg



f. $x = 2.73$ diam, $\theta = 22.5$ deg
Figure 18. Continued.

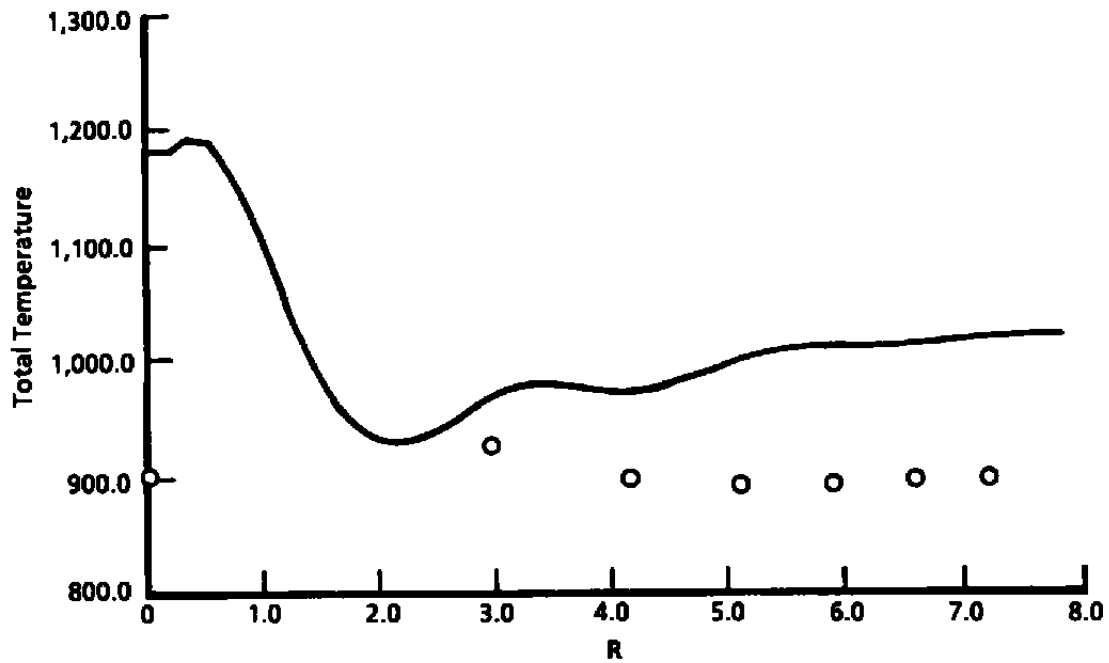


g. $x = 4.78$ diam, $\theta = 0$ deg

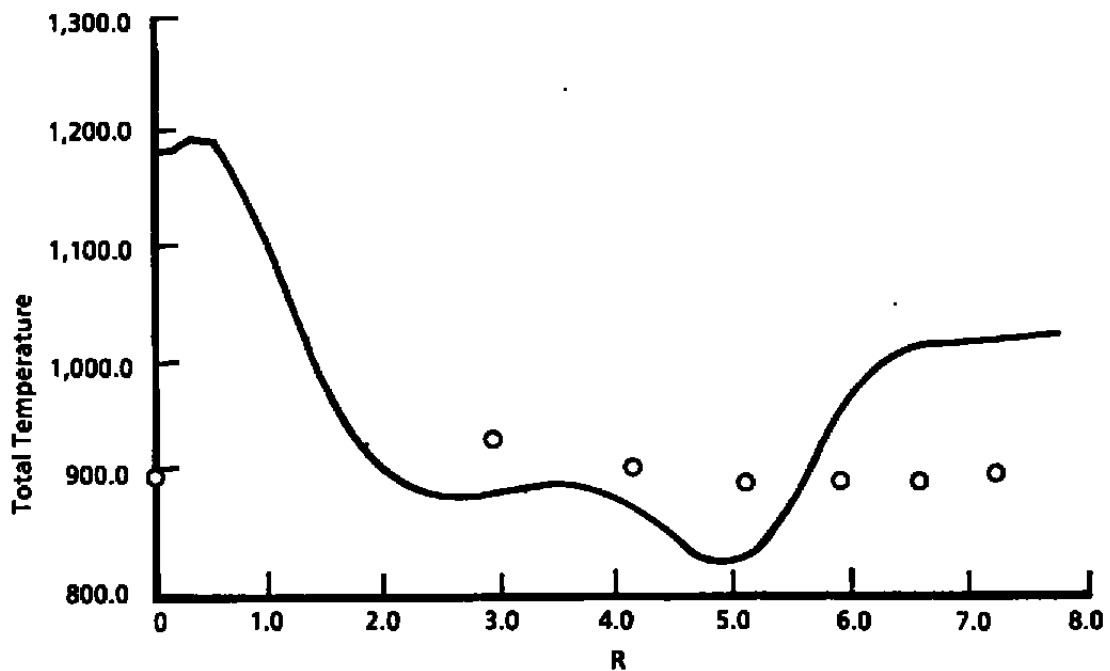


h. $x = 4.78$ diam, $\theta = 22.5$ deg

Figure 18. Concluded.

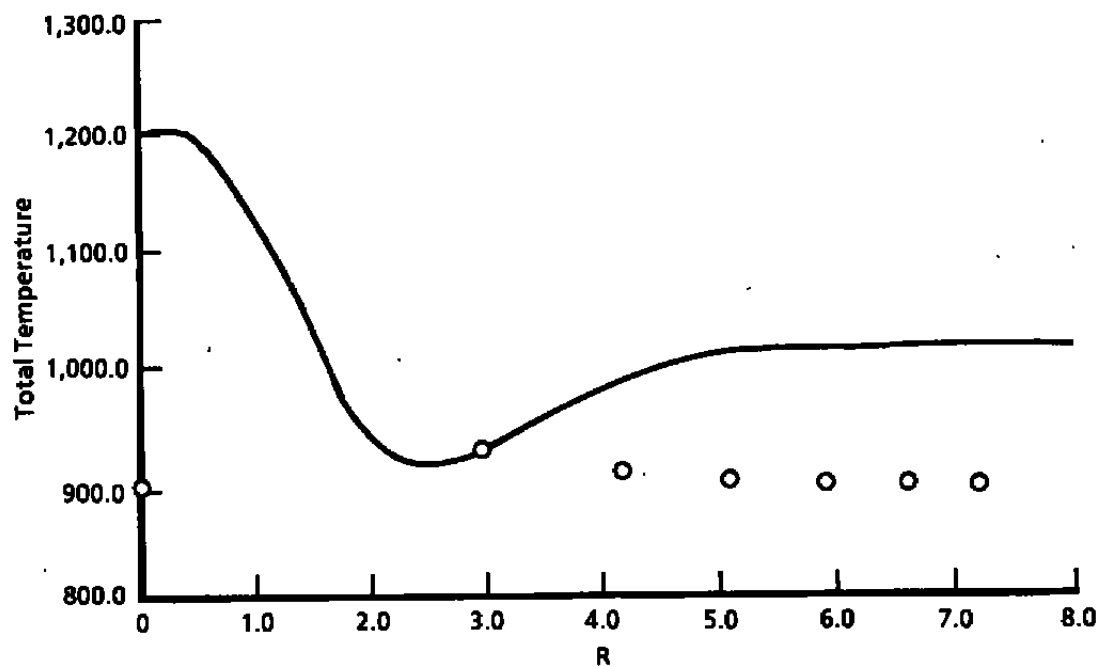


a. $x = 1.19$ diam, $\theta = 0$ deg

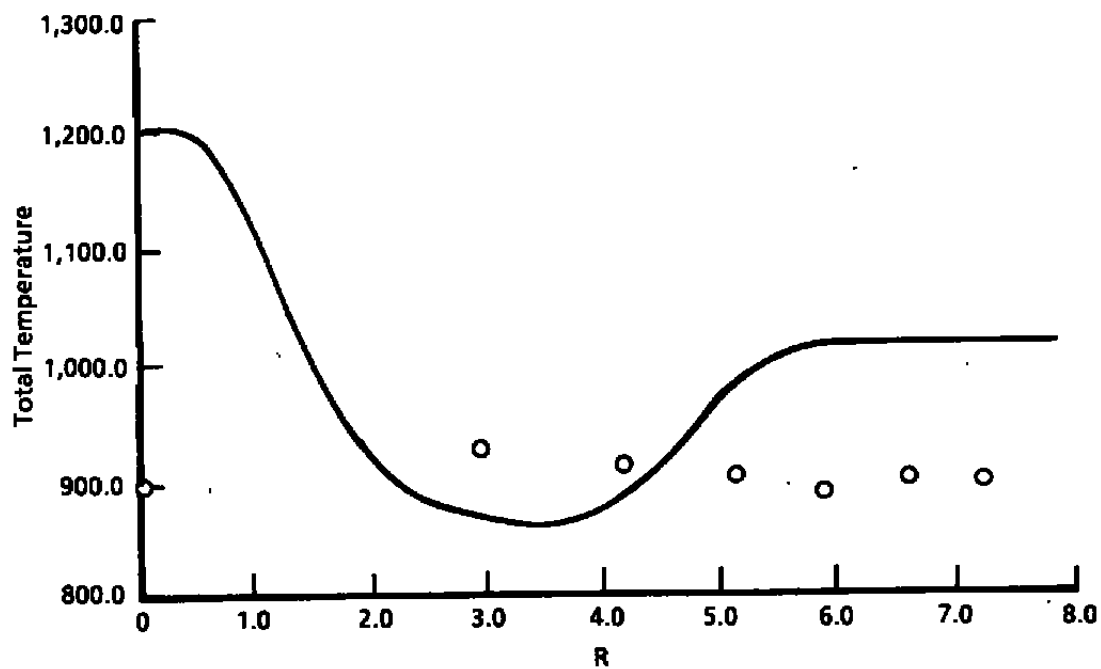


b. $x = 1.19$ diam, $\theta = 22.5$ deg

Figure 19. PARC prediction of total temperature versus experimental data, Case 3.

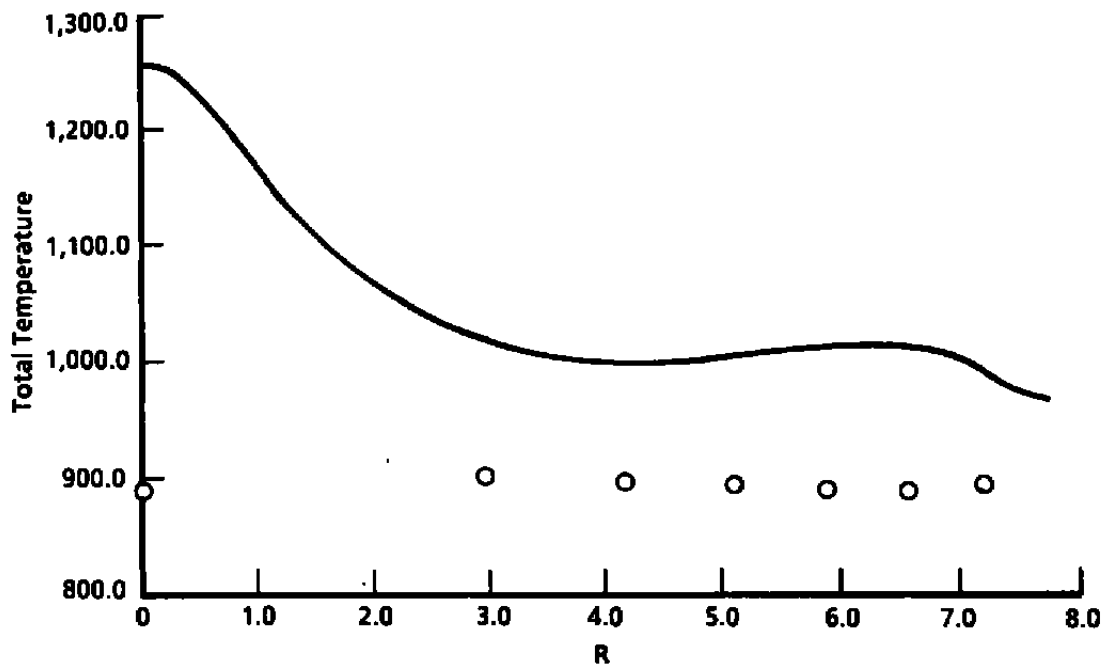


c. $x = 1.71$ diam, $\theta = 0$ deg

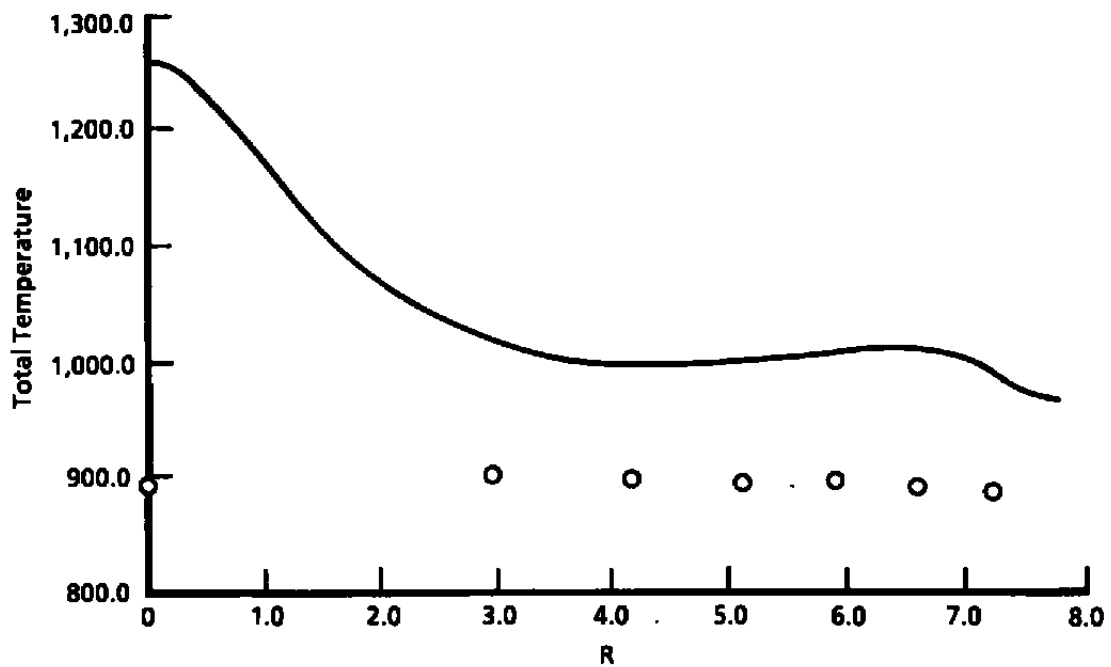


d. $x = 1.71$ diam, $\theta = 22.5$ deg

Figure 19. Continued.

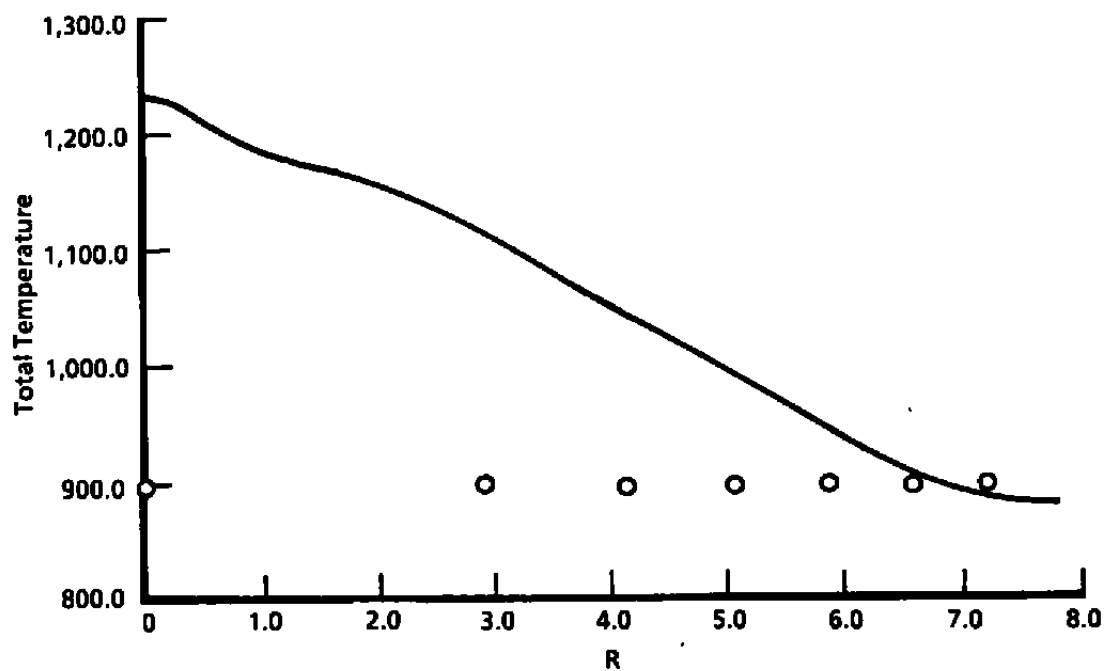


e. $x = 2.73 \text{ diam}$, $\theta = 0 \text{ deg}$

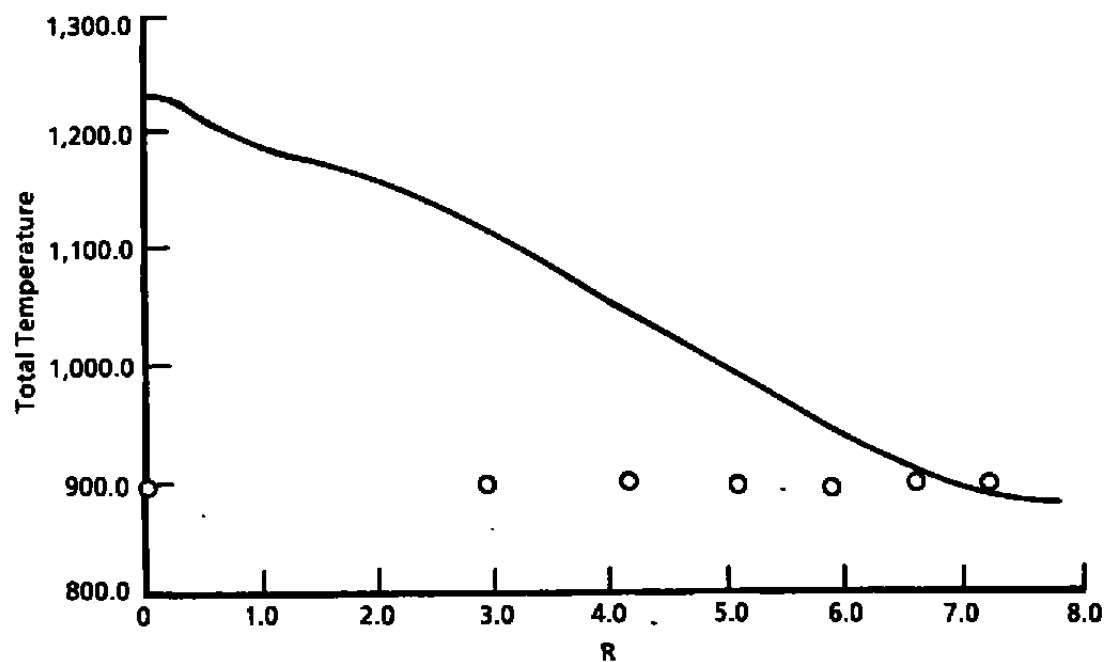


f. $x = 2.73 \text{ diam}$, $\theta = 22.5 \text{ deg}$

Figure 19. Continued.

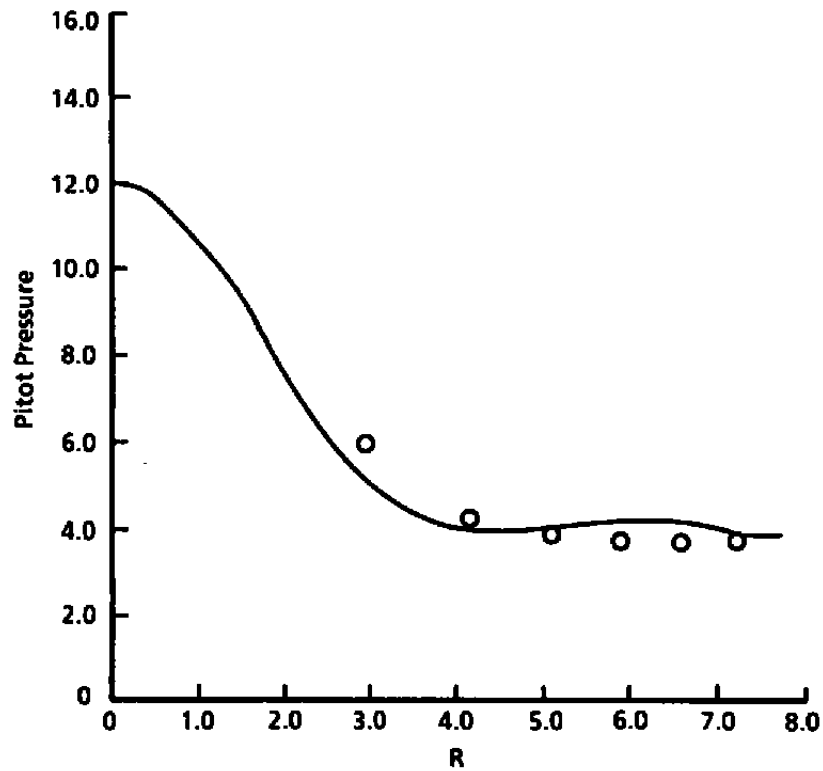


g. $x = 4.78$ diam, $\theta = 0$ deg

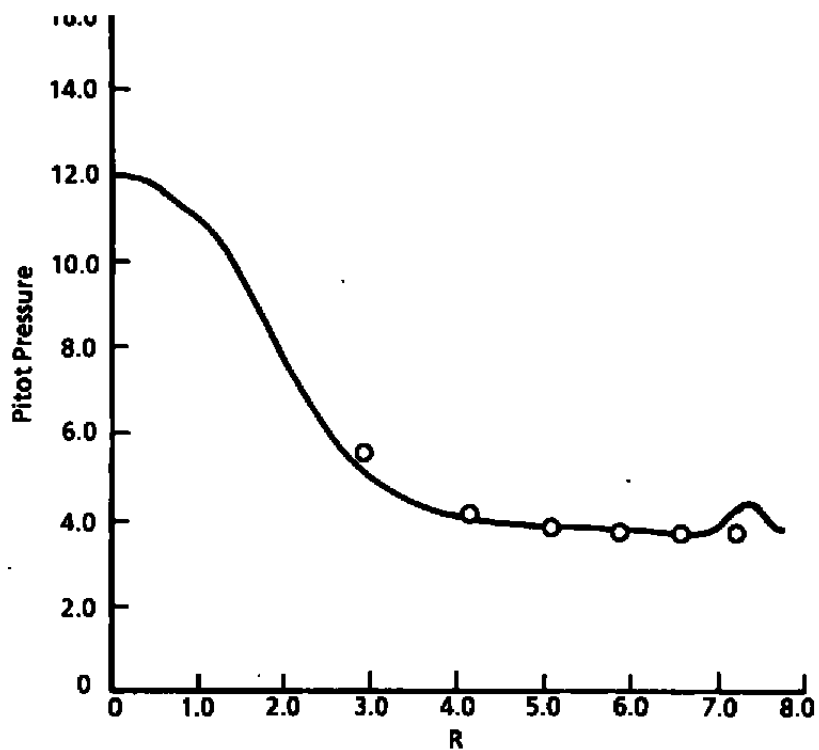


h. $x = 4.78$ diam, $\theta = 22.5$ deg

Figure 19. Concluded.

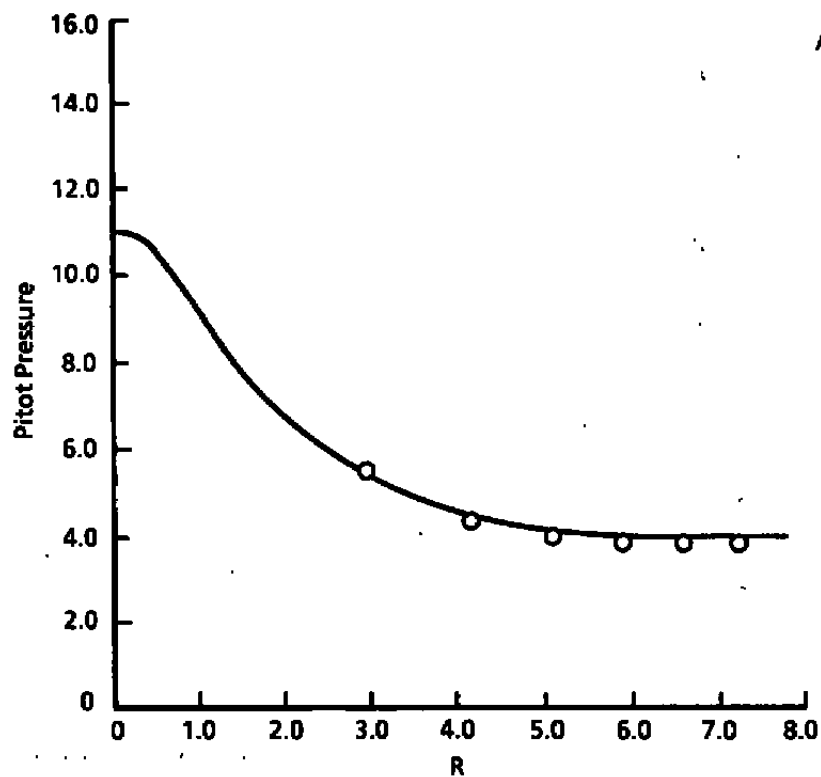


a. $x = 1.19$ diam, $\theta = 0$ deg

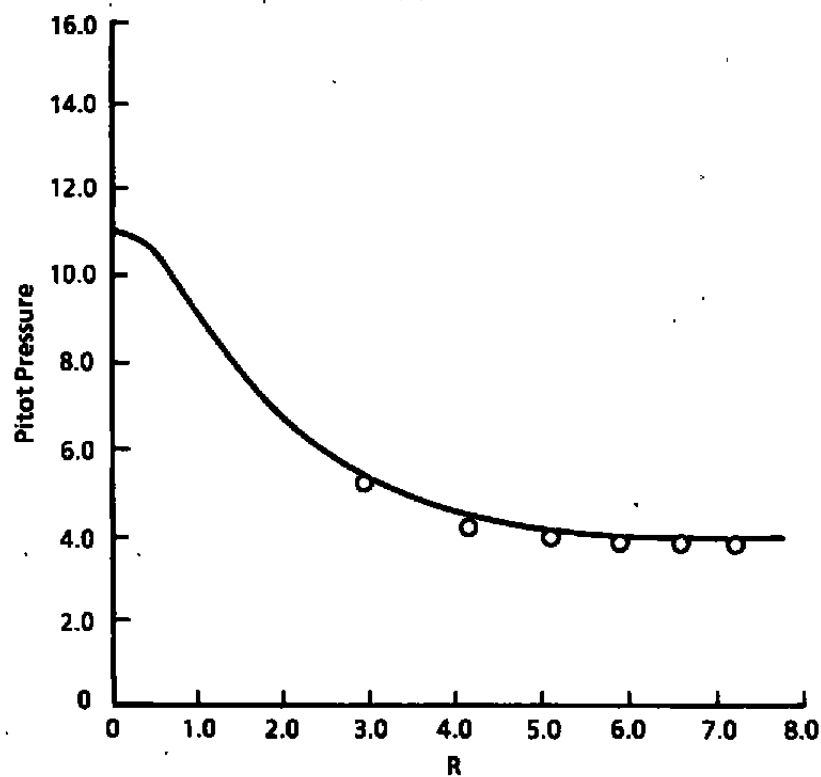


b. $x = 1.19$ diam, $\theta = 22.5$ deg

Figure 20. PARC prediction of pitot pressure versus experimental data, Case 2.

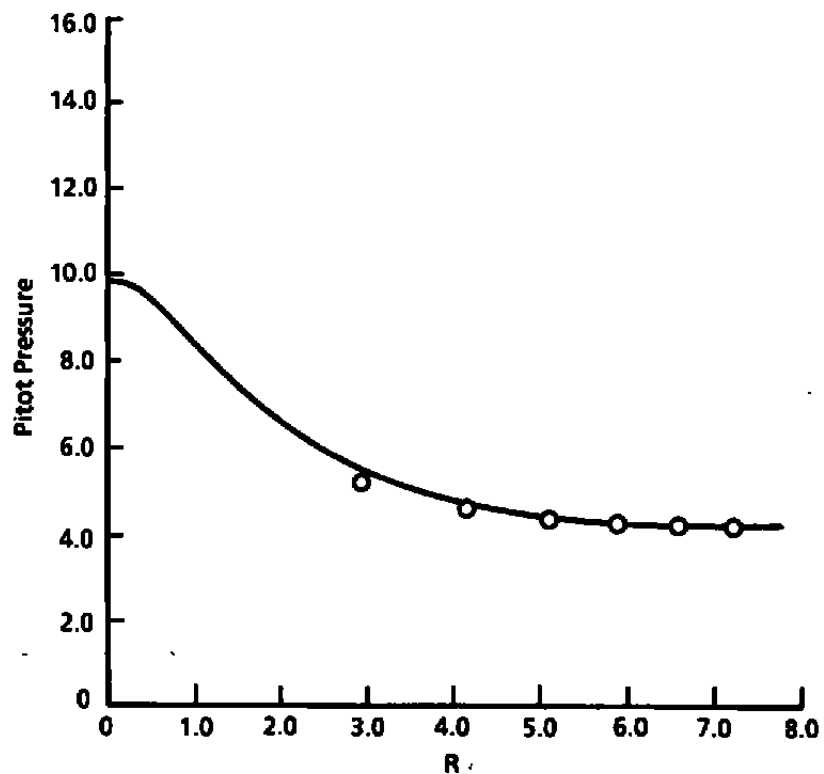
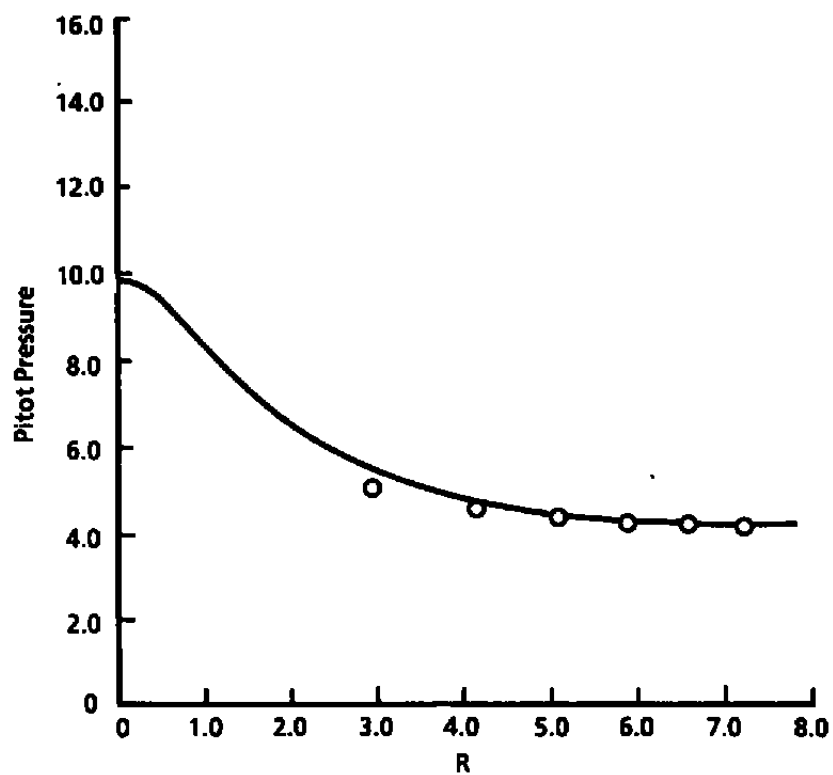


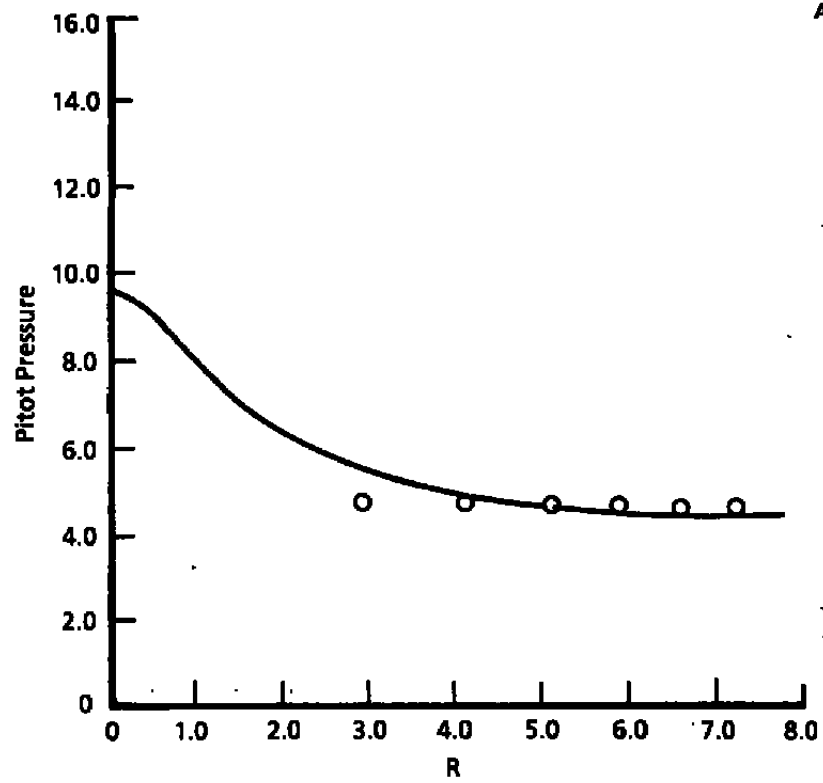
c. $x = 1.71$ diam, $\theta = 0$ deg



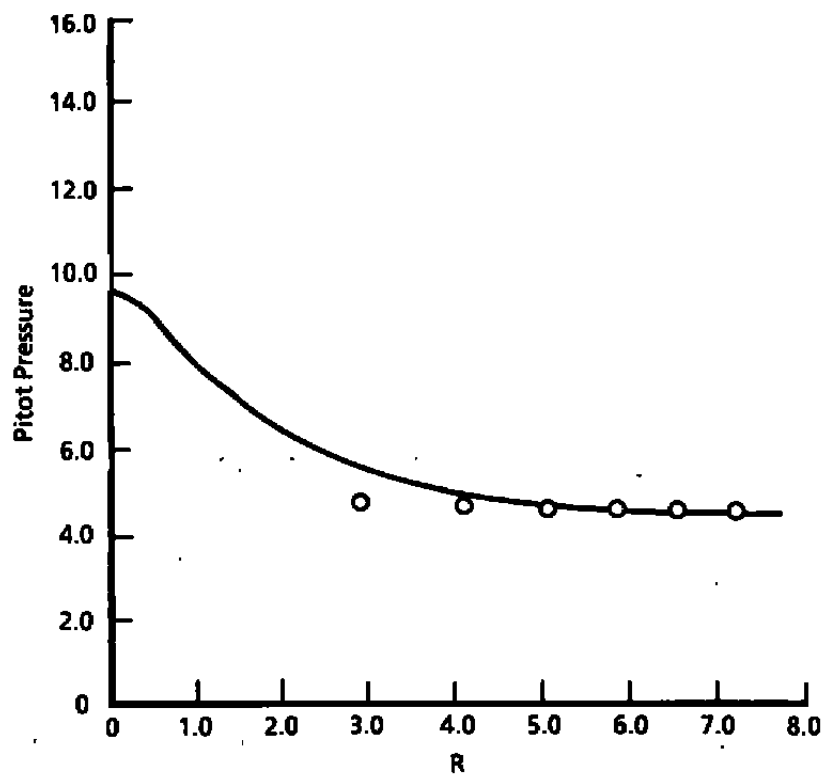
d. $x = 1.71$ diam, $\theta = 22.5$ deg

Figure 20. Continued.

e. $x = 2.73$ diam, $\theta = 0$ degf. $x = 2.73$ diam, $\theta = 22.5$ deg
Figure 20. Continued.

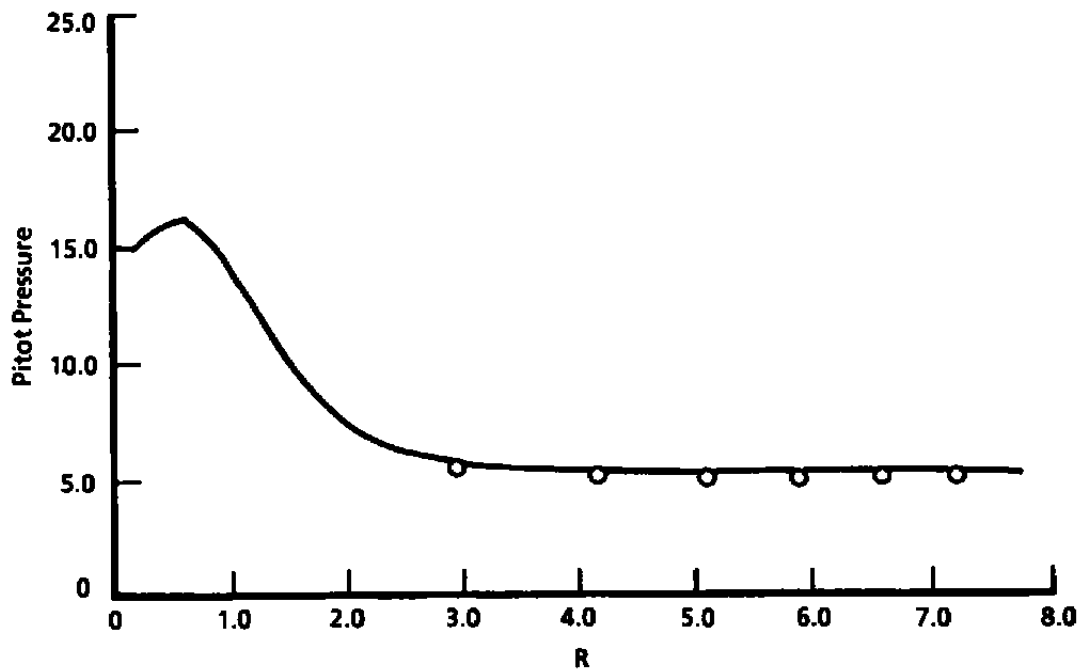


g. $x = 4.78$ diam, $\theta = 0$ deg

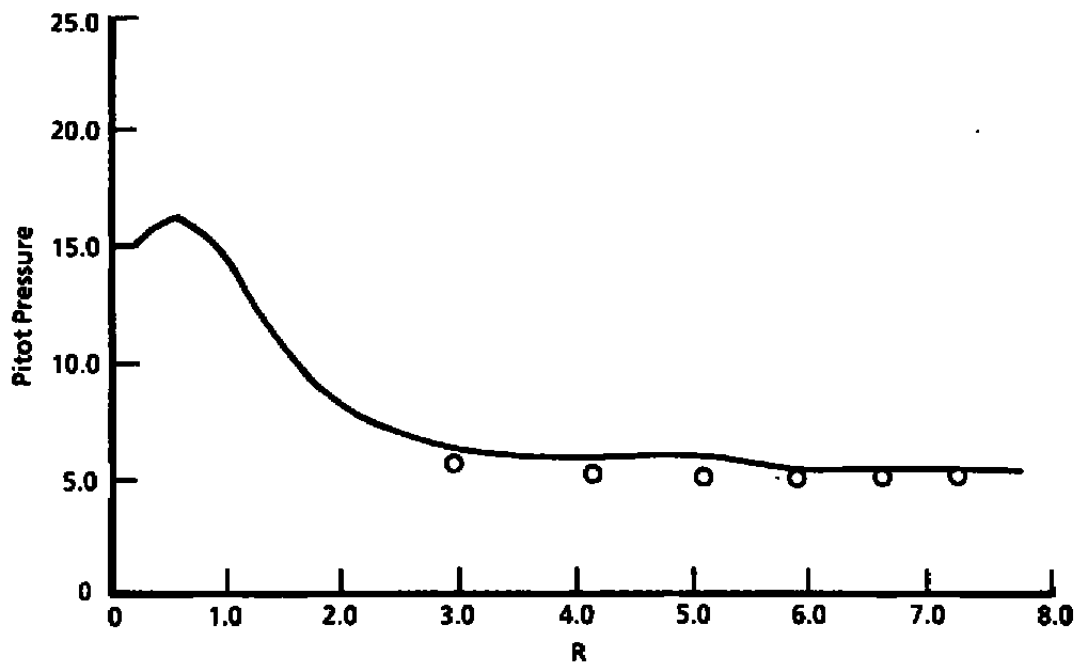


h. $x = 4.78$ diam, $\theta = 22.5$ deg

Figure 20. Concluded.

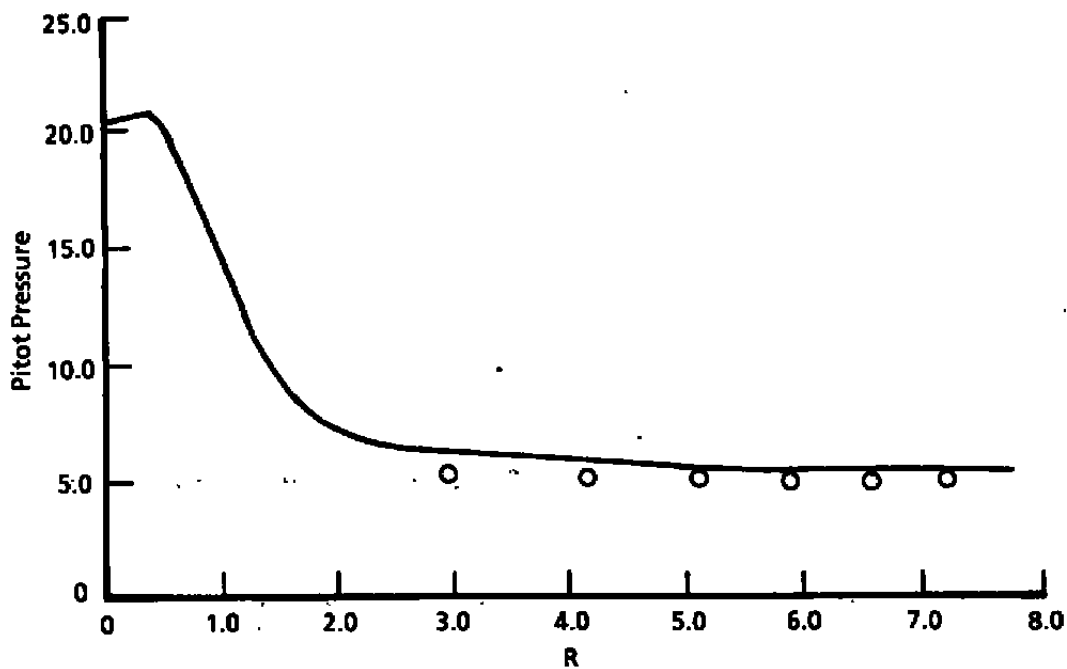


a. $x = 1.19 \text{ diam}$, $\theta = 0 \text{ deg}$

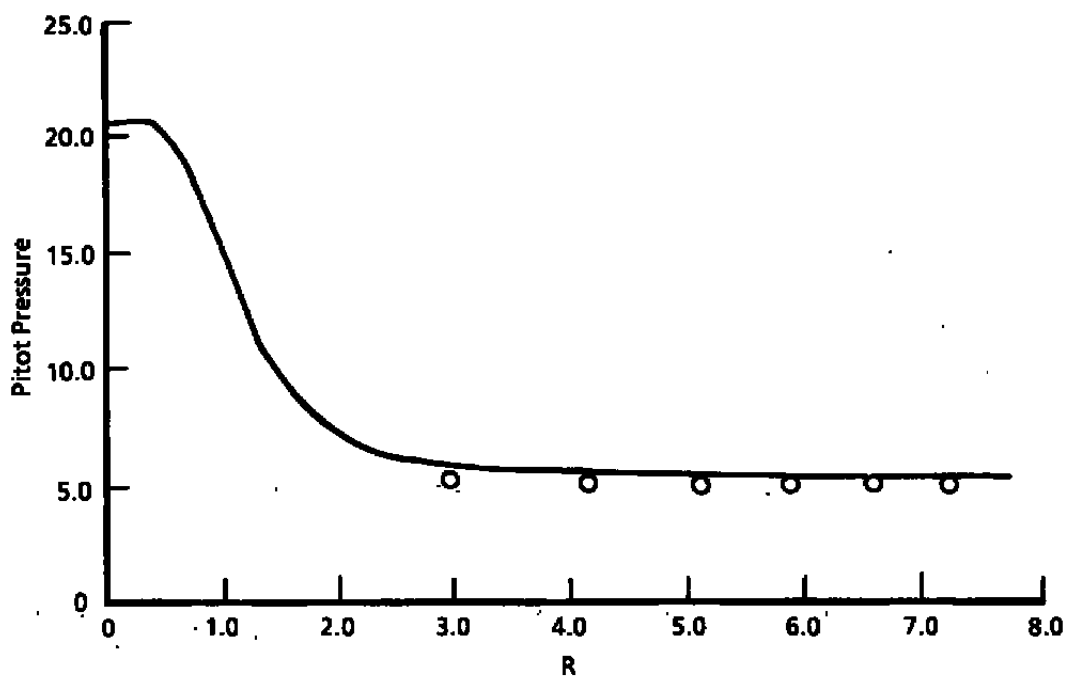


b. $x = 1.19 \text{ diam}$, $\theta = 22.5 \text{ deg}$

Figure 21. PARC prediction of pitot pressure versus experimental data, Case 3.

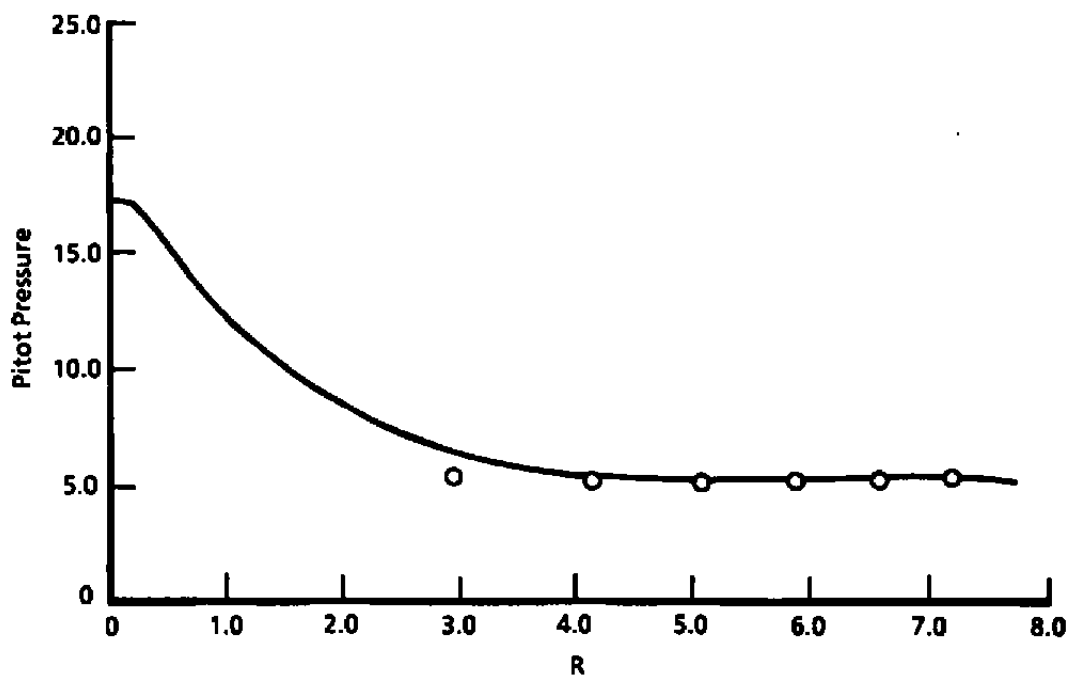


c. $x = 1.71 \text{ diam}, \theta = 0 \text{ deg}$

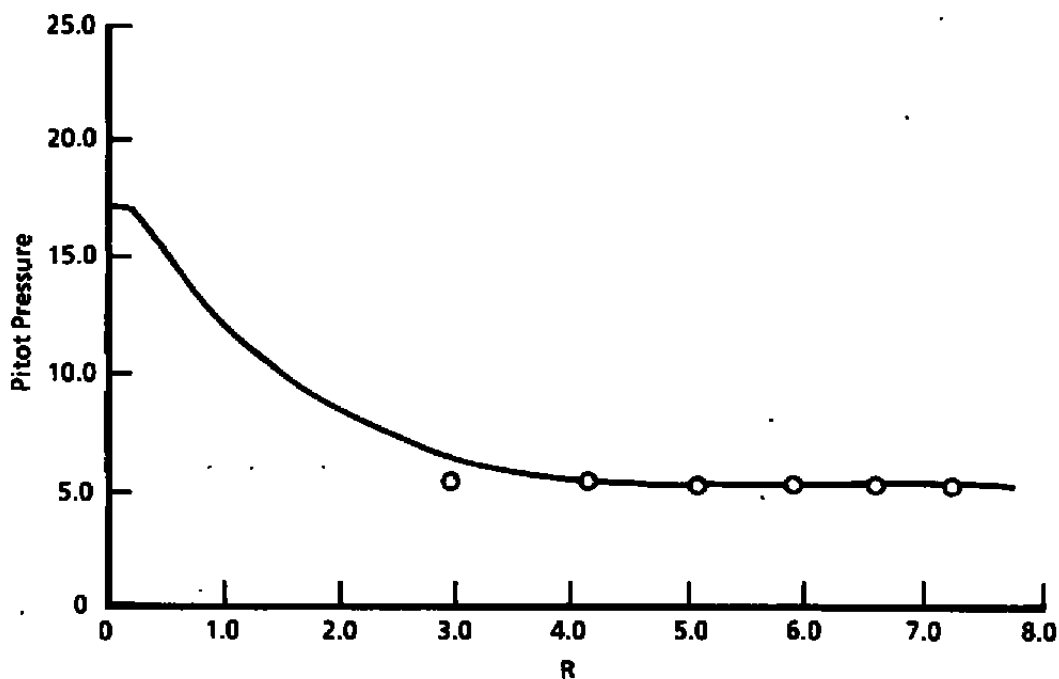


d. $x = 1.71 \text{ diam}, \theta = 22.5 \text{ deg}$

Figure 21. Continued.

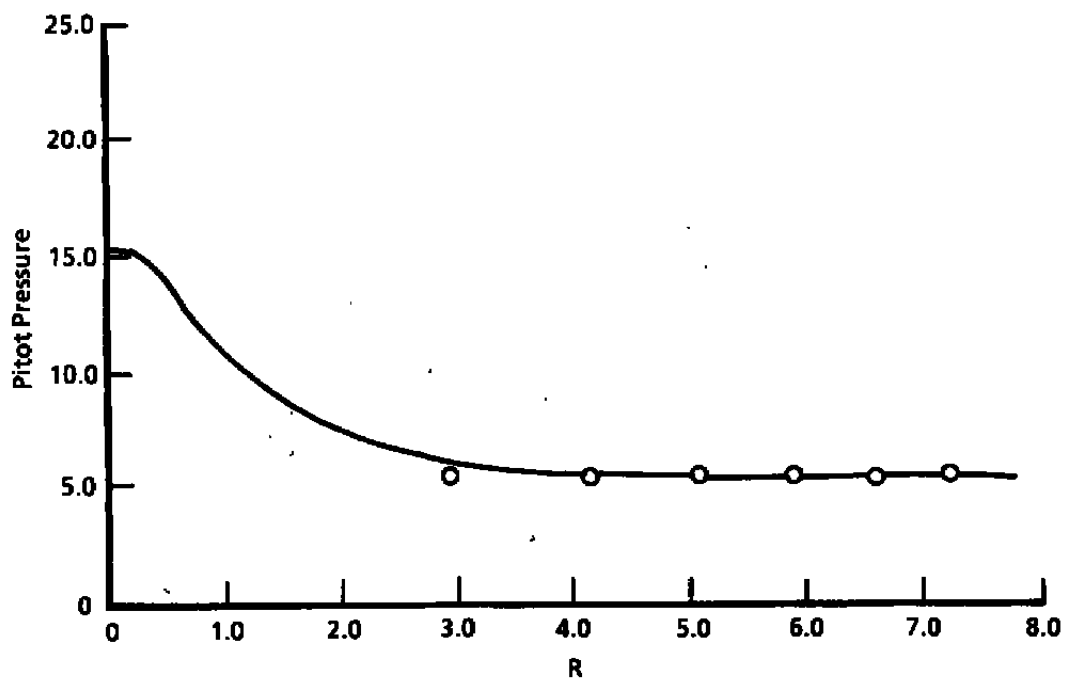


e. $x = 2.73 \text{ diam}$, $\theta = 0 \text{ deg}$

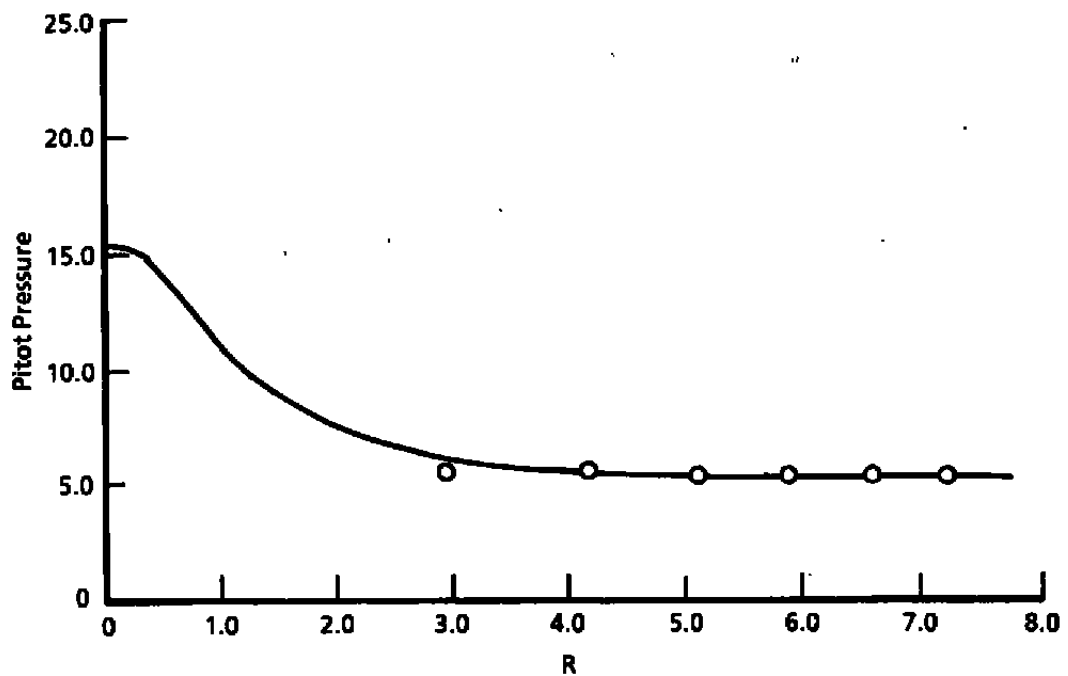


f. $x = 2.73 \text{ diam}$, $\theta = 22.5 \text{ deg}$

Figure 21. Continued.



g. $x = 4.78$ diam, $\theta = 0$ deg



h. $x = 4.78$ diam, $\theta = 22.5$ deg

Figure 21. Concluded.

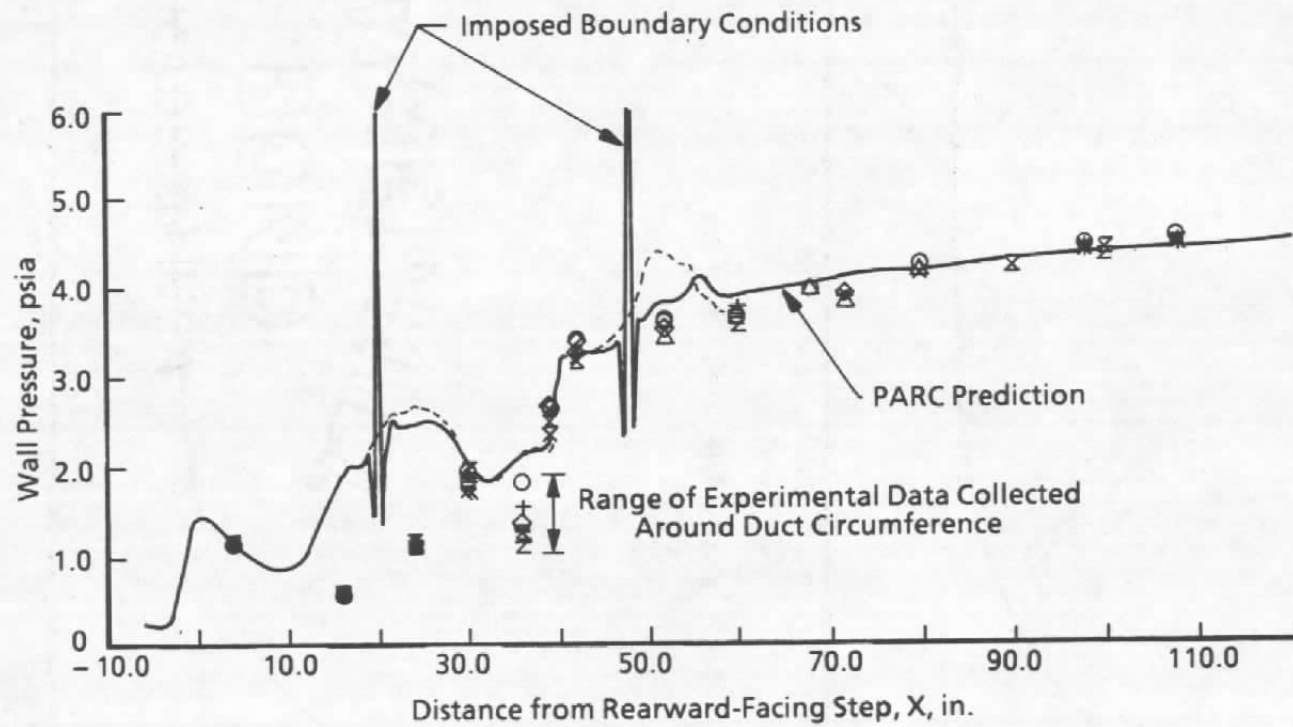


Figure 22. PARC prediction of wall pressure, Case 2.

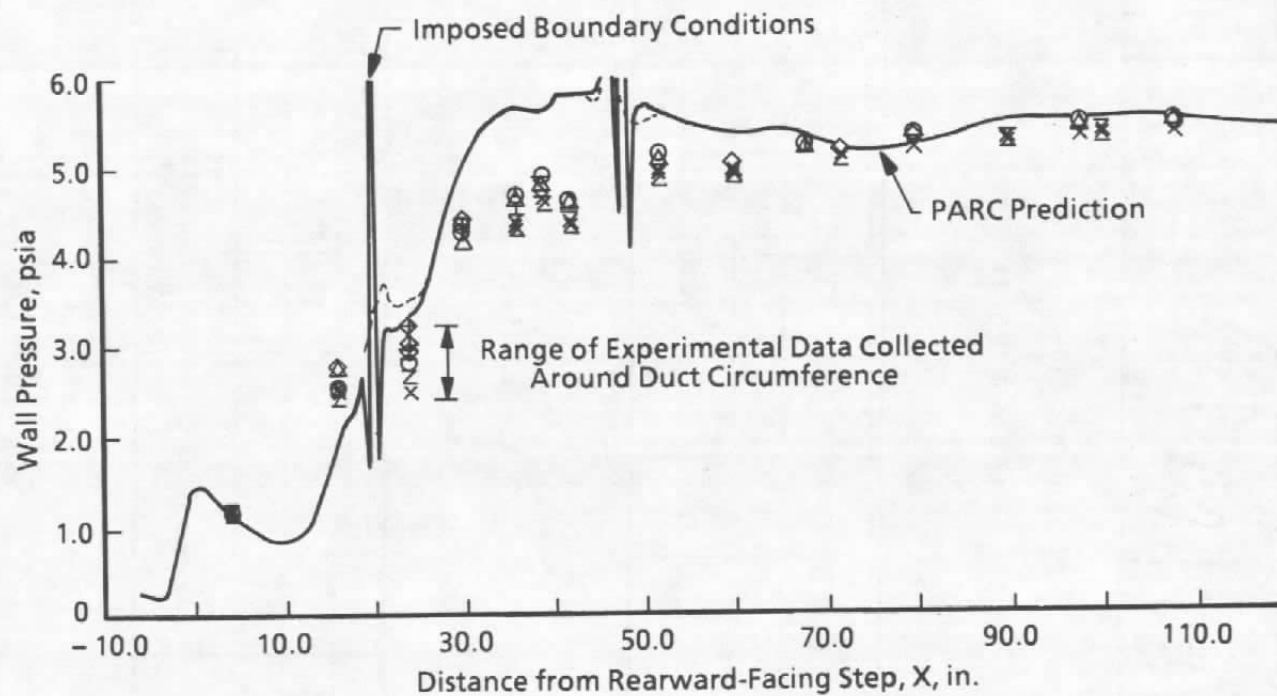
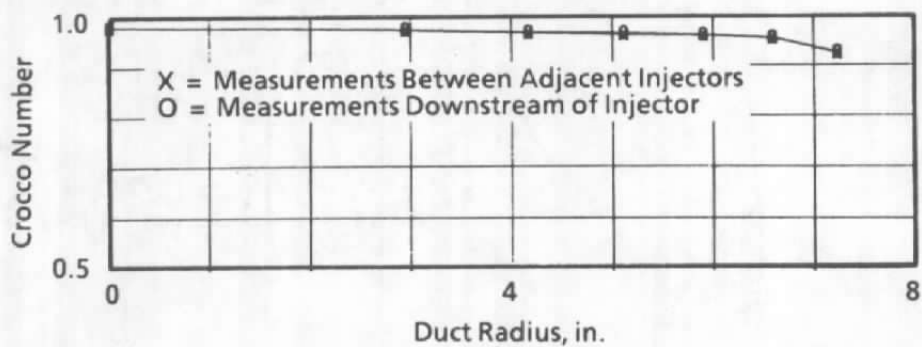
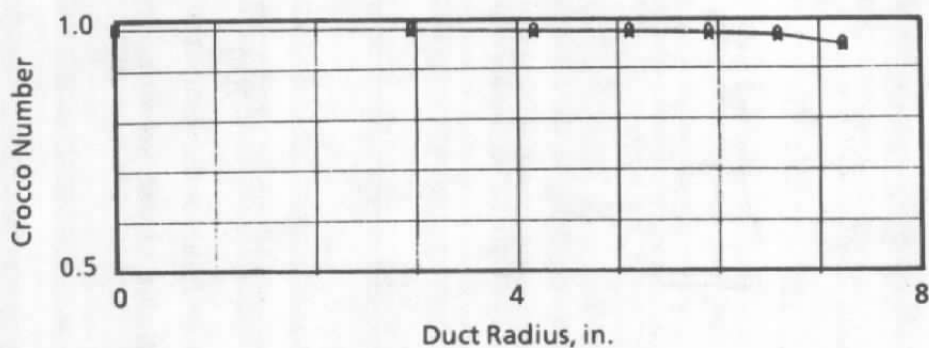


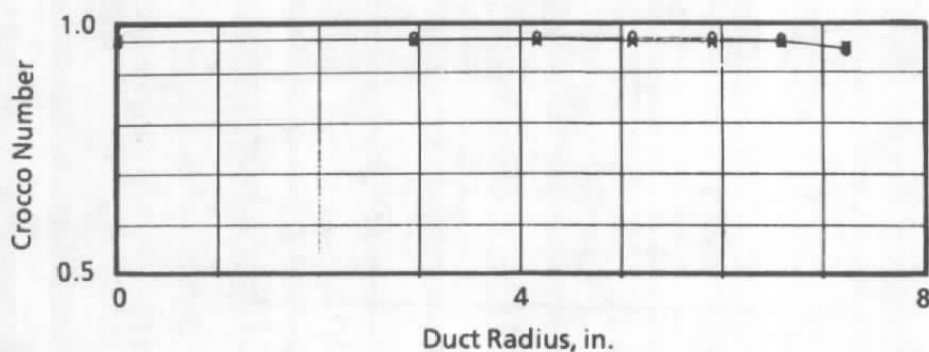
Figure 23. PARC prediction of wall pressure, Case 3.



a. $x = 1.19 L/D$

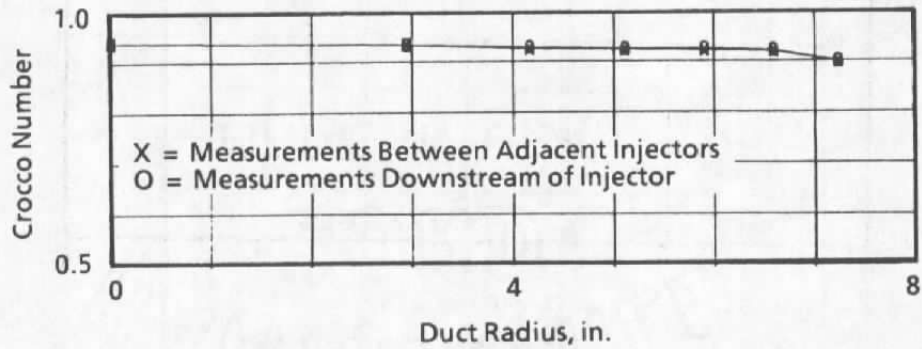


b. $x = 1.71 L/D$

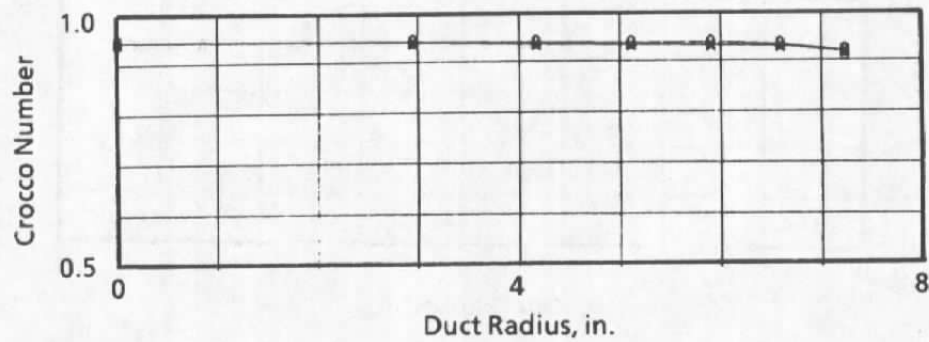


c. $x = 4.78 L/D$

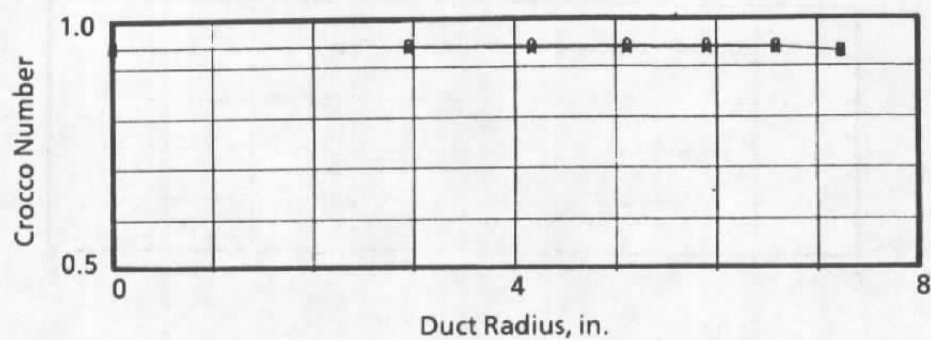
Figure 24. Crocco number — Mach 0.8 configuration, no injection.



a. $x = 1.19 L/D$

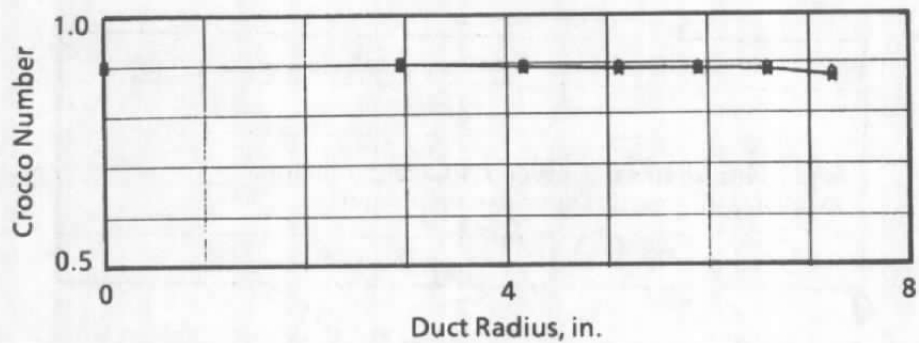


b. $x = 1.71 L/D$

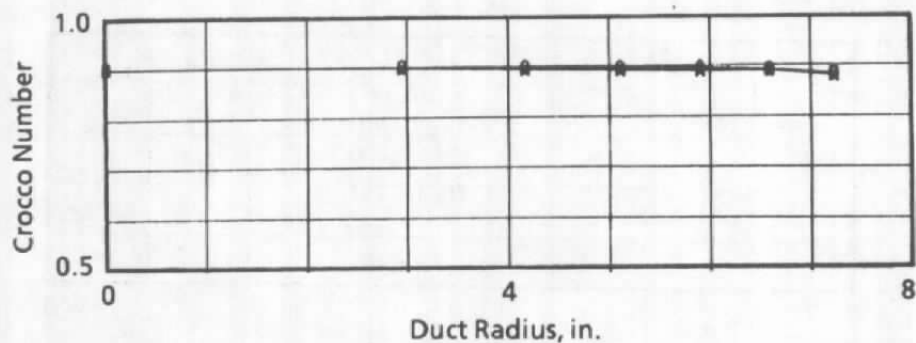


c. $x = 4.78 L/D$

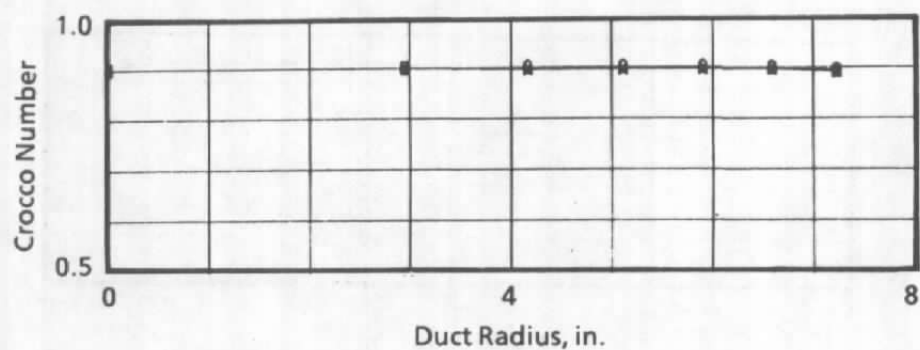
Figure 25. Crocco number — upstream injection = 0.25 lbm/sec.



a. $x = 1.19 L/D$

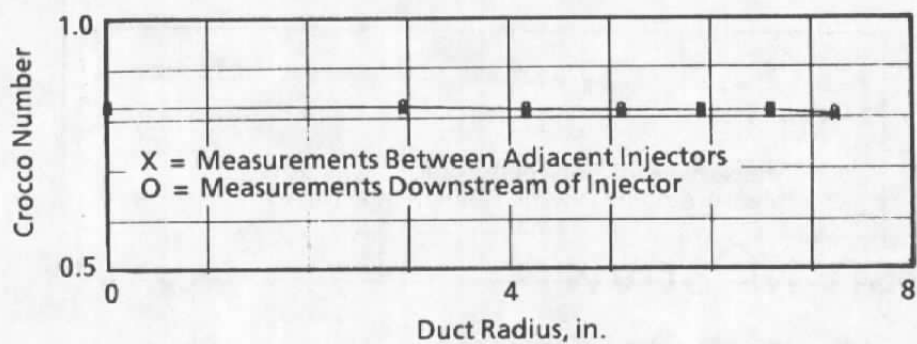


b. $x = 1.71 L/D$

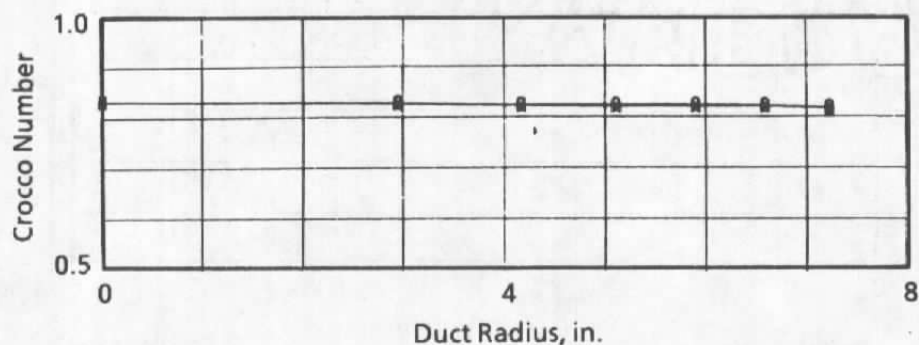


c. $x = 4.78 L/D$

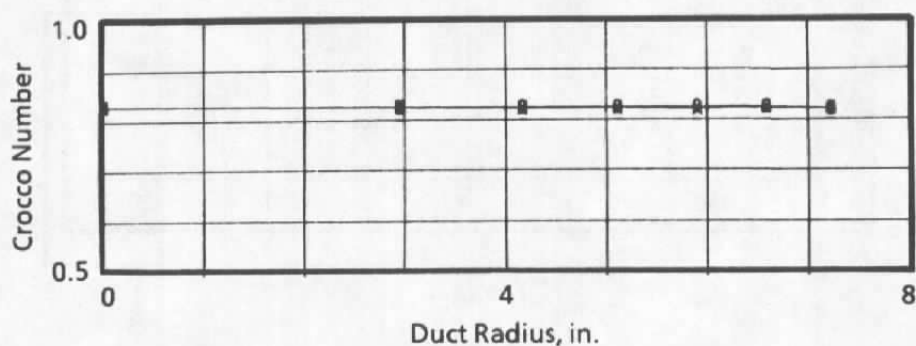
Figure 26. Crocco number — upstream injection = 0.50 lbm/sec.



a. $x = 1.19 \text{ L/D}$

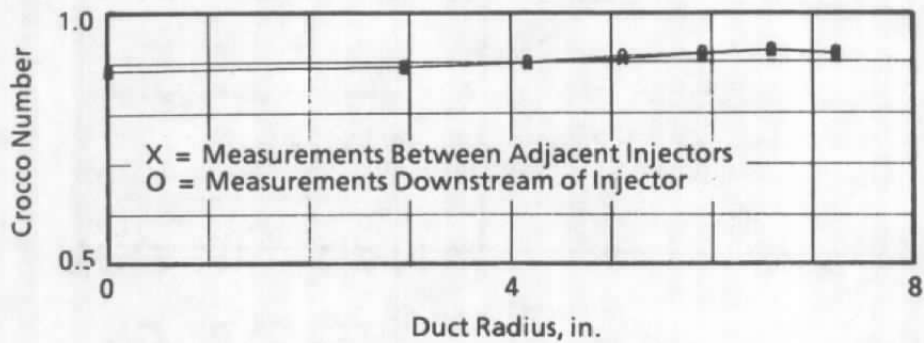


b. $x = 1.71 \text{ L/D}$

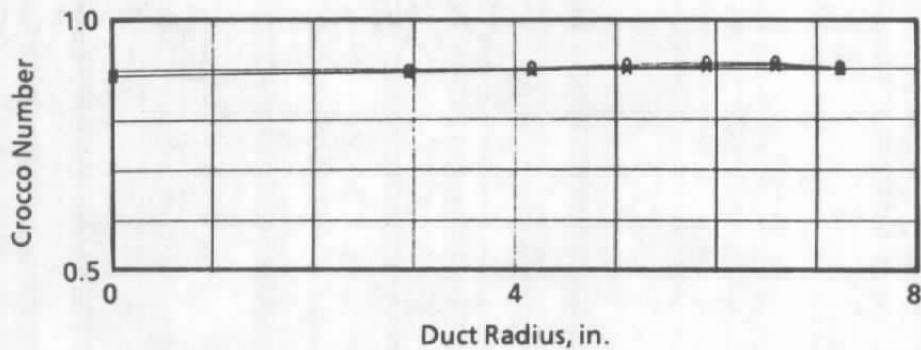


c. $x = 4.78 \text{ L/D}$

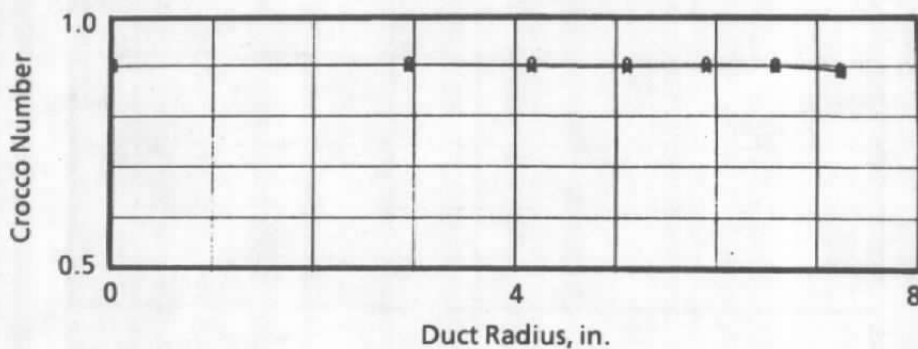
Figure 27. Crocco number — upstream injection = 1.0 lbm/sec.



a. $x = 1.19 \text{ L/D}$

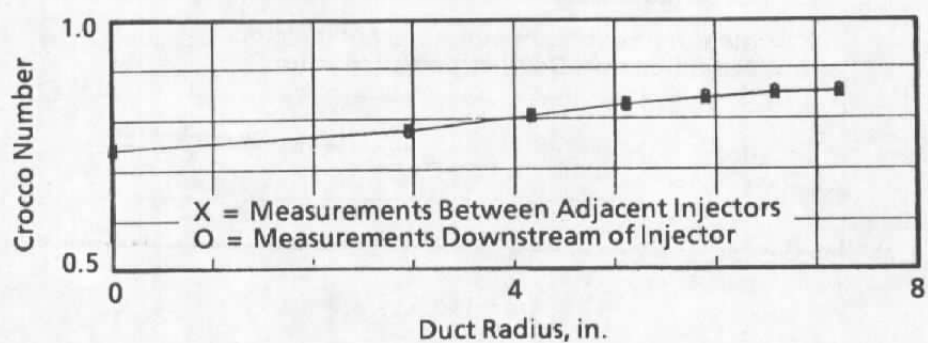


b. $x = 1.71 \text{ L/D}$

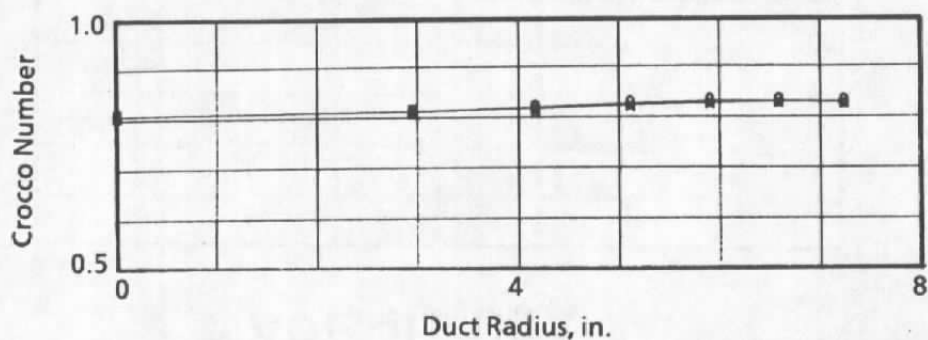


c. $x = 4.78 \text{ L/D}$

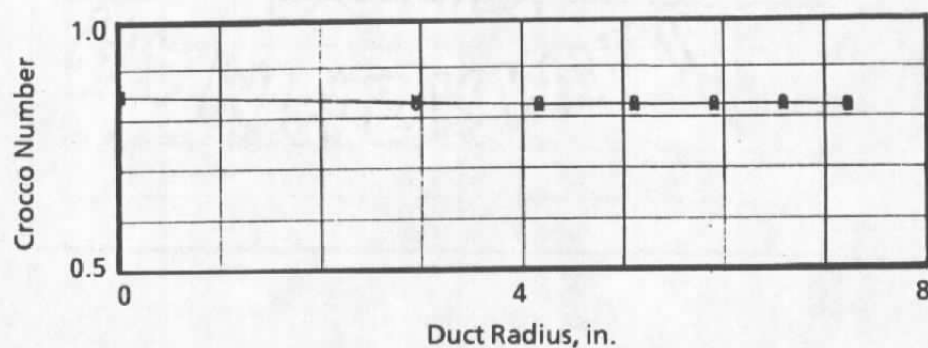
Figure 28. Crocco number — downstream injection = 0.50 lbm/sec.



a. $x = 1.19 \text{ L/D}$

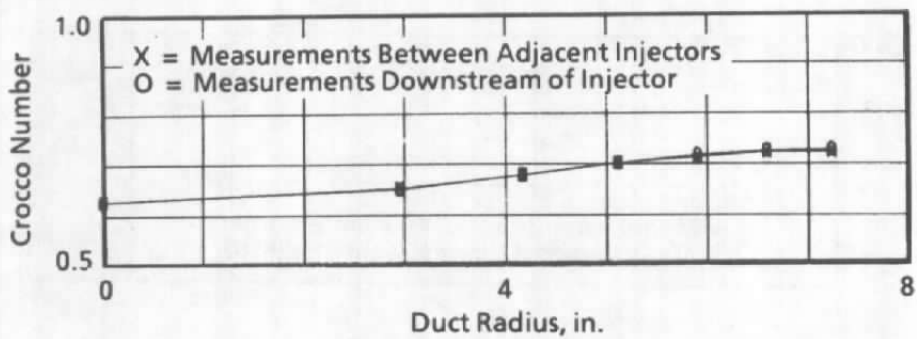


b. $x = 1.71 \text{ L/D}$

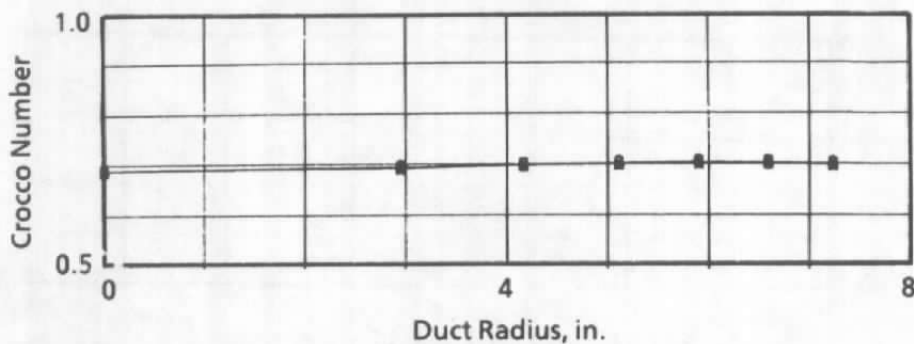


c. $x = 4.78 \text{ L/D}$

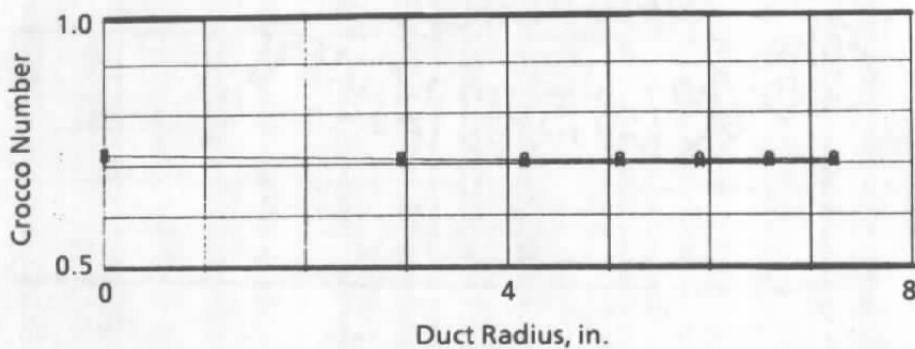
Figure 29. Crocco number — downstream injection = 1.0 lbm/sec.



a. $x = 1.19 \text{ L/D}$

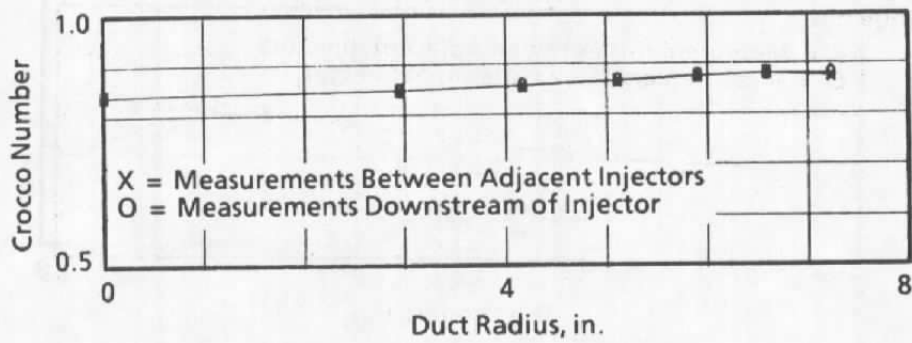


b. $x = 1.71 \text{ L/D}$

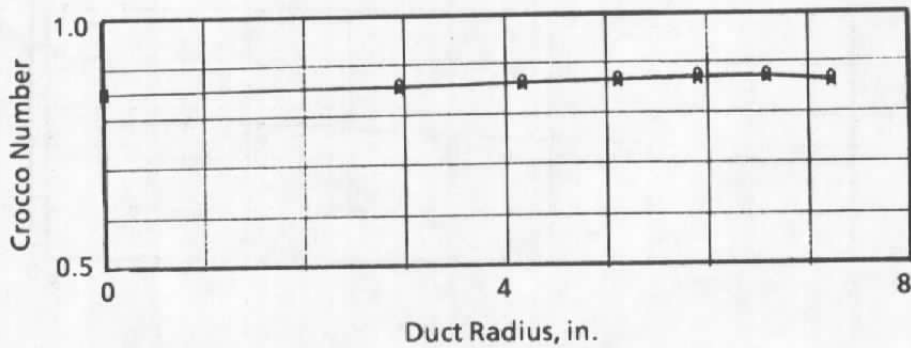


c. $x = 4.78 \text{ L/D}$

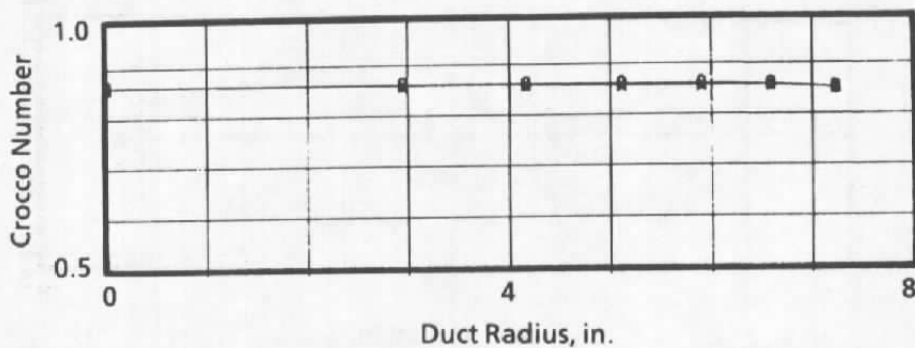
Figure 30. Crocco number — downstream injection = 2.0 lbm/sec.



a. $x = 1.19 L/D$

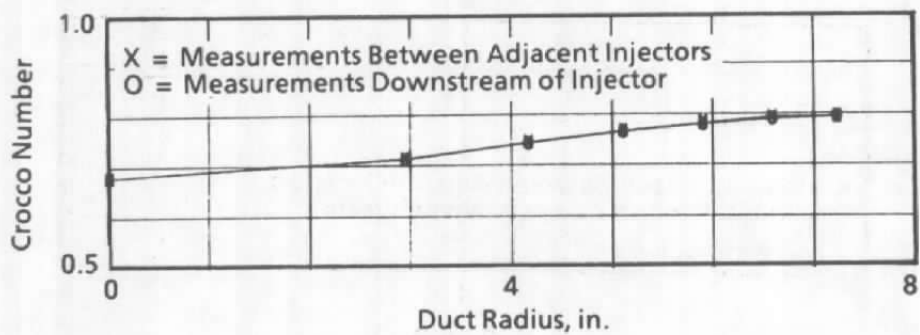


b. $x = 1.71 L/D$

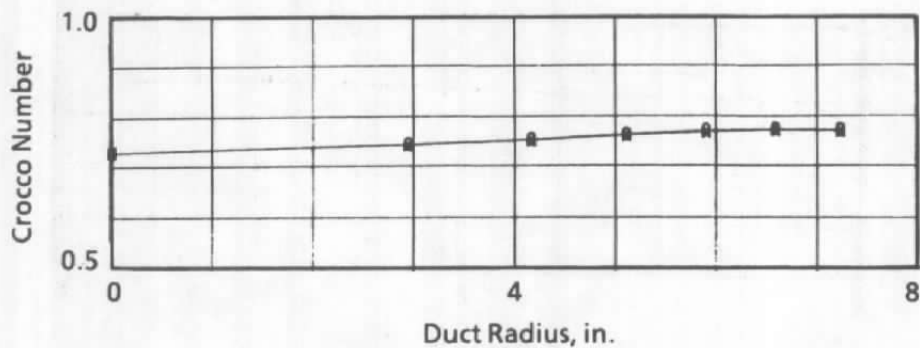


c. $x = 4.78 L/D$

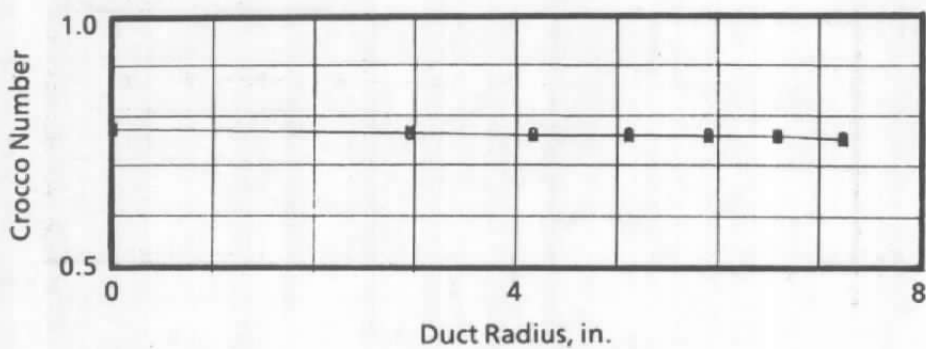
Figure 31. Crocco number — combined injection = 0.75 lbm/sec.



a. $x = 1.19 L/D$

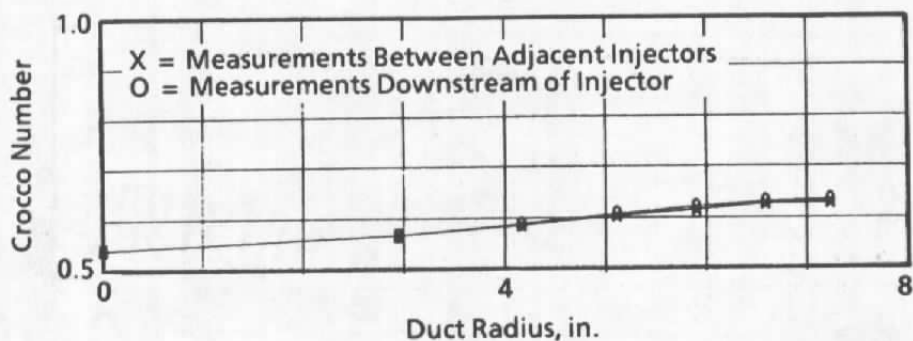


b. $x = 1.71 L/D$

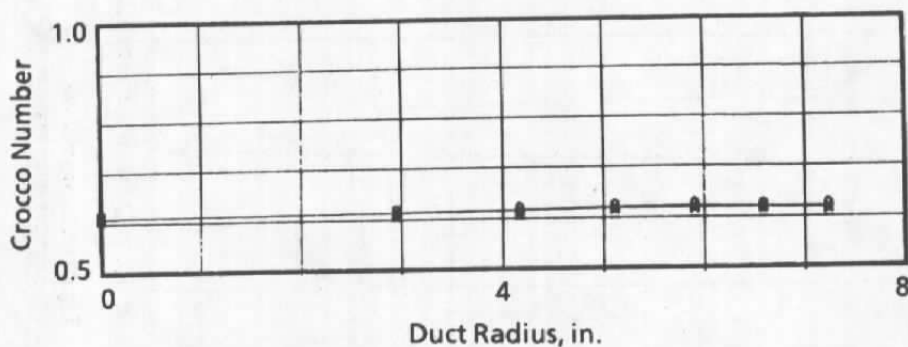


c. $x = 4.78 L/D$

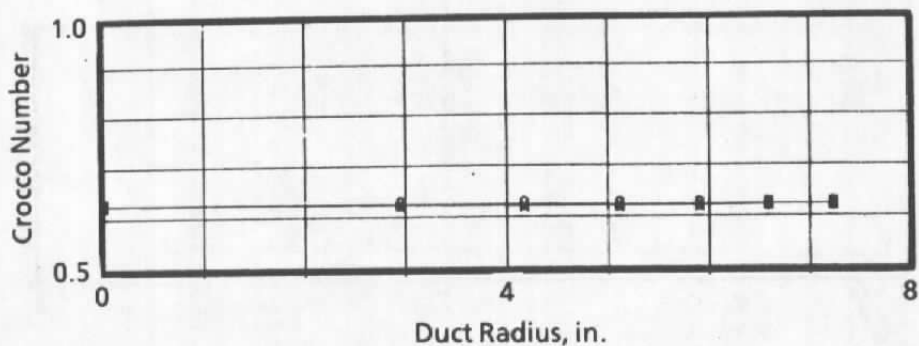
Figure 32. Crocco number — combined injection = 1.50 lbm/sec.



a. $x = 1.19 L/D$

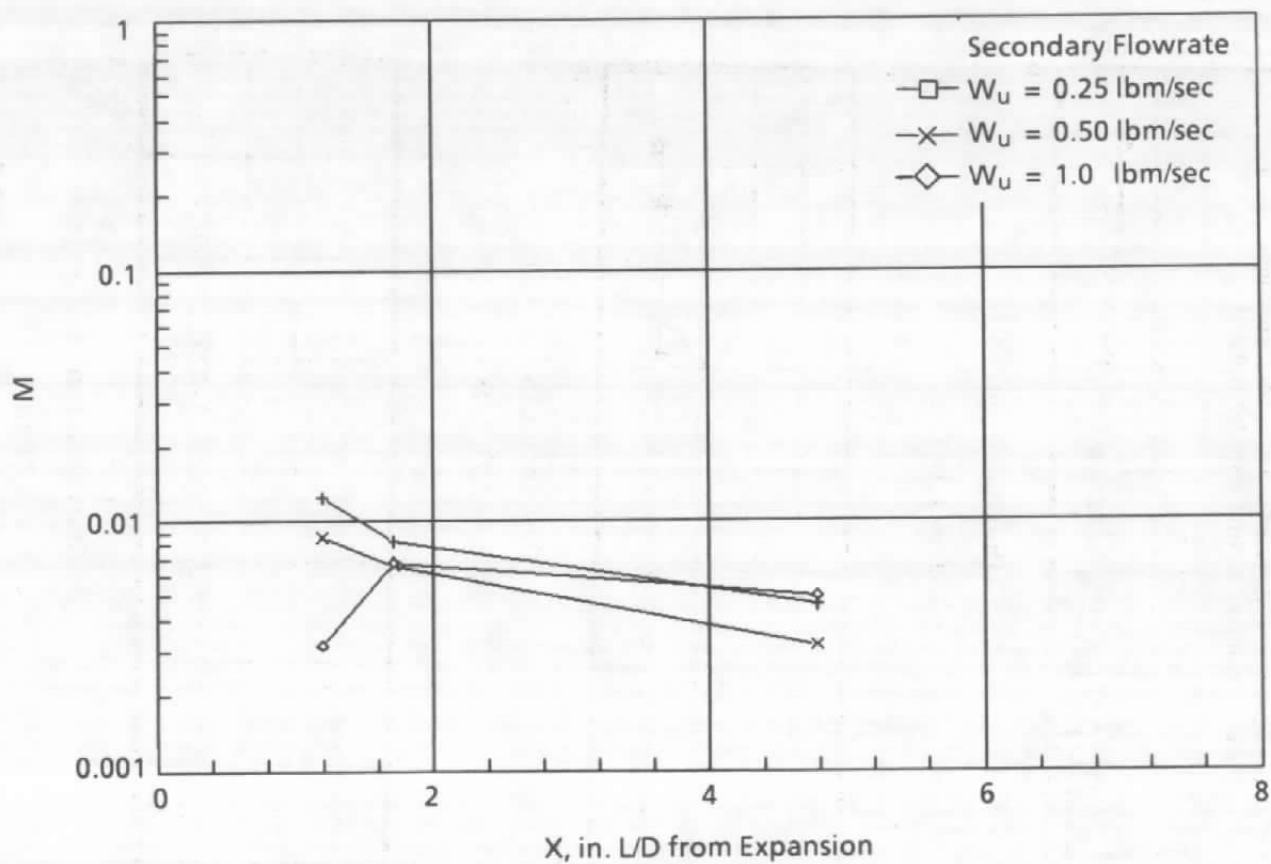


b. $x = 1.71 L/D$



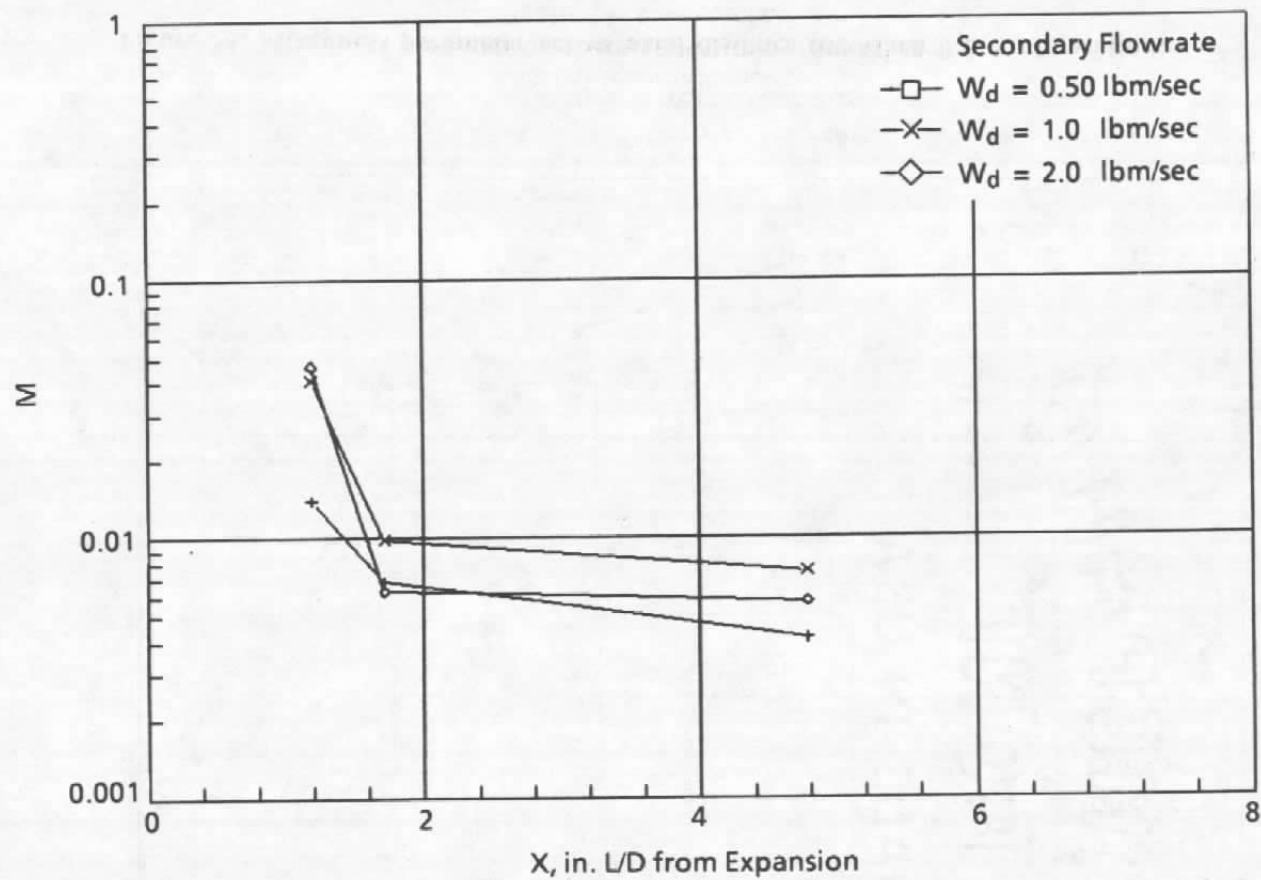
c. $x = 4.78 L/D$

Figure 33. Crocco number — combined injection = 3.0 lbm/sec.

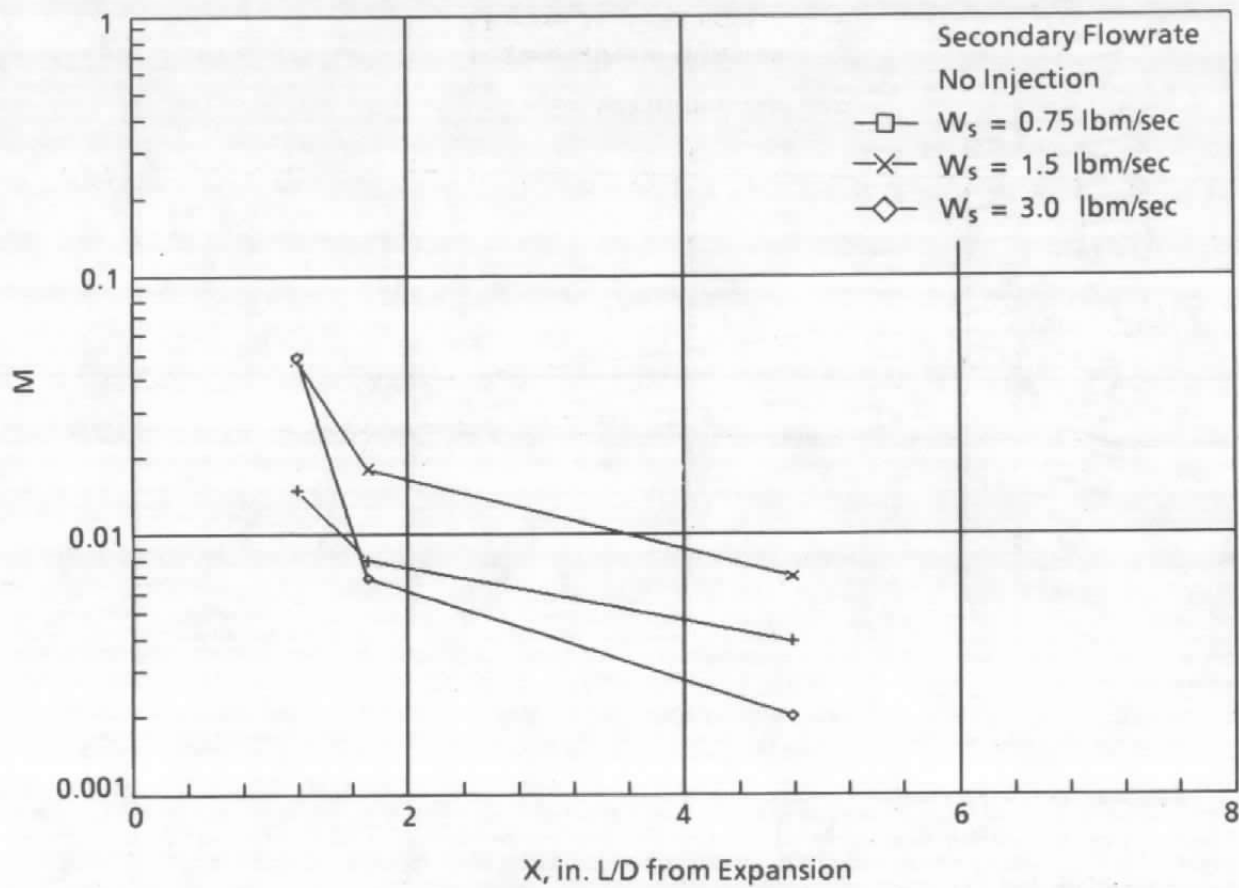


a. Upstream injection

Figure 34. Mixedness parameter versus axial distance for Mach 0.8 configuration.



b. Downstream injection
Figure 34. Continued.



c. Combined upstream/downstream injection
Figure 34. Concluded.

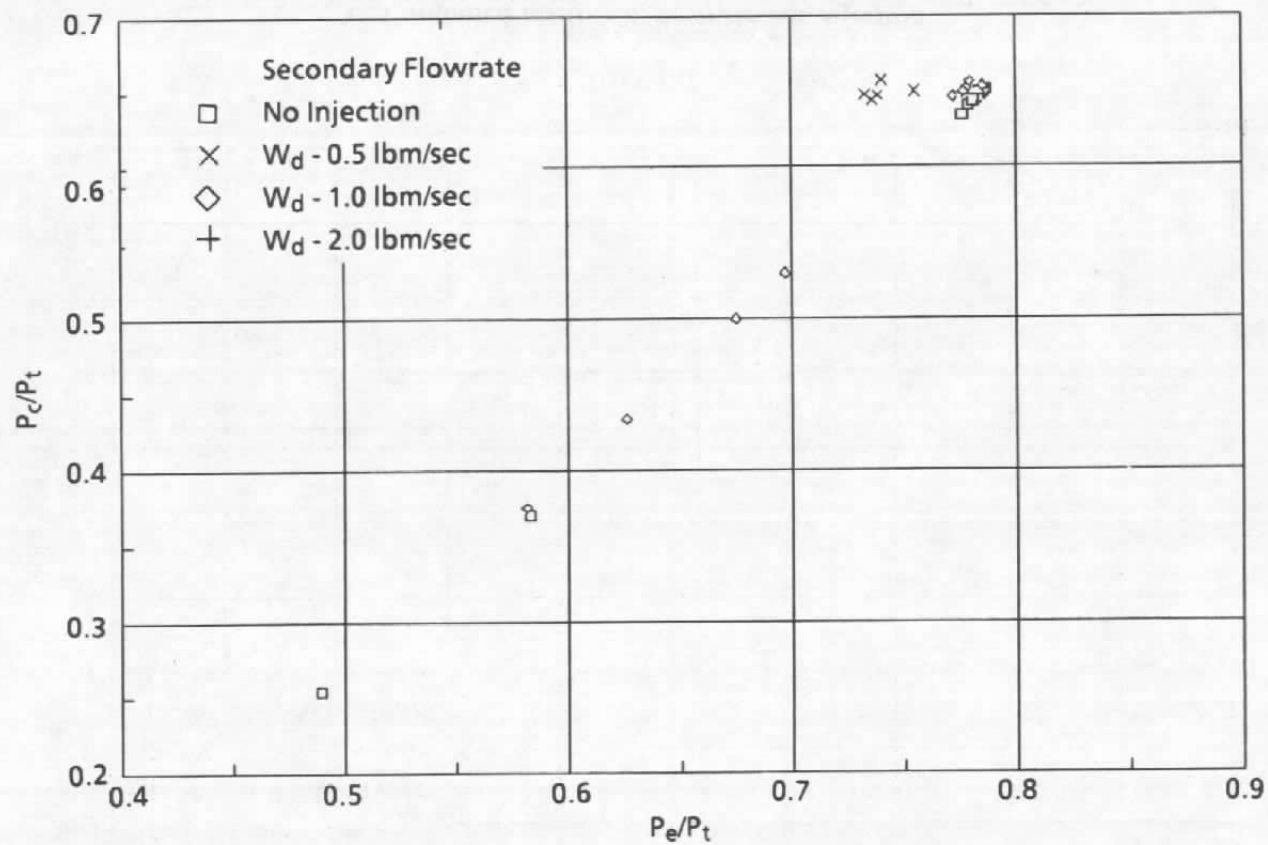
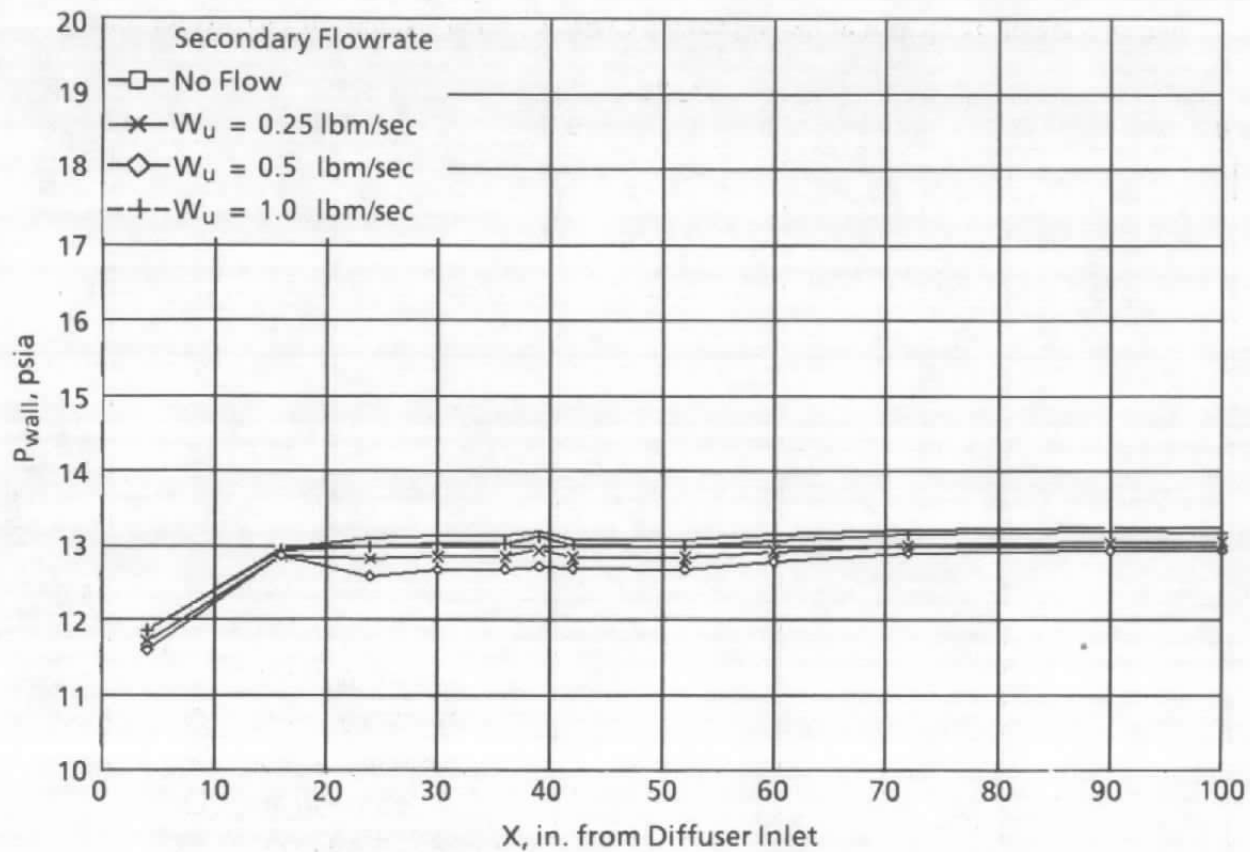
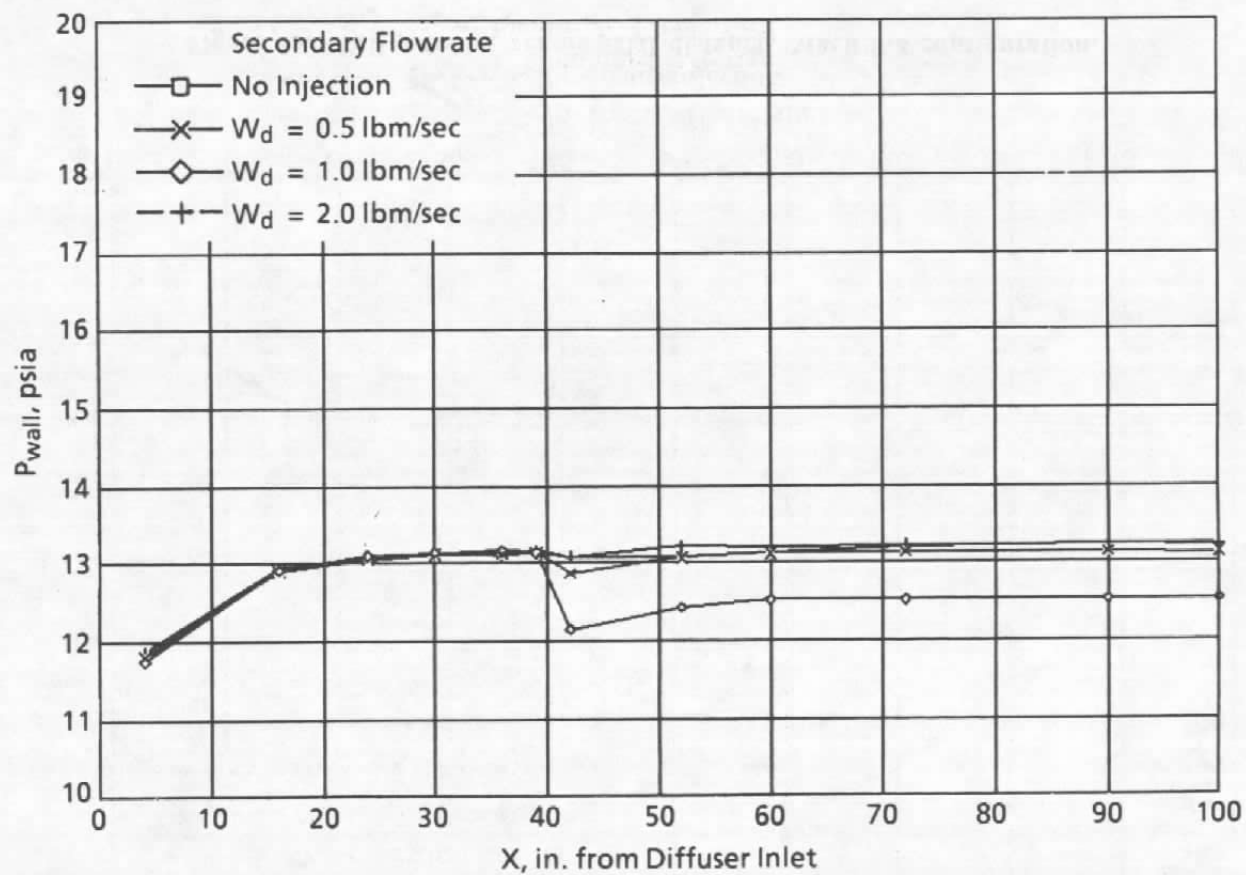


Figure 35. Diffuser breakdown curve for Mach 0.8 configuration with downstream injection.

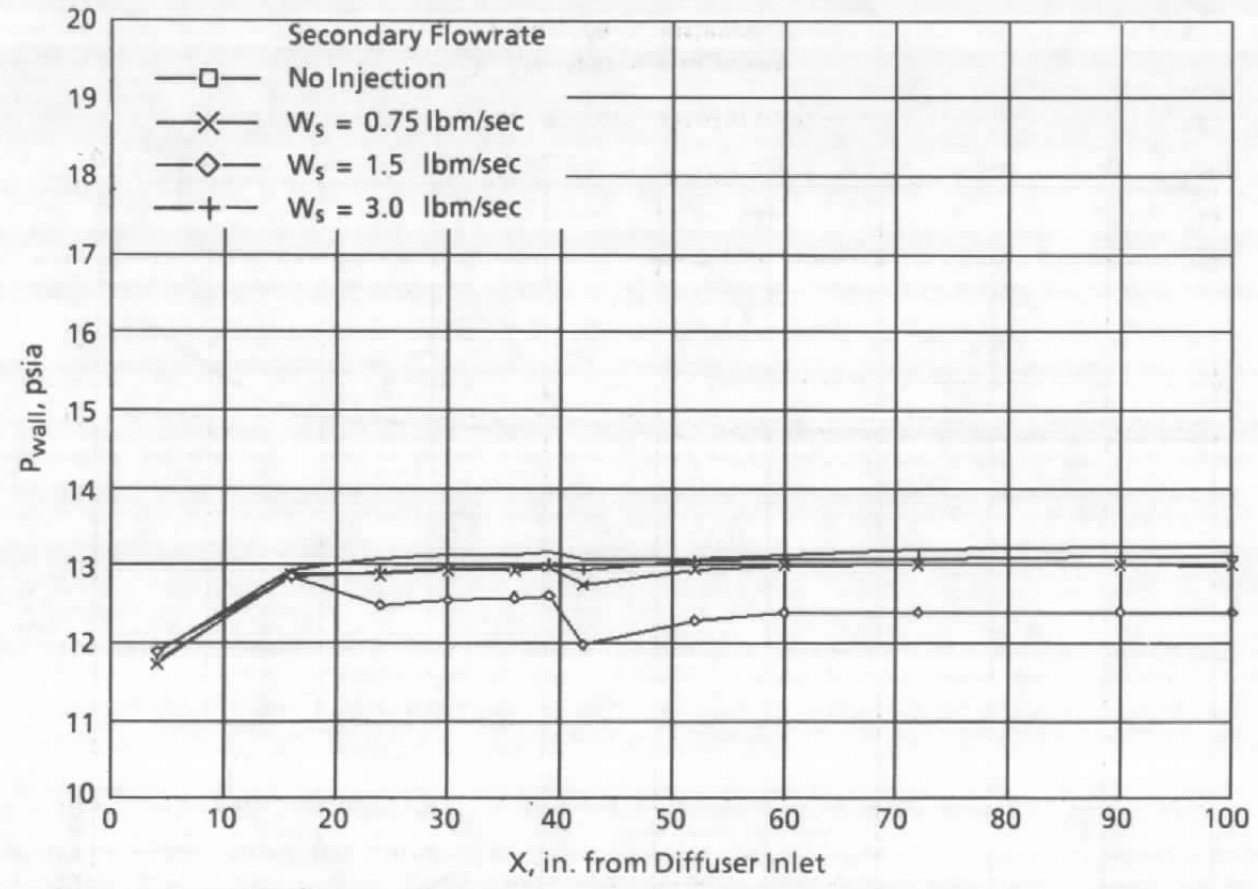


a. Upstream injection

Figure 36. Wall pressure versus axial distance, Mach 0.8 configuration.



b. Downstream injection
Figure 36. Continued.



c. Combined injection
Figure 36. Concluded.

Table 1. Measurement Uncertainties

Parameter Designation	Bias (B), Percent Reading	Degree of Freedom	Precision (S), Percent Reading	Uncertainty $U = \pm (B + t_{95}S)$, Percent Reading	Range	Sensor Manufacturer
PSEW1 to PSEW24	± 0.7	> 30	± 0.15	± 1.0	25 psia	Taber
PTR-1 to PTR12	± 0.7	> 30	± 0.15	± 1.0	25 psia	Taber
PTPV	± 0.7	> 30	± 0.15	± 1.0	500 psia	Taber
PSPV	± 0.7	> 30	± 0.15	± 1.0	100 psia	Taber
PTNC-1	± 0.7	> 30	± 0.15	± 1.0	100 psia	Dynisco
PTNC-2	± 0.7	> 30	± 0.15	± 1.0	100 psia	Dynisco
PCELL-1	± 0.7	> 30	± 0.15	± 1.0	20 psia	Taber
PCELL-2	± 0.7	> 30	± 0.15	± 1.0	20 psia	Taber
PEX	± 0.7	> 30	± 0.15	± 1.0	20 psia	Taber
PTUV	± 0.7	> 30	± 0.15	± 1.0	200 psia	Taber
PSUV	± 0.7	> 30	± 0.15	± 1.0	100 psia	Dynisco
PTDV	± 0.7	> 30	± 0.15	± 1.0	200 psia	Taber
PSDV	± 0.7	> 30	± 0.15	± 1.0	100 psia	Dynisco
PTVM1 to PTUM3	± 0.7	> 30	± 0.15	± 1.0	200 psia	Taber
PTDM1 to PTDM3	± 0.7	> 30	± 0.15	± 1.0	200 psia	Taber
PSSA	± 0.7	> 30	± 0.15	± 1.0	200 psia	Taber
PEX-2	± 0.7	> 30	± 0.15	± 1.0	20 psia	Taber
TEX	± 0.7	> 30	± 0.15	$\pm (4\% + 2^\circ\text{R})$	0 to 640°F	Type C/A
TSEW-1 to TSEW-4	± 0.7	> 30	± 0.15	$\pm (4\% + 2^\circ\text{R})$	0 to 640°F	Type C/A
TTDM-1 to TTDM-2	± 0.7	> 30	± 0.15	$\pm (4\% + 2^\circ\text{R})$	0 to 400°F	Type C/A
TTDV	± 0.7	> 30	± 0.15	$\pm (4\% + 2^\circ\text{R})$	0 to 100°F	Type C/C
TTNC-1 and TTNC-2	± 0.7	> 30	± 0.15	$\pm (4\% + 2^\circ\text{R})$	0 to 640°F	Type C/A
TTPV	± 0.7	> 30	± 0.15	$\pm (4\% + 2^\circ\text{R})$	0 to 640°F	Type C/A
TTR-01 to TTR-13	± 0.7	> 30	± 0.15	$\pm (4\% + 2^\circ\text{R})$	0 to 640°F	Type C/A
TTUM-1 and TTUM-2	± 0.7	> 30	± 0.15	$\pm (4\% + 2^\circ\text{R})$	0 to 100°F	Type C/A
TTUV	± 0.7	> 30	± 0.15	$\pm (4\% + 2^\circ\text{R})$	0 to 100°F	Type C/C

NOMENCLATURE

CA	Chromel® -Alumel®
CC	Copper-constantan
CR	Crocco number
CRT	Cathode Ray Tube
D	Duct diameter, in.
EUD	Engineering units data
FLCL	Fuel lean combustion limit
HPA	High-pressure air
L	Duct length, in.
L/D	Length-to-diameter ratio
M	Mixedness parameter
MN	Mach number
n	Parameter index
NIST	National Institute of Standards and Technology
OLCL	Oxidizer lean combustion limit
PCELL-n	Test cabin pressure, psia
PEX	Exhaust duct pressure, psia
PSEW-n	Exhaust duct wall static pressure, psia
PSDV	Downstream venturi throat static pressure, psia

PSPV	Primary air venturi throat static pressure, psia
PSUV	Secondary air upstream venturi throat static pressure, psia
PSSA	Supply air static pressure, psia
PTDMn	Secondary air downstream manifold pressure, psia
PTDV	Secondary air downstream venturi throat static pressure, psia
PTNC-n	Primary air nozzle chamber pressure, psia
PTPV	Primary air venturi total pressure, psia
PTR-n	Mixing rake total pressure, psia
PTUV	Secondary air upstream venturi pressure, psia
PTUM-n	Secondary air upstream manifold pressure, psia
TEX	Exhaust duct gas temperature, °F
TSEW-n	Exhaust duct wall temperature, °F
TTDV	Secondary air downstream venturi total temperature, °F
TTPV	Primary air venturi total temperature, °F
TTR-n	Mixing rake total temperature, °F
TTNC-n	Primary nozzle chamber total temperature, °F
TTDM-n	Secondary air downstream manifold temperature, °F
TTUM-n	Secondary air upstream manifold temperature, °F
TTUV	Secondary air upstream venturi total temperature, °F
x	Axial Distance from sudden expansion

Y	Species mass fraction
θ	Angular Position, degrees
ϕ	Diameter